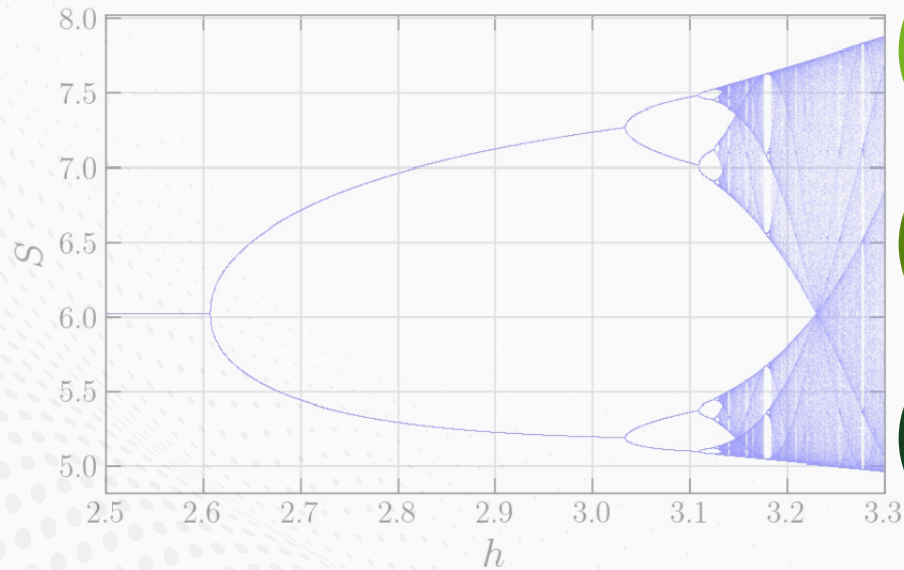


ISSN ONLINE
2980-1869



BULLETIN OF
BIOMATHEMATICS



2024

YEAR

2

VOLUME

2

ISSUE



Editor-in-Chief
Mehmet Yavuz, PhD

www.bulletinbiomath.org

VOLUME: 2 ISSUE: 2
ISSN ONLINE: 2980-1869

October 2024
<https://bulletinbiomath.org>



B U L L E T I N O F
BIOMATHEMATICS

BULLETIN OF BIOMATHEMATICS

Editor-in-Chief

Mehmet Yavuz
Department of Mathematics and Computer Sciences,
Faculty of Science, Necmettin Erbakan University,
Meram Yeniyol, 42090 Meram, Konya / TÜRKİYE
mehmetyavuz@erbakan.edu.tr

Publisher

Fırat Evirgen
Department of Mathematics,
Faculty of Science and Arts, Balıkesir University,
Çağış Campus, 10145 Çağış, Balıkesir / TÜRKİYE
fevirgen@balikesir.edu.tr

Editorial Board

Abdeljawad, Thabet
Prince Sultan University
Saudi Arabia

Agarwal, Praveen
Anand International College of Engineering
India

Aguilar, José Francisco Gómez
CONACyT- National Center for Technological Research
and Development
Mexico

Ahmad, Hijaz
International Telematic University Uninettuno
Italy

Arqub, Omar Abu
Al-Balqa Applied University
Jordan

Asjad, Muhammad Imran
University of Management and Technology
Pakistan

Atangana, Abdon
University of the Free State
South Africa

Baleanu, Dumitru
Cankaya University, *Türkiye*;
Institute of Space Sciences, Bucharest, *Romania*

Başkonus, Hacı Mehmet
Harran University
Türkiye

Biswas, Md. Haider Ali
Khulna University
Bangladesh

Bonyah, Ebenezer
Department of Mathematics Education
Ghana

Bulai, Iulia Martina
University of Basilicata
Italy

Cabada, Alberto
University of Santiago de Compostela
Spain

Dassios, Ioannis
University College Dublin
Ireland

Eskandari, Zohreh
Shahrekord University
Iran

Flaut, Cristina
Ovidius University of Constanta
Romania

González, Francisco Martínez
Universidad Politécnica de Cartagena
Spain

Gürbüz, Burcu
Johannes Gutenberg-University Mainz, Institute of
Mathematics, *Germany*

Hammouch, Zakia
ENS Moulay Ismail University Morocco;
Thu Dau Mot University Vietnam and China Medical
University, *Taiwan*

Hristov, Jordan
University of Chemical Technology and Metallurgy
Bulgaria

Jafari, Hossein
University of Mazandaran, *Iran*;
University of South Africa, *South Africa*

Jajarmi, Amin
University of Bojnord
Iran

Lupulescu, Vasile
Constantin Brâncuși University of Târgu-Jiu
Romania

Naik, Parvaiz Ahmad
Department of Mathematics and Computer Science,
Youjiang Medical University for Nationalities, *China*

Owolabi, Kolade
Federal University of Technology
Nigeria

Otero-Espinar, Maria Victoria
University of Santiago de Compostela
Spain

Özdemir, Necati
Balıkesir University
Türkiye

Pinto, Carla M.A.
ISEP, *Portugal*

Povstenko, Yuriy
Jan Długosz University in Czestochowa
Poland

Qureshi, Sania
Mehran University of Engineering and Technology
Pakistan

Sabatier, Jocelyn
Bordeaux University
France

Safaei, Mohammad Reza
Florida International University
USA

Salahshour, Soheil
Bahçeşehir University
Türkiye

Sarı, Murat
Yıldız Technical University
Türkiye

Sarris, Ioannis E.
University of West Attica
Greece

Sene, Ndolane
Cheikh Anta Diop University
Senegal

Stamova, Ivanka
University of Texas at San Antonio
USA

Torres, Delfim F. M.
University of Aveiro
Portugal

Townley, Stuart
University of Exeter
United Kingdom

Valdés, Juan Eduardo Nápoles
Universidad Nacional del Nordeste
Argentina

Yang, Xiao-Jun
China University of Mining and Technology
China

Yuan, Sanling
University of Shanghai for Science and Technology
China

Technical Editor

Kerim Sarıgöl
Research Information System, Gazi University,
Ankara / TÜRKİYE
kerimsarigul@gazi.edu.tr

English Editors (In Alphabetical Order)

- **Abdulkadir Ünal** - School of Foreign Languages, Foreign Languages, Alanya Alaaddin Keykubat University, Antalya Türkiye.
- **Ahmet Sınak** - Necmettin Erbakan University, Department of Mathematics and Computer Sciences, Konya, Türkiye.
- **Faruk Türk** - Karamanoğlu Mehmetbey University, School of Foreign Languages, Karaman, Türkiye.

Editorial Secretariat

Fatma Özlem Coşar
Department of Mathematics and Computer Sciences,
Faculty of Science, Necmettin Erbakan University,
Meram Yeniyol, 42090 Meram, Konya / TÜRKİYE

Müzeyyen Akman
Department of Mathematics and Computer Sciences,
Faculty of Science, Necmettin Erbakan University,
Meram Yeniyol, 42090 Meram, Konya / TÜRKİYE

Contents

Research Articles

- 1 A fractional-order model of COVID-19 and Malaria co-infection
Livinus Loko Iwa, Andrew Omame, Simeon Chioma Inyama 133-161
- 2 A stochastic approach to tumor modeling incorporating macrophages
Sümevra Uçar, Ilknur Koca, Necati Özdemir, Tarık İnci 162-181
- 3 Bifurcations on a discrete-time SIS-epidemic model with saturated infection rate
Hasan S. Panigoro, Emli Rahmi, Salmun K. Nasib, Nur'ain Putri H. Gawa, Olumuyiwa James Peter 182-197
- 4 The effect of amyloid beta, membrane, and ER pathways on the fractional behavior of neuronal calcium
Brajesh Kumar Jha, Vora Hardagna Vatsal, Tajinder Pal Singh 198-217
- 4 A mathematical model for the study of HIV/AIDS transmission with PrEP coverage increase and parameter estimation using MCMC with a Bayesian approach
Erick Manuel Delgado Moya, Ranses Alfonso Rodriguez, Alain Pietrus 218-244

RESEARCH PAPER

A fractional-order model of COVID-19 and Malaria co-infection

Livinus Loko Iwa ^{1,*,‡}, Andrew Omame ^{1,2,‡} and Simeon Chioma Inyama ^{1,‡}

¹Department of Mathematics, Federal University of Technology, Owerri, Nigeria, ²Abdus Salam School of Mathematical Sciences, Government College University, Lahore, Pakistan

* Corresponding Author

‡ iwa.livinus@gmail.com (Livinus Loko Iwa); andrew.omame@futo.edu.ng (Andrew Omame); scinyama2011@yahoo.com (Simeon Chioma Inyama)

Abstract

This paper explores the co-infection dynamics of coronavirus disease 2019 (COVID-19) and Malaria using Caputo-type fractional derivative to further understand the disease interactions and implement effective control strategies. We demonstrate the positivity and boundedness of the solution through Laplace transform techniques and establish the existence and uniqueness of the solution, showcasing model stability using fractional-order stability theory. Simulation experiments across varying fractional orders and disease classes offer insights into the co-infection dynamics. This is a new model and the findings underscore the potential impact of control measures on mitigating co-infection under endemic conditions. We conclude that infection with malaria does not guarantee immunity to COVID-19 and infection with COVID-19 as well does not guarantee immunity to malaria.

Keywords: COVID-19; Malaria; vaccination; co-infection; model-fitting; simulations

AMS 2020 Classification: 92D30; 92D25; 92C42; 34C60

1 Introduction

Malaria is one of the most deadly diseases in the world's history. It is caused by Plasmodium parasite [1] and transmitted to humans through the bites of infectious female Anopheles mosquitoes. First discovered in 1880 in a military hospital in Algiers, Algeria [2], malaria has caused millions of deaths in the past and still poses a great threat despite scientific investigations for hundreds of years [3]. Although some countries in the world have attained an indigenous malaria-free state in some particular years [4], most others still suffer the menace. In 2015, about 218 million malaria cases were recorded worldwide with 453,000 cases of death [5]. Also, in 2019, about 229 million cases of malaria with another estimated 409 thousand deaths were recorded in the world [6].

► Received: 22.09.2023 ► Revised: 16.05.2024 ► Accepted: 10.07.2024 ► Published: 31.10.2024

According to the 2020 World Malaria Report, Nigeria's malaria prevalence rate is at 303 per 1000 of its population [7]. The malaria prevalence rate is affected significantly by regions, rural-urban, and socio-economic differences [8]. In Nigeria for instance, the malaria prevalence rate ranges from 16 percent in the South-South and South-East regions to 34 percent in the North-West region and 2.4 times in rural population than in urban population as reported by United States Agency for International Development [9]. Also in socioeconomic groups, there is a seven times positive difference between children in lower and higher socio-economic groups.

The COVID-19 pandemic has recently joined the league of most common deadly diseases in the world. [10] described it as a positive-sense RNA virus that originated in the seafood market of live animals with its first case traced to the city of Wuhan, China [11] in December 2019. COVID-19 is highly contagious with three main routes; respiratory droplets, contact, and airborne [12]. Infected individuals become symptomatic in stages, although its complete clinical manifestation is still not clear as of the time of this research [13]. Symptoms include fever, dry cough, sore throat, loss of smell and fatigue but in acute cases, it can lead to severe shortness of breath, hypoxia, and death [12, 14]. Evidence suggests that older individuals and those with compromised immune systems (from pre-existing conditions) are more likely to develop severe forms of COVID-19 [15]. In 2020, there were about 2,804,796 confirmed cases of COVID-19 in the world and 193,710 confirmed deaths [16]. Also, a total of 585,086,861 confirmed cases worldwide with a total of 6,422,914 deaths as of August 11, 2022 [17].

Malaria and COVID-19 are two life-threatening diseases that concurrently distort normal human activities. Realizing the transmissible routes of COVID-19, the government placed restrictions in markets, worship centers, airports, viewing centers, and other social gatherings to help reduce unguided transmission of the disease. These unusual by-laws lasted for weeks and even months interrupted routine malaria prevention and control measures and treatments, and by extension increased new malaria cases and exacerbated untreated ones [18]. This suggests that COVID-19 has caused havoc on every aspect of human life ranging from social, health, economy, and education [19]. About 241 million malaria cases and 627 thousand deaths were recorded in 2020 worldwide as against the previous year, which makes about 14 million extra cases and 69 thousand extra deaths in the latter year [18]. Approximately two-thirds of these increased deaths (47,000) were caused by the unavailability of malaria prevention, diagnosis and treatment linked to COVID-19 disruptions [18]. Confirming the possible link between COVID-19 and Malaria [20] found different types of Malaria associated with COVID-19 and stated that the prevalence of Malaria among COVID-19 patients in Sudan is 32.4 percent.

Mathematical models have been so important in studying the behavioral pattern of infectious diseases [21–28]. The mathematical model of malaria transmission was first developed by Ross [26]. His report showed that reducing the vector population to below a certain threshold can help eradicate malaria. Chiyaka et al. [23] formulated a deterministic model with two latent periods in the non-constant host and vector populations. While checking for ways to eradicate the disease, they uniquely analyzed the spread of resistance and combined effects of intervention strategies such as personal protection, vaccination and treatment with the assumption that the treated individuals remain infectious for a while and discovered that personal control has a positive impact on disease control. To ascertain the level of awareness of COVID-19 virus [28] studied the mathematical model of COVID-19 which incorporates awareness programs and different hospitalization strategies for mild and severe cases while [29] proposed an SEIQCWR transmission model which adopts the SEIR model to study the current outbreak of COVID-19 in Nigeria with nonlinear forces on infection. While considering the complexity of the disease [19] formulated a stochastic model of COVID-19 under environmental white noise and recognized the random nature of the input components. Several other mathematical models on COVID-19 are found in

the literature, some of which are co-infection models [30–33].

Fractional differential equations have been widely used in recent years in modeling physical and biological processes [33–41]. This is mainly because of some level of limitations exhibited by mathematical models in integer-order derivatives. Although classical integer-order derivatives yield good results, fractional-order derivatives are non-local operators and produce better and more realistic results for a given real-life problem [41]. To further understand the different fractional order operators and models, see [42–46]. Caputo fractional derivative as one of the fractional differential operators is mostly used in modeling feasible real-life problems. This is because of its convenience for the initial condition of the fractional differential equations. It has long-term memory effects [21], and is very useful in translating higher fractional-order differential systems to lower ones [47] with well-understood physical meaning compared to other fractional operators [48]. [49] confirmed this when they analyzed the co-infection of HPV-CT in fractional order using Caputo fractional derivative. Also [50] compared Caputo, Caputo-Fabrizio and Atangana-Baleanu derivatives in their work. Their comparison shows that the Caputo derivative presents better results in the form of stability. Other mathematical models with fractional-order derivatives can be found in the works of [38, 51].

There are so many separate mathematical models in the literature on malaria and COVID-19 pandemic, however [27] started the work on the co-infection of the two diseases. They first derived the sufficient conditions for the stability of the two diseases separately before considering their entire equilibria where their findings suggest that using Malaria and COVID-19 protection measures concurrently is best compared to dealing with them separately. [52] studied the fractional-order mathematical model of COVID-19 and Malaria using the Atangana-Baleanu derivative and discovered they could reduce the risk factor of getting COVID-19 after contracting Malaria and vice versa. Still on the co-infection of COVID-19 and malaria [53] worked on the impact of COVID-19 and Malaria co-infection on clinical outcomes and discovered that patients with concurrent malaria and COVID-19 infection had greater mortality risk compared to mono-infection with Severe Acute Respiratory Syndrome Coronavirus 2 (SARS-CoV-2). Inspired by the above literature, especially the work performed by [27] and the beautiful patterns and results gotten from fractional derivatives as put together by [21, 41, 52, 54], we present this study of the co-infection of COVID-19 and malaria in fractional order derivative using Caputo fractional operator since the works of [27] and [53] are in integer derivative and [52] used Atangana-Baleanu fractional derivative. We expect to obtain better results considering the stated advantages.

The ensuing parts of this paper (in sections) are as follows: **Section 2** captures the preliminaries where major definitions of the various fractional-order derivative operators are stated for easy and better understanding of the whole work. In **Section 3**, we formulated the fractional mathematical model and also carried out some vital analysis on the formulated model which included analysis on the invariant domain, positivity, basic reproduction number, locally asymptotic stability, existence and uniqueness of the solution and lastly the generalized Ulam-Hyers-Rassias stability. In **Section 4** we performed some numerical simulations and discussed our results therein. Lastly, we concluded **Section 5** based on our findings.

2 Preliminaries

This particular section presents some definitions of fractional derivatives and integrals that are of great relevance to modeling real-life problems.

Definition 1 [55]: The Caputo fractional derivative of order $\omega > 0$ of a function $f(t)$ of order $\omega \in \mathbb{R}^+$ is given as

$${}^C D_t^\omega f(t) = J_t^{n-\omega} D^n f(t) = \frac{1}{\Gamma(n-\omega)} \int_0^t (t-\tau)^{n-\omega-1} f^{(n)}(\tau) d\tau, \quad (1)$$

with the positive integer n given as $n-1 < \omega \leq n$. As $0 < \omega \leq 1$, the Caputo fractional derivative of order $\omega > 0$ above becomes

$${}^C D_t^\omega f(t) = \frac{1}{\Gamma(1-\omega)} \int_0^t (t-\tau)^{-\omega} f'(\tau) d\tau. \quad (2)$$

Definition 2 [54]: Suppose that a function $f \in C^1(0, Y)$ is such that $T > 0$ and $0 < \omega \leq 1$, then Atangana-Baleanu derivative in Caputo sense is presented as

$${}^{ABC} D_t^\omega f(t) = \frac{S(\omega)}{1-\omega} \int_a^t E_\omega \left(-\omega \frac{(t-\tau)^\omega}{1-\omega} \right) f'(\tau) d\tau, \quad t > 0, \quad (3)$$

where $S(\omega) = (1-\omega) + \frac{\omega}{\Gamma(\omega)}$, denotes a normalization function satisfying $S(0) = S(1) = 1$.

Definition 3 [48]: The fractional integral of order $\omega > 0$ of any function $f \in C^1(0, Y)$ is presented as

$$J_t^\omega f(t) = \frac{1}{\Gamma(\omega)} \int_0^t (t-\tau)^{\omega-1} f(\tau) d\tau, \quad t > 0, \quad (4)$$

as long as the integral part is integrable in \mathbb{R}^+ . In other words, suppose that $f(t) = P$, where P is a constant and results to;

$$J_t^\omega(P) = \frac{1}{\Gamma(\omega)} \int_0^t (t-\tau)^{\omega-1} (P) d\tau = P \frac{t^\omega}{\Gamma(\omega+1)}. \quad (5)$$

Definition 4 The solution of the Caputo fractional derivative can be written in the form of the Volterra integral as given below;

$$f - f(0) = \frac{1}{\Gamma(\omega)} \int_0^t (t-\tau)^{\omega-1} K(\tau, f(\tau)) d\tau,$$

where the fractional order $\omega > 0$.

Definition 5 [55]: The Laplace transform of Caputo fractional derivative (2) is presented as;

$$\mathcal{L}\{D_t^\omega f(t)\} = s^\omega \tilde{f}(s) - s^{\omega-1} f(0), \quad 0 < \omega \leq 1, \quad (6)$$

with \mathcal{L} as the Laplace transform operator.

3 Mathematical model formulation

The fractional-order model under this study is an interaction between human and vector populations. The human population at time t , denoted by $N_H(t)$ is sub-divided into seven distinct classes,

namely; susceptible humans $S_H(t)$, susceptible humans vaccinated against COVID-19 $V_{HC}(t)$, individuals infected with malaria $I_{HM}(t)$, recovered individuals from malaria $R_{HM}(t)$, individuals infected with COVID-19 $I_{HC}(t)$, recovered individuals from COVID-19 $R_{HC}(t)$ and individuals co-infected with malaria and COVID-19 $I_{MC}(t)$. Therefore,

$$N_H(t) = S_H(t) + V_{HC}(t) + I_{HM}(t) + R_{HM}(t) + I_{HC}(t) + R_{HC}(t) + I_{MC}(t).$$

We considered the last stage of the mosquito life cycle and sub-divided the vector population at time t , denoted by $N_V(t)$ into two distinct classes; susceptible vectors $S_V(t)$ and infectious vectors with malaria $I_{VM}(t)$ hence the vector population is given by

$$N_V(t) = S_V(t) + I_{VM}(t).$$

The model flow diagram is depicted in Figure 1 while the parameters of the model are described properly in Table 1 below.

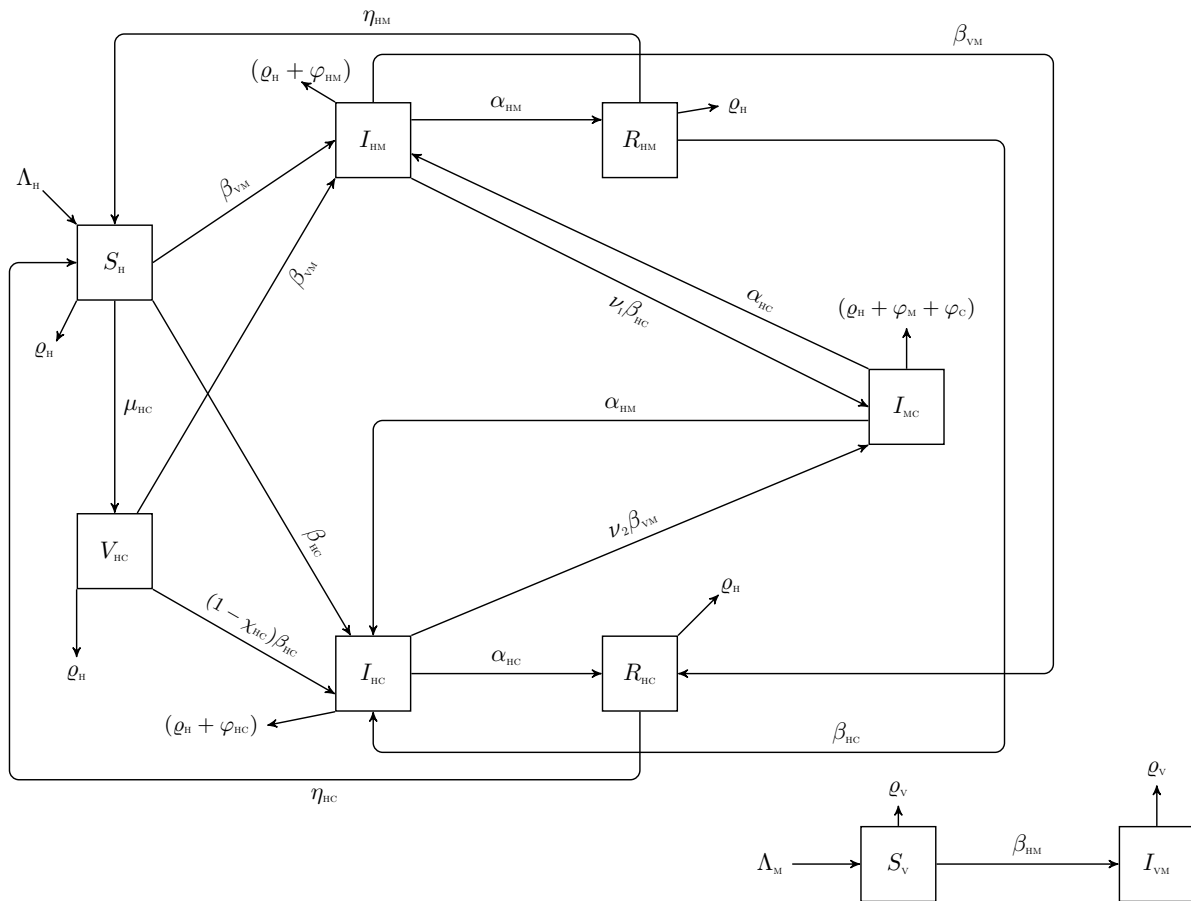


Figure 1. Model diagram

The rate of recruitment into the susceptible human population is given by Λ_H and that of the vector population is given by Λ_M . The parameter ρ_H is the natural human mortality rate. It is assumed that infectious individuals can contact Malaria and/or COVID-19 individuals at the rates ϑ_{HM} and ϑ_{HC} , respectively. The interacting ability between the human and vector population warrants that individuals can move from one class to another. When treated, humans infected with Malaria move to the recovered class at the rate α_{HM} . Also, the human-to-unvaccinated human transmission

Table 1. Description of variables and parameters in the above model equation

Variable	Description		
S_H	Susceptible humans		
V_{HC}	Susceptible humans vaccinated against COVID-19		
I_{HM}	Individuals infected with Malaria		
R_{HM}	Recovered individuals from Malaria		
I_{HC}	Individuals infected with COVID-19		
R_{HC}	Recovered individuals from COVID-19		
I_{MC}	Infectious individuals co-infected with Malaria and COVID-19		
S_V	Susceptible vectors		
I_{VM}	Infectious vectors with Malaria		
Parameter	Description	Value	Reference
Λ_H	Human recruitment rate	$\frac{206,139,587}{54,69 \times 365} \text{ day}^{-1}$	[56, 57]
Λ_V	Vector recruitment rate	$\frac{10^4}{21}$	[56]
θ_2	Human contact rate with COVID-19 patients	0.4531	[58]
ϱ_H	Human natural death rate	$\frac{1}{54.69 \times 365} \text{ day}^{-1}$	[56, 57]
η_{HM}	Loss of infection acquired immunity to Malaria	0.005	Assumed
η_{HC}	Loss of infection acquired immunity to COVID-19	0.005	Assumed
μ_{HC}	Fraction of susceptible humans vaccinated against COVID-19	0.025	[59]
χ_{HC}	COVID-19 vaccine efficacy	0.95	[14]
θ_1	Effective contact rate for vector to human transmission of Malaria	0.125 - 0.5	[60]
θ_3	Effective contact rate for human to vector transmission of Malaria	0.48	[61]
α_{HM}	Malaria recovery rate	0.25	[56]
α_{HC}	COVID-19 recovery rate	0.3	[62]
ϑ_1	Modification parameter accounting for susceptibility of Malaria-infected individuals to COVID-19	1	Assumed
ϑ_2	Modification parameter accounting for susceptibility of COVID-19-infected individuals to Malaria	1	Assumed
φ_{HM}	Malaria-induced death rate	0.000153	[7]
φ_{HC}	COVID-19-induced death rate	0.015	[63]
ϱ_V	Vector removal rate	$\frac{1}{21}$	[56, 57]

of COVID-19 is possible at the rate θ_2 , especially when safety measures are neglected and the recovery rate of infected humans with COVID-19 is α_{HC} . χ_{HC} is the COVID-19 vaccine efficacy and θ_1 is the contact rate for vector to human transmission of Malaria. ϑ_1 is the modification parameter accounting for the susceptibility of Malaria-infected individuals to COVID-19 and ϑ_2 is the modification parameter accounting for susceptibility of COVID-19 infected individuals to Malaria. Mosquitoes are recruited into the population at the rate Λ_V and noting that the adult mosquito has a life span, we have the vector removal rate as ϱ_V .

Following the assumptions above, the COVID-19 and Malaria co-infection model is given by the following fractional differential equations;

$$\begin{aligned}
 {}^C D_t^\omega S_H(t) &= \Lambda_H - \left(\frac{\beta_{VM} I_{VM}}{N_H} + \frac{\beta_{HC} (I_{HC} + I_{MC})}{N_H} \right) S_H - \varrho_H S_H - \mu_{HC} S_H + \eta_{HM} R_{HM} + \eta_{HC} R_{HC}, \\
 {}^C D_t^\omega V_{HC}(t) &= \mu_{HC} S_H - (1 - \chi_{HC}) \frac{\beta_{HC} (I_{HC} + I_{MC})}{N_H} V_{HC} - \varrho_V V_{HC} - \frac{\beta_{VM} I_{VM}}{N_H} V_{HC}, \\
 {}^C D_t^\omega I_{HM}(t) &= \frac{\beta_{VM} I_{VM}}{N_H} (S_H + V_{HC} + R_{HC}) - (\alpha_{HM} + \varrho_H + \varphi_{HM}) I_{HM} - \vartheta_1 \frac{\beta_{HC} (I_{HC} + I_{MC})}{N_H} I_{HM} + \alpha_{HC} I_{MC},
 \end{aligned}$$

$$\begin{aligned}
 {}^C D_t^\omega R_{HM}(t) &= \alpha_{HM} I_{HM} - \varrho_H R_{HM} - \eta_{HM} R_{HM} - \frac{\beta_{HC}(I_{HC} + I_{MC})}{N_H} R_{HM}, \\
 {}^C D_t^\omega I_{HC}(t) &= \frac{\beta_{HC}(I_{HC} + I_{MC})}{N_H} (S_H + (1 - \chi_{HC}) V_{HC} + R_{HM}) - (\alpha_{HC} + \varrho_H + \varphi_{HC}) I_{HC} - \vartheta_2 \frac{\beta_{VM} I_{VM}}{N_H} I_{HC} + \alpha_{HM} I_{MC}, \\
 {}^C D_t^\omega R_{HC}(t) &= \alpha_{HC} I_{HC} - \varrho_H R_{HC} - \eta_{HC} R_{HC} + \frac{\beta_{VM} I_{VM}}{N_H} R_{HC}, \\
 {}^C D_t^\omega I_{MC}(t) &= \vartheta_1 \frac{\beta_{HC}(I_{HC} + I_{MC})}{N_H} I_{HM} + \vartheta_2 \frac{\beta_{VM} I_{VM}}{N_H} I_{HC} - (\varrho_H + \varphi_{HM} + \varphi_{HC} + \alpha_{HM} + \alpha_{HC}) I_{MC}, \\
 {}^C D_t^\omega S_V(t) &= \Lambda_M - \frac{\beta_{HM}(I_{HM} + I_{MC})}{N_H} S_V - \varrho_V S_V, \\
 {}^C D_t^\omega I_{VM}(t) &= \frac{\beta_{HM}(I_{HM} + I_{MC})}{N_H} S_V - \varrho_V I_{VM},
 \end{aligned}$$

with the corresponding initial conditions $S_H \geq (0)$, $V_{HC} \geq (0)$, $I_{HM} \geq (0)$, $R_{HM} \geq (0)$, $I_{HC} \geq (0)$, $R_{HC} \geq (0)$, $I_{MC} \geq (0)$, $S_V \geq (0)$, $I_{VM} \geq (0)$.

Invariant domain

Theorem 1 Suppose $S_H(t), V_{HC}(t), I_{HM}(t), R_{HM}(t), I_{HC}(t), R_{HC}(t), I_{MC}(t)$ are solutions of the system of equations for the human population, then the set

$$\begin{aligned}
 \Delta_h = \left\{ (S_H(t), V_{HC}(t), I_{HM}(t), R_{HM}(t), I_{HC}(t), R_{HC}(t), I_{MC}(t)) \in \mathbb{R}_+^7 : S_H \right. \\
 \left. + V_{HC} + I_{HM} + R_{HM} + I_{HC} + R_{HC} + I_{MC} \leq \frac{\Lambda_H}{\varrho_H} \right\}, \tag{7}
 \end{aligned}$$

is positively invariant with respect to the model concerned.

For the vector population, Suppose $S_V(t), I_{VM}(t)$ are any solution of the system, then the set

$$\Delta_v = \left\{ (S_V(t), I_{VM}(t)) \in \mathbb{R}_+^2 : S_V + I_{VM} \leq \frac{\Lambda_V}{\varrho_V} \right\}, \tag{8}$$

is positively invariant with respect to the model concerned.

Proof We shall adopt the proof put together by [64].

Positivity

Following the pattern in the work of [48], by contradiction, we assume that equation three of the model is false. Then let $t_1 = \min\{t : S_H(t) V_{HC}(t) I_{HM}(t) R_{HM}(t) I_{HC}(t) R_{HC}(t) I_{MC}(t) S_V(t) I_{VM}(t) = 0\}$. Suppose $I_{HM}(t_1) = 0$, it implies that $S_H(t) > 0$, $V_{HC}(t) > 0$, $R_{HM}(t) > 0$, $I_{HC}(t) > 0$, $R_{HC}(t) > 0$, $I_{MC}(t) > 0$, $S_V(t) > 0$, $I_{VM}(t) > 0$ for all $[0, t_1]$. We can assume that there exists the following expression,

$$\theta_1 = \min_{0 \leq t \leq t_1} \left\{ \frac{(\beta_{VM} I_{VM} S_H + \beta_{VM} I_{VM} R_{HC} + \beta_{VM} I_{VM} R_{HC} - \vartheta_1 \beta_{HC} I_{HC} - \vartheta_1 \beta_{HC} I_{MC})}{I_{HM}} - (\alpha_{HM} + \varrho_H + \varphi_{HM} + \alpha_{HC} I_{MC}) \right\}.$$

It follows that

$${}^C D_t^\omega I_{HM} - \theta_1 I_{HM} > 0. \tag{9}$$

We can also determine a continuous function Φ_1 to ascertain the following equation

$${}^C D_t^\omega I_{HM} - \theta_1 I_{HM} = -\Phi_1(t).$$

By Laplace transform, the above inequality becomes

$$s^\omega \tilde{I}_{HM}(s) - s^{\omega-1} I_{HM}(0) - \theta_1 \tilde{I}_{HM}(s) = -\tilde{\Phi}_1(s),$$

from which

$$\begin{aligned} \tilde{I}_{HM}(s) &= I_{HM}(0) \frac{s^{\omega-1}}{s^\omega - \theta_1} - \frac{\Phi_1(s)}{s^\omega - \theta_1} \\ &= \frac{I_{HM}(0)}{s} \left(1 - \frac{\theta_1}{s^\omega}\right)^{-1} - \frac{\Phi_1(s)}{s^\omega} \left(1 - \frac{\theta_1}{s^\omega}\right)^{-1} \\ &= I_{HM}(0) \sum_{k=0}^{\infty} \frac{\theta_1^k}{s^{\omega k + 1}} - \Phi_1(s) \sum_{k=0}^{\infty} \frac{\theta_1^k}{s^{\omega k + \omega}}. \end{aligned} \tag{10}$$

Ignoring the non-positive term, the inverse Laplace transform gives the solution of (9) (using Mittag-Leffler function), which satisfies the following expression:

$$I_{HM} > I_{HM}(0) \sum_{k=0}^{\infty} \frac{(\theta_1 t^\omega)^k}{\Gamma(\omega k + 1)} = I_{HM}(0) E_\omega(\theta_1 t^\omega),$$

such that the positivity of the solution I_{HM} is given by

$$I_{HM} > I_{HM}(0) E_\omega(\theta_1 t^\omega) > 0,$$

which contradicts $I_{HM}(t_1) = 0$. Similarly, suppose $I_{MC}(t_1) = 0$ which implies that $S_H(t) > 0$, $V_{HC}(t) > 0$, $R_{HM}(t) > 0$, $I_{HM}(t) > 0$, $R_{HC}(t) > 0$, $I_{HC}(t) > 0$, $S_V(t) > 0$, $I_{VM}(t) > 0$ for all $0 \leq t \leq t_1$. We assume that there exists the following expression:

$$\theta_2 = \min_{0 \leq t \leq t_1} \left\{ \frac{(\varphi_1 \beta_{HC} I_{HC} I_{HM} + \varphi_1 \beta_{HC} I_{HM} + \varphi_2 \beta_{VM} I_{VM} I_{HM})}{I_{MC}} - (\varrho_H + \vartheta_M + \vartheta_C + \alpha_{HM} + \alpha_{HC}) \right\},$$

so that

$${}^C D_t^\omega I_{MC}(t) > \theta_2 I_{MC}(t). \tag{11}$$

We can still determine a continuous function $\Phi_2(t)$ to ascertain the following equation

$${}^C D_t^\omega I_{MC}(t) - \theta_2 I_{MC}(t) = -\Phi_2(t).$$

By applying the Laplace transform, the above inequality becomes

$$s^\omega \tilde{I}_{MC}(s) - s^{\omega-1} I_{MC}(0) - \theta_2 \tilde{I}_{MC}(s) = -\tilde{\Phi}_2(s),$$

from which

$$\tilde{I}_{MC}(s) = I_C(0) \sum_{k=0}^{\infty} \frac{\theta_2^k}{s^{\omega k + 1}} - \Phi_2(s) \sum_{k=0}^{\infty} \frac{\theta_2^k}{s^{\omega k + \omega}}.$$

Ignoring the non-positive term, the inverse Laplace transform gives the solution of Eq. (11) (using Mittag-Leffler function), satisfying the following expression:

$$I_{MC}(t) > I_{MC}(0) \sum_{k=0}^{\infty} \frac{(\theta_2 t^\omega)^k}{\Gamma(\omega k + 1)} = I_{MC}(0) E_\omega(\theta_2 t^\omega). \tag{12}$$

Hence the positivity of this other solution I_{MC} is given by $I_{MC}(t) > I_{MC}(0) E_\omega(\theta_2 t^\omega) > 0$, which contradicts $I_{MC}(t_1) = 0$. More so, since the above have similar results, the same pattern will show that the positivity of the solutions $S_H, V_{HC}, R_{HM}, R_{HC}, S_V$ and V_{HC} respectively are given by

$$\begin{aligned} I_{HC}(t) &> I_{HC}(0) E_\omega(\theta_3 t^\omega) > 0, \\ S_H(t) &> S_H(0) E_\omega(\theta_4 t^\omega) > 0, \\ V_{HC}(t) &> V_{HC}(0) E_\omega(\theta_5 t^\omega) > 0, \\ R_{HM}(t) &> R_{HM}(0) E_\omega(\theta_6 t^\omega) > 0, \\ R_{HC}(t) &> R_{HC}(0) E_\omega(\theta_7 t^\omega) > 0, \\ S_V(t) &> S_V(0) E_\omega(\theta_8 t^\omega) > 0, \\ I_{VM}(t) &> I_{VM}(0) E_\omega(\theta_9 t^\omega) > 0. \end{aligned}$$

Basic reproduction number of the mathematical model

The Malaria-COVID-19 co-infection model has a disease-free equilibrium (DFE) as given below. First, we set the right-hand side of the equations to zero to obtain

$$\begin{aligned} \xi_0 &= (S_H^0, V_{HC}^0, I_{HM}^0, R_{HM}^0, I_{HC}^0, R_{HC}^0, I_{MC}^0, S_V^0, I_{VM}^0) \\ &= \left(\frac{\Lambda_H}{\rho_H + \mu_{HC}}, \frac{\mu_{HC} S_H}{\rho_H}, 0, 0, 0, 0, 0, \frac{\Lambda_H}{\rho_V}, 0 \right). \end{aligned} \tag{13}$$

We apply the next-generation operator method to the model. Matrix F is of new infection and matrix V is the transfer of infection in and out of the disease classes. Thus, we have

$$F = \begin{pmatrix} 0 & 0 & 0 & \beta_{VM} \\ 0 & \frac{\beta_{HC} Q_1}{N_H} & \frac{\beta_{HC} Q_1}{N_H} & 0 \\ 0 & 0 & 0 & 0 \\ \frac{\beta_{HM} S_V}{N_H} & 0 & \frac{\beta_{HM} S_V}{N_H} & 0 \end{pmatrix}, \tag{14}$$

where $Q_1 = [S_H + (1 - \chi_{HC})] V_{HC}$.

$$V = \begin{pmatrix} k_1 & 0 & -\alpha_{HC} & 0 \\ 0 & k_2 & -\alpha_{HM} & 0 \\ 0 & 0 & k_3 & 0 \\ 0 & 0 & 0 & \rho_V \end{pmatrix}, \tag{15}$$

where $k_1 = \alpha_{HM} + \varrho_H + \varphi_{HM}$, $k_2 = \alpha_{HC} + \varrho_H + \varphi_{HC}$, $k_3 = \varrho_H + \varphi_M + \varphi_C + \alpha_{HM} + \alpha_{HC}$. The basic reproduction number of the Malaria-COVID-19 co-infection model, denoted by \mathcal{R}_0 as illustrated in [65], is presented as $\mathcal{R}_0 = \max\{\mathcal{R}_{0M}, \mathcal{R}_{0C}\}$ where \mathcal{R}_{0M} and \mathcal{R}_{0C} are respectively the Malaria and COVID-19 associated reproduction numbers, given by

$$\mathcal{R}_{0M} = \sqrt{\frac{\beta_{HM}\beta_{VM}S_V^*}{\varrho_V k_1 N_H^*}}, \quad \text{and} \quad \mathcal{R}_{0C} = \frac{\beta_{HC}[S_H^* + (1 - \chi_{HC})V_{HC}^*]}{k_2 N_H^*}.$$

Local asymptotic stability of disease-free equilibrium (DFE) of the co-infection model

Theorem 2 *At Disease-Free Equilibrium (DFE), the mathematical model is locally asymptotically stable (LAS) if $\mathcal{R}_0 < 1$, and unstable if $\mathcal{R}_0 > 1$.*

Proof The local stability of the model is analyzed using the Jacobean square matrix of the whole system, evaluated at COVID-19-Malaria-free equilibrium, given by;

$$J = \begin{pmatrix} -(\varrho_H + \mu_{HC}) & 0 & 0 & \eta_{HM} & \frac{\beta_{HC}S_H}{N_H} & \eta_{HC} & \frac{\beta_{HC}S_H}{N_H} & 0 & \frac{\beta_{VM}S_H}{N_H} \\ \mu_{HC} & \varrho_H & 0 & 0 & -\frac{(1-\chi_{HC})\beta_{HC}V_{HC}}{N_H} & 0 & -\frac{(1-\chi_{HC})\beta_{HC}V_{HC}}{N_H} & 0 & \frac{\beta_{VM}V_{HC}}{N_H} \\ 0 & 0 & -k_1 & 0 & 0 & 0 & \alpha_{HC} & 0 & \frac{\beta_{VM}(S_H + V_{HC})}{N_H} \\ 0 & 0 & \alpha_{HM} & -(\varrho_H + \eta_{HM}) & 0 & 0 & 0 & 0 & 0 \\ 0 & 0 & 0 & 0 & H - k_2 & 0 & H + \alpha_{HM} & 0 & 0 \\ 0 & 0 & 0 & 0 & \alpha_{HC} & -(\varrho_H + \eta_{HC}) & 0 & 0 & 0 \\ 0 & 0 & 0 & 0 & 0 & 0 & -k_3 & 0 & 0 \\ 0 & 0 & -\frac{\beta_{HM}S_V}{N_H} & 0 & 0 & 0 & -\frac{\beta_{HM}S_V}{N_H} & -\varrho_V & 0 \\ 0 & 0 & \frac{\beta_{HM}S_V}{N_H} & 0 & 0 & 0 & \frac{\beta_{HM}S_V}{N_H} & 0 & -\varrho_V \end{pmatrix}, \tag{16}$$

where $H = \frac{\beta_{HC}[S_H + (1 - \chi_{HC})V_{HC}]}{N_H}$.

The first three eigenvalues are $\lambda_1 = -(\eta_{HC} + \varrho_H)$, $\lambda_2 = -\varrho_V$ (twice), while the remaining eigenvalues will as well satisfy the negativity requirement for stability (following the method of Routh-Hurwitz).

Epidemiologically, **Theorem 2** implies that the prevalence of COVID-19 and Malaria can be eradicated from the population when $\mathcal{R}_0 < 1$ and if the initial population of the model is in the region of attraction of the DFE. Hence, the DFE is locally asymptotically stable if $\mathcal{R}_0 = \max(\mathcal{R}_{0C}, \mathcal{R}_{0M}) < 1$.

Existence and uniqueness of solution of the model

As significantly demonstrated by [66], we show the existence and uniqueness of the solution of the fractional-order model. When we apply the fractional integral to the Caputo fractional derivative model of order $\omega > 0$ while maintaining its initial conditions, we have the following Volterra-integral equations as a solution to the fractional model. This theory validates our claim that a solution to our model equations exists and is unique:

$$\begin{aligned} S_H - S_H(0) &= \frac{1}{\Gamma(\omega)} \int_0^t (t - \tau)^{\omega-1} K(\tau, S_H(\tau)) d\tau, \\ V_{HC} - V_{HC}(0) &= \frac{1}{\Gamma(\omega)} \int_0^t (t - \tau)^{\omega-1} Q(\tau, V_{HM}(\tau)) d\tau, \\ I_{HM} - I_{HM}(0) &= \frac{1}{\Gamma(\omega)} \int_0^t (t - \tau)^{\omega-1} V(\tau, I_{HM}(\tau)) d\tau, \end{aligned} \tag{17}$$

$$\begin{aligned}
 R_{HM}(t) - R_{HM}(0) &= \frac{1}{\Gamma(\omega)} \int_0^t (t - \tau)^{\omega-1} F(\tau, R_{HM}(\tau)) d\tau, \\
 I_{HC}(t) - I_{HC}(0) &= \frac{1}{\Gamma(\omega)} \int_0^t (t - \tau)^{\omega-1} H(\tau, I_{HC}(\tau)) d\tau, \\
 R_{HC}(t) - R_{HC}(0) &= \frac{1}{\Gamma(\omega)} \int_0^t (t - \tau)^{\omega-1} G(\tau, R_{HC}(\tau)) d\tau, \\
 I_{MC}(t) - I_{MC}(0) &= \frac{1}{\Gamma(\omega)} \int_0^t (t - \tau)^{\omega-1} U(\tau, I_{MC}(\tau)) d\tau, \\
 S_v(t) - S_v(0) &= \frac{1}{\Gamma(\omega)} \int_0^t (t - \tau)^{\omega-1} P(\tau, S_v(\tau)) d\tau, \\
 I_{VM}(t) - I_{VM}(0) &= \frac{1}{\Gamma(\omega)} \int_0^t (t - \tau)^{\omega-1} W(\tau, I_{VM}(\tau)) d\tau.
 \end{aligned}$$

We assume that the functions $(K, Q, V, F, H, G, U, P, W) : [0, b] \times \mathbb{R} \rightarrow \mathbb{R}$ are continuous so that $(\mathbb{R}, \|\cdot\|)$ is the Banach space and $\mathbb{H}^1([0, b])$ is that of all the continuous function defined in $[0, b] \rightarrow \mathbb{R}$ carved with Chebychev norm. We now prove that the continuous functions K, Q, V, F, H, G, U, P and W satisfy the Lipschitz condition when

$$\sup_{0 < t \leq Y} \left\| \frac{I_{HM}}{N_H} \right\| \leq \Theta_1, \quad \sup_{0 < t \leq Y} \left\| \frac{I_{HC}}{N_H} \right\| \leq \Theta_2, \quad \sup_{0 < t \leq Y} \left\| \frac{I_{MC}}{N_H} \right\| \leq \Theta_3, \quad \sup_{0 < t \leq Y} \left\| \frac{I_{VM}}{N_H} \right\| \leq \Theta_4.$$

Thus, firstly we have

$$\begin{aligned}
 \|K(S_{H1}) - K(S_{H2})\| &= \left\| \Lambda_H - \left(\frac{\beta_{VM} I_{VM}}{N_H} + \frac{\beta_{HC} (I_{HC} + I_{MC})}{N_H} + \varrho_H + \mu_{HC} - \eta_{HM} R_{HM} - \eta_{HC} R_{HC} \right) S_{H1} \right. \\
 &\quad \left. - \left(\Lambda_H - \left(\frac{\beta_{VM} I_{VM}}{N_H} + \frac{\beta_{HC} (I_{HC} + I_{MC})}{N_H} + \varrho_H + \mu_{HC} - \eta_{HM} R_{HM} - \eta_{HC} R_{HC} \right) S_{H2} \right) \right\| \\
 &= \left\| -\frac{\beta_{VM} I_{VM}}{N_H} (S_{H1} - S_{H2}) - \frac{\beta_{HC} I_{HC}}{N_H} (S_{H1} - S_{H2}) - \frac{\beta_{HC} I_{MC}}{N_H} (S_{H1} - S_{H2}) - \varrho_H (S_{H1} - S_{H2}) \right. \\
 &\quad \left. - \mu_{HC} (S_{H1} - S_{H2}) + \eta_{HM} R_{HM} (S_{H1} - S_{H2}) + \eta_{HC} R_{HC} (S_{H1} - S_{H2}) \right\| \\
 &\leq \beta_{VM} \sup_{0 \leq t \leq Y} \left\| \frac{I_{VM}}{N_H} \right\| \|S_{H1} - S_{H2}\| + \beta_{HC} \sup_{0 \leq t \leq Y} \left\| \frac{I_{HC}}{N_H} \right\| \|S_{H1} - S_{H2}\| \\
 &\quad + \beta_{HC} \sup_{0 \leq t \leq Y} \left\| \frac{I_{MC}}{N_H} \right\| \|S_{H1} - S_{H2}\| + \varrho_H \|S_{H1} - S_{H2}\| + \mu_{HC} \|S_{H1} - S_{H2}\| \\
 &\quad + \eta_{HM} R_{HM} \|S_{H1} - S_{H2}\| + \eta_{HC} R_{HC} \|S_{H1} - S_{H2}\| \\
 &\leq L_K \|S_{H1} - S_{H2}\|, \tag{18}
 \end{aligned}$$

where

$$L_K = \beta_{VM} \Theta_4 + \beta_{HC} \Theta_2 + \beta_{HC} \Theta_3 + \varrho_H + \mu_{HC} + \eta_{HM} R_{HM} + \eta_{HC} R_{HC} > 0.$$

Secondly,

$$\|Q(V_{HC1}) - Q(V_{HC2})\| = \left\| \mu_{HC} S_H - \left(\frac{\beta_{HC} I_{HC}}{N_H} + \frac{\chi_{HC} I_{MC}}{N_H} - \varrho_H - \frac{\beta_{VM} I_{VM}}{N_H} \right) V_{HC1} \right\|$$

$$\begin{aligned}
 & - \left(\mu_{\text{HC}} S_{\text{H}} - \left(\frac{\beta_{\text{HC}} I_{\text{HC}}}{N_{\text{H}}} + \frac{\chi_{\text{HC}} I_{\text{MC}}}{N_{\text{H}}} - \varrho_{\text{H}} - \frac{\beta_{\text{VM}} I_{\text{VM}}}{N_{\text{H}}} \right) V_{\text{HC}2} \right) \Big\| \tag{19} \\
 & = - \left(\frac{\beta_{\text{HC}} I_{\text{HC}}}{N_{\text{H}}} + \frac{\chi_{\text{HC}} I_{\text{MC}}}{N_{\text{H}}} - \varrho_{\text{H}} - \frac{\beta_{\text{VM}} I_{\text{VM}}}{N_{\text{H}}} \right) \|V_{\text{HC}1} - V_{\text{HC}2}\| \\
 & \leq \left(\beta_{\text{HC}} \sup_{0 \leq t \leq Y} \left\| \frac{I_{\text{HC}}}{N_{\text{H}}} \right\| + \chi_{\text{HC}} \sup_{0 \leq t \leq Y} \left\| \frac{I_{\text{MC}}}{N_{\text{H}}} \right\| + \beta_{\text{VM}} \sup_{0 \leq t \leq Y} \left\| \frac{I_{\text{VM}}}{N_{\text{H}}} \right\| + \varrho_{\text{H}} \right) \|V_{\text{HC}1} - V_{\text{HC}2}\| \\
 & \leq L_{\text{Q}} \|V_{\text{HC}1} - V_{\text{HC}2}\|,
 \end{aligned}$$

where

$$L_{\text{Q}} = \beta_{\text{HC}} \Theta_2 + \chi_{\text{HC}} \Theta_3 + \beta_{\text{VM}} \Theta_4 + \varrho_{\text{H}} > 0.$$

Applying a similar approach gives the following

$$\begin{aligned}
 \|V(I_{\text{HM}1}) - V(I_{\text{HM}2})\| & = \left\| \frac{\beta_{\text{VM}} I_{\text{VM}} S_{\text{H}}}{N_{\text{H}}} + \frac{\beta_{\text{VM}} I_{\text{VM}} V_{\text{HC}}}{N_{\text{H}}} + \frac{\beta_{\text{VM}} I_{\text{VM}} R_{\text{HC}}}{N_{\text{H}}} - \left(\alpha_{\text{HM}} + \varrho_{\text{H}} + \varphi_{\text{HM}} + \frac{\vartheta_1 B_{\text{HC}} I_{\text{HC}}}{N_{\text{H}}} + \frac{\vartheta_1 I_{\text{MC}}}{N_{\text{H}}} - \alpha_{\text{HM}} \right) I_{\text{HM}1} \right\| \\
 & - \left\| \frac{\beta_{\text{VM}} I_{\text{VM}} S_{\text{H}}}{N_{\text{H}}} + \frac{\beta_{\text{VM}} I_{\text{VM}} V_{\text{HC}}}{N_{\text{H}}} + \frac{\beta_{\text{VM}} I_{\text{VM}} R_{\text{HC}}}{N_{\text{H}}} - \left(\alpha_{\text{HM}} + \varrho_{\text{H}} + \varphi_{\text{HM}} + \frac{\vartheta_1 B_{\text{HC}} I_{\text{HC}}}{N_{\text{H}}} + \frac{\vartheta_1 I_{\text{MC}}}{N_{\text{H}}} - \alpha_{\text{HM}} \right) I_{\text{HM}2} \right\| \\
 & = \left(\alpha_{\text{HM}} + \varrho_{\text{H}} + \varphi_{\text{HM}} + \left(\frac{\vartheta_1 B_{\text{HC}} I_{\text{HC}}}{N_{\text{H}}} + \frac{\vartheta_1 I_{\text{MC}}}{N_{\text{H}}} \right) \right) \|I_{\text{HM}1} - I_{\text{HM}2}\| \\
 & \leq L_{\text{V}} \|I_{\text{HM}1} - I_{\text{HM}2}\|, \tag{20}
 \end{aligned}$$

where

$$L_{\text{V}} = \vartheta_1 B_{\text{HC}} \Theta_2 + \vartheta_1 \Theta_3 + \alpha_{\text{HM}} + \varrho_{\text{H}} + \varphi_{\text{HM}} > 0.$$

$$\begin{aligned}
 \|F(R_{\text{HM}1}) - F(R_{\text{HM}2})\| & = \left\| \alpha_{\text{HM}} I_{\text{HM}} - \varrho_{\text{H}} - \eta_{\text{HM}} - \left(\frac{\beta_{\text{HC}} I_{\text{HC}}}{N_{\text{H}}} - \frac{\beta_{\text{HC}} I_{\text{MC}}}{N_{\text{H}}} \right) R_{\text{HM}1} \right. \\
 & - \left. \left(\alpha_{\text{HM}} I_{\text{HM}} - \varrho_{\text{H}} - \eta_{\text{HM}} - \left(\frac{\beta_{\text{HC}} I_{\text{HC}}}{N_{\text{H}}} - \frac{\beta_{\text{HC}} I_{\text{MC}}}{N_{\text{H}}} \right) R_{\text{HM}2} \right) \right\| \\
 & \leq L_{\text{F}} \|R_{\text{HM}1} - R_{\text{HM}2}\|, \tag{21}
 \end{aligned}$$

where

$$L_{\text{F}} = \beta_{\text{HC}} \Theta_2 + \beta_{\text{HC}} \Theta_3 > 0.$$

$$\begin{aligned}
 \|H(I_{\text{HC}1}) - H(I_{\text{HC}2})\| & = \left\| \left(\frac{\beta_{\text{HC}} S_{\text{H}}}{N_{\text{H}}} + \frac{\beta_{\text{HC}} I_{\text{MC}} S_{\text{H}}}{N_{\text{H}}} + \frac{\beta_{\text{HC}} V_{\text{HC}}}{N_{\text{H}}} + \frac{\beta_{\text{HC}} I_{\text{MC}} V_{\text{HC}}}{N_{\text{H}}} - \frac{\beta_{\text{HC}} \chi_{\text{HC}} V_{\text{HC}}}{N_{\text{H}}} - \frac{\beta_{\text{HC}} I_{\text{MC}} \chi_{\text{HC}} V_{\text{HC}}}{N_{\text{H}}} \right. \right. \\
 & + \left. \frac{\beta_{\text{HC}} R_{\text{HC}}}{N_{\text{H}}} + \frac{\beta_{\text{HC}} I_{\text{MC}} R_{\text{HC}}}{N_{\text{H}}} - \alpha_{\text{HC}} - \varrho_{\text{H}} + \varphi_{\text{HC}} - \frac{\vartheta_2 \beta_{\text{VM}} I_{\text{VM}}}{N_{\text{H}}} + \alpha_{\text{HM}} I_{\text{MC}} \right) I_{\text{HC}1} \\
 & - \left(\frac{\beta_{\text{HC}} S_{\text{H}}}{N_{\text{H}}} + \frac{\beta_{\text{HC}} I_{\text{MC}} S_{\text{H}}}{N_{\text{H}}} + \frac{\beta_{\text{HC}} V_{\text{HC}}}{N_{\text{H}}} + \frac{\beta_{\text{HC}} I_{\text{MC}} V_{\text{HC}}}{N_{\text{H}}} - \frac{\beta_{\text{HC}} \chi_{\text{HC}} V_{\text{HC}}}{N_{\text{H}}} - \frac{\beta_{\text{HC}} I_{\text{MC}} \chi_{\text{HC}} V_{\text{HC}}}{N_{\text{H}}} \right. \\
 & + \left. \frac{\beta_{\text{HC}} R_{\text{HC}}}{N_{\text{H}}} + \frac{\beta_{\text{HC}} I_{\text{MC}} R_{\text{HC}}}{N_{\text{H}}} - \alpha_{\text{HC}} - \varrho_{\text{H}} + \varphi_{\text{HC}} - \frac{\vartheta_2 \beta_{\text{VM}} I_{\text{VM}}}{N_{\text{H}}} + \alpha_{\text{HM}} I_{\text{MC}} \right) I_{\text{HC}2} \Big\| \\
 & \leq L_{\text{H}} \|I_{\text{HC}1} - I_{\text{HC}2}\|, \tag{22}
 \end{aligned}$$

where

$$L_H = \beta_{HC}\chi_{HC}\Theta_1 + \beta_{HC}\chi_{HC}\Theta_2 + \vartheta_2\beta_{VM}\Theta_4 + \alpha_{HC} + \varrho_H > 0.$$

$$\begin{aligned} \|G(R_{HC1}) - G(R_{HC2})\| &= \left\| \left(\alpha_{HC}I_{HC} - \varrho_H - \eta_{HC} - \frac{\beta_{VM}I_{VM}}{N_H} \right) R_{HC1} \right. \\ &\quad \left. - \left(\alpha_{HC}I_{HC} - \varrho_H - \eta_{HC} - \frac{\beta_{VM}I_{VM}}{N_H} \right) R_{HC2} \right\| \\ &\leq L_G \|R_{HC1} - R_{HC2}\|, \end{aligned} \tag{23}$$

where

$$L_G = \beta_{VM}\Theta_4 + \varrho_H + \eta_{HC} > 0.$$

$$\begin{aligned} \|U(I_{MC1}) - U(I_{MC2})\| &= \left\| \left(\frac{\vartheta_1\beta_{HC}I_{HC}\mathcal{I}_{HM}}{N_H} + \frac{\vartheta_1\beta_{HC}I_{HM}}{N_H} + \frac{\vartheta_2\beta_{VM}I_{VM}I_{HM}}{N_H} - \varrho_H - \varphi_M - \varphi_C - \alpha_{HM} - \alpha_{HC} \right) I_{MC1} \right. \\ &\quad \left. - \left(\frac{\vartheta_1\beta_{HC}I_{HC}\mathcal{I}_{HM}}{N_H} + \frac{\vartheta_1\beta_{HC}I_{HM}}{N_H} + \frac{\vartheta_2\beta_{VM}I_{VM}I_{HM}}{N_H} - \varrho_H - \varphi_M - \varphi_C - \alpha_{HM} - \alpha_{HC} \right) I_{MC2} \right\| \\ &\leq L_U \|I_{MC1} - I_{MC2}\|, \end{aligned} \tag{24}$$

where

$$L_U = \varrho_H + \varphi_M + \varphi_C + \alpha_{HM} + \alpha_{HC} > 0.$$

$$\begin{aligned} \|P(S_{V1}) - P(S_{V2})\| &= \left\| \left(\Lambda_M - \frac{\beta_{HM}I_{HM}}{N_H} - \frac{\beta_{HM}I_{MC}}{N_H} - \varrho_V \right) S_{V1} - \left(\Lambda_M - \frac{\beta_{HM}I_{HM}}{N_H} - \frac{\beta_{HM}I_{MC}}{N_H} - \varrho_V \right) S_{V2} \right\| \\ &\leq L_P \|S_{V1} - S_{V2}\|, \end{aligned} \tag{25}$$

where

$$L_P = \beta_{HM}\Theta_1 + \beta_{HM}\Theta_2 + \varrho_V > 0.$$

$$\begin{aligned} \|W(I_{VM1}) - W(I_{VM2})\| &= \left\| \left(\frac{\beta_{HM}I_{HM}S_{VM}}{N_H} + \frac{\beta_{HM}I_{MC}S_{VM}}{N_H} - \varrho_V I_{VM} \right) I_{VM1} - \left(\frac{\beta_{HM}I_{HM}S_{VM}}{N_H} + \frac{\beta_{HM}I_{MC}S_{VM}}{N_H} - \varrho_V I_{VM} \right) I_{VM2} \right\| \\ &\leq L_W \|I_{VM1} - I_{VM2}\|, \end{aligned} \tag{26}$$

where

$$L_W = \varrho_V > 0.$$

Theorem 3 Suppose $(L_K, L_Q, L_V, L_F, L_H, L_G, L_U, L_P, L_W) \frac{\Gamma(1-\omega)\sin(\pi\omega)Y^\omega}{\omega\pi} < 1$, we then say that the fractional model has a unique solution on the interval $[0, b]$, letting $(K, Q, V, F, H, G, U, P, W) : [0, b] \times$

$\mathbb{R} \rightarrow \mathbb{R}$ be continuous and satisfying the Lipschitz condition.

Proof We can see the proof in the work of [67–69].

Furthermore, we look at the existence of solutions of the fractional model using Schaefer’s fixed point theorem.

Theorem 4 Suppose that $(K, Q, V, F, H, G, U, P, W) : [0, b] \times \mathbb{R} \rightarrow \mathbb{R}$ are continuous and that there exists constants $(L_{K1}, L_{Q1}, L_{V1}, L_{F1}, L_{H1}, L_{G1}, L_{U1}, L_{P1}, L_{W1}) > 0$ such that

$$\|K(t, S_H)\| \leq L_{K1} (g + \|S_H\|), \quad \|Q(t, V_{HC})\| \leq L_{Q1} (g + \|V_{HC}\|), \quad \|V(t, I_{HM})\| \leq L_{V1} (g + \|I_{HM}\|),$$

$$\|F(t, R_{HM})\| \leq L_{F1} (g + \|R_{HM}\|), \quad \|H(t, I_{HC})\| \leq L_{H1} (g + \|I_{HC}\|), \quad \|G(t, R_{HC})\| \leq L_{G1} (g + \|R_{HC}\|),$$

$$\|U(t, I_{MC})\| \leq L_{U1} (g + \|I_{MC}\|), \quad \|P(t, S_V)\| \leq L_{P1} (g + \|S_V\|), \quad \|W(t, I_{VM})\| \leq L_{W1} (g + \|I_{VM}\|),$$

where $0 < g \leq 1$ is an arbitrary number, then the system has at least one solution.

Proof The proof of this result is similar to the approach used in ([67–69], and therefore omitted.

Generalized Ulam-Hyers-Rassias stability

This particular stability for fractional systems has been studied in a few literature. In this section we will adopt a similar approach in [70] to show that our fractional model is generalized Ulam-Hyers-Rassias (UHR) stable. Following [70], we have the definition below.

Definition 6 The fractional model above is generalized UHR stable with respect to $\Omega(t) \in \mathbb{H}^1([0, b], \mathbb{R})$ if there exists a real value $\kappa_\psi > 0$ such that $\epsilon > 0$ and for every solution $(S_H, V_{HM}, I_{HM}, R_{HM}, I_{HC}, R_{HC}, I_{MC}, S_V, I_{VM}) \in \mathbb{H}^1([0, b], \mathbb{R})$ of the following inequalities

$$\left| D_t^\psi S_H(t) - K(t, S_H) \right| \leq \Omega(t), \quad \left| D_t^\psi V_{HM} - Q(t, V_{HM}) \right| \leq \Omega(t), \quad \left| D_t^\psi I_{HM} - V(t, I_{HM}) \right| \leq \Omega(t),$$

$$\left| D_t^\psi R_{HM}(t) - F(t, R_{HM}(t)) \right| \leq \Omega(t), \quad \left| D_t^\psi I_{HC}(t) - H(t, I_{HC}(t)) \right| \leq \Omega(t), \quad \left| D_t^\psi R_{HC}(t) - G(t, R_{HC}(t)) \right| \leq \Omega(t),$$

$$\left| D_t^\psi I_{MC}(t) - U(t, I_{MC}(t)) \right| \leq \Omega(t), \quad \left| D_t^\psi S_V(t) - P(t, S_V(t)) \right| \leq \Omega(t),$$

$$\left| D_t^\psi I_{VM}(t) - W(t, I_{VM}(t)) \right| \leq \Omega(t), \quad \left| D_t^\psi S_V(t) - P(t, S_V(t)) \right| \leq \Omega(t),$$

there exists a solution $(\bar{S}_H, \bar{V}_{HM}, \bar{I}_{HM}, \bar{R}_{HM}, \bar{I}_{HC}, \bar{R}_{HC}, \bar{I}_{MC}, \bar{S}_V, \bar{I}_{VM}) \in \mathbb{H}^1([0, b], \mathbb{R})$ of the fractional model with

$$|S_H(t) - \bar{S}_H| \leq \kappa_\psi \Omega(t), \quad |V_{HM} - \bar{V}_{HM}| \leq \kappa_\psi \Omega(t), \quad |I_{HM} - \bar{I}_{HM}| \leq \kappa_\psi \Omega(t), \quad |R_{HM}(t) - \bar{R}_{HM}(t)| \leq \kappa_\psi \Omega(t),$$

$$|I_{HC}(t) - \bar{I}_{HC}(t)| \leq \kappa_\psi \Omega(t), \quad |R_{HC}(t) - \bar{R}_{HC}(t)| \leq \kappa_\psi \Omega(t), \quad |I_{MC}(t) - \bar{I}_{MC}(t)| \leq \kappa_\psi \Omega(t),$$

$$|S_v(t) - \bar{S}_v(t)| \leq \kappa_\psi \Omega(t), \quad |I_{VM}(t) - \bar{I}_{VM}(t)| \leq \kappa_\psi \Omega(t).$$

Theorem 5 *The fractional model is generalized Ulam-Hyers-Rassias stable with respect to $\Omega \in \mathbb{H}^1([0, b], \mathbb{R})$ if*

$$(L_K, L_Q, L_V, L_F, L_H, L_G, L_U, L_P, L_W) T^\psi < 1.$$

Proof From [Definition 6](#), let Ω denote the non-decreasing function of t , then there exists $\epsilon > 0$ such that

$$\int_0^t (t - \tau)^{\psi-1} \Omega(\tau) d\tau \leq \epsilon \Omega(t),$$

for every $t \in [0, b]$. The functions $K, Q, V, F, H, G, U, P, W$ have been shown to be continuous and

$$(L_K, L_Q, L_V, L_F, L_H, L_G, L_U, L_P, L_W) > 0,$$

satisfies the Lipschitz condition as shown in the previous section. From [Theorem 3](#), the fractional model has the unique solution

$$\bar{S}_h = S_h(0) + \frac{1}{\Gamma(\psi)} \int_0^t (t - \tau)^{\psi-1} K(\tau, \bar{S}_h(\tau)) d\tau.$$

Integrating the inequalities in [Definition 6](#) we get

$$\begin{aligned} \left| S_h - S_h(0) - \frac{1}{\Gamma(\psi)} \int_0^t (t - \tau)^{\psi-1} K(\tau, S_h(\tau)) d\tau \right| &\leq \frac{1}{\Gamma(\psi)} \int_0^t (t - \tau)^{\psi-1} \Omega(\tau) d\tau \\ &\leq \frac{\epsilon \Omega(t) \Gamma(1 - \psi) \sin(\pi\psi)}{\pi}. \end{aligned} \quad (27)$$

Using [\(27\)](#) and the Lemma we get

$$\begin{aligned} |S_h - \bar{S}_h| &\leq \left| S_h - \left(S_h(0) + \frac{1}{\Gamma(\psi)} \int_0^t (t - \tau)^{\psi-1} K(\tau, \bar{S}_h(\tau)) d\tau \right) \right| \\ &\leq \left| S_h - S_h(0) - \left(\frac{1}{\Gamma(\psi)} \int_0^t (t - \tau)^{\psi-1} K(\tau, \bar{S}_h(\tau)) d\tau + \frac{1}{\Gamma(\psi)} \int_0^t (t - \tau)^{\psi-1} K(\tau, S_h(\tau)) d\tau \right. \right. \\ &\quad \left. \left. - \frac{1}{\Gamma(\psi)} \int_0^t (t - \tau)^{\psi-1} K(\tau, S_h(\tau)) d\tau \right) \right| \\ &\leq \left| S_h - S_h(0) - \frac{1}{\Gamma(\psi)} \int_0^t (t - \tau)^{\psi-1} K(\tau, S_h(\tau)) d\tau \right| \\ &\quad + \frac{1}{\Gamma(\psi)} \int_0^t (t - \tau)^{\psi-1} |K(\tau, S_h(\tau)) - K(\tau, \bar{S}_h(\tau))| d\tau \\ &\leq \frac{\epsilon \Omega(t) \Gamma(1 - \psi) \sin(\pi\psi)}{\pi} + \frac{L_K \Gamma(1 - \psi) \sin(\pi\psi)}{\pi} \int_0^t (t - \tau)^{\psi-1} |S_h(\tau) - \bar{S}_h(\tau)| d\tau \\ &\leq \frac{\epsilon \Omega(t) \Gamma(1 - \psi) \sin(\pi\psi)}{\pi} E_\psi \left(L_{KT}^\psi \right). \end{aligned}$$

By setting $\kappa_\psi = \frac{\epsilon\Gamma(1-\psi)\sin(\pi\psi)}{\pi} E_\psi \left(L_{\text{KT}}^\psi \right)$, we have

$$|S_H - \bar{S}_H| \leq \kappa_\psi \Omega(t), \quad t \in [0, b].$$

Applying the similar approach we get

$$|V_{\text{HM}} - \bar{V}_{\text{HM}}| \leq \kappa_\psi \Omega(t), \quad |I_{\text{HM}} - \bar{I}_{\text{HM}}| \leq \kappa_\psi \Omega(t),$$

$$|R_{\text{HM}}(t) - \bar{R}_{\text{HM}}(t)| \leq \kappa_\psi \Omega(t), \quad |I_{\text{HC}}(t) - \bar{I}_{\text{HC}}(t)| \leq \kappa_\psi \Omega(t),$$

$$|R_{\text{HC}}(t) - \bar{R}_{\text{HC}}(t)| \leq \kappa_\psi \Omega(t), \quad |I_{\text{MC}}(t) - \bar{I}_{\text{MC}}(t)| \leq \kappa_\psi \Omega(t),$$

$$|S_v(t) - \bar{S}_v(t)| \leq \kappa_\psi \Omega(t), \quad |I_{\text{VM}}(t) - \bar{I}_{\text{VM}}(t)| \leq \kappa_\psi \Omega(t),$$

for every $t \in [0, b]$. Hence, we conclude that the fractional model is generalized Ulam-Hyers-Rassias stable with respect to $\Omega(t)$.

4 Numerical scheme and simulations

We carried out some numerical simulations to further explain the analytical results we presented earlier. Most of our parameters are obtained from previous works of renowned authors who have done similar works like this. However, there are few cases where certain parameters are unavailable in the literature, such cases gave us room to assume relevant values for the sake of this study.

The fractional predictor-corrector method was used in carrying out numerical simulations and the numerical scheme was derived using the Adams-Bashforth linear multi-step method in the Caputo sense, taking into consideration the convergence of the numerical method. The model is simulated using parameters provided based on dynamical data relevant to COVID-19 and Malaria co-infection in Nigeria. The total human population of Nigeria is estimated to be 206,139,587 as of 2020 and its life expectancy is estimated at 54.69 years according to WHO, hence the natural death rate ϱ_H is set at $\frac{1}{54.69 \times 365}$ per day and the recruitment rate Λ_H set at $\frac{206,139,597}{54.69 \times 365}$ per day. Under normal biological interpretation, we let all parameters used to be non-negative and considered the following initial conditions; we assume that the total susceptible population is $S_H(0) = 200,000,000$ and the total human population vaccinated against COVID-19, $V_{\text{HC}}(0) = 8,000,000$. Hence we set $I_{\text{HM}}(0) = 700,000$, $R_{\text{HM}}(0) = 100,000$, $I_{\text{HC}}(0) = 77,239$, $R_{\text{HC}}(0) = 72,350$, $I_{\text{MC}}(0) = 200,000$. We also assume susceptible vector population $S_v(0) = 50,000$, $I_{\text{VM}}(0) = 40,000$. It is important to state that very scanty data is available in the literature on the co-infection of COVID-19 and Malaria as of October 2021.

Let the uniform grid points be $t_k = kh$, where $k = 0, 1, 2, \dots, m$ with some integer m and the grid step size $h = T/m$. Then by piece-wise interpolation with nodes and knots taken at t_j , $j = 0, 1, 2, \dots, k+1$, Eq. (17) becomes the fractional variant of the one-step Adam-Moulton method (Corrector formula);

$$\begin{aligned}
S_H(t_{k+1}) - S_H(0) &= \frac{h^\omega}{\Gamma(\omega + 2)} \left(\sum_{j=0}^k u_{j,k+1} K(t_j, S_H(t_j)) + K(t_{k+1}, S_H^p(t_{k+1})) \right), \\
V_{HC}(t_{k+1}) - V_{HC}(0) &= \frac{h^\omega}{\Gamma(\omega + 2)} \left(\sum_{j=0}^k u_{j,k+1} Q(t_j, V_{HC}(t_j)) + Q(t_{k+1}, V_{HC}^p(t_{k+1})) \right), \\
I_{HM}(t_{k+1}) - I_{HM}(0) &= \frac{h^\omega}{\Gamma(\omega + 2)} \left(\sum_{j=0}^k u_{j,k+1} V(t_j, I_{HM}(t_j)) + H(t_{k+1}, I_{HM}^p(t_{k+1})) \right), \\
R_{HM}(t_{k+1}) - R_{HM}(0) &= \frac{h^\omega}{\Gamma(\omega + 2)} \left(\sum_{j=0}^k u_{j,k+1} F(t_j, R_{HM}(t_j)) + K(t_{k+1}, R_{HM}^p(t_{k+1})) \right), \\
I_{HC}(t_{k+1}) - I_{HC}(0) &= \frac{h^\omega}{\Gamma(\omega + 2)} \left(\sum_{j=0}^k u_{j,k+1} H(t_j, I_{HC}(t_j)) + Q(t_{k+1}, I_{HC}^p(t_{k+1})) \right), \\
R_{HC}(t_{k+1}) - R_{HC}(0) &= \frac{h^\omega}{\Gamma(\omega + 2)} \left(\sum_{j=0}^k u_{j,k+1} G(t_j, R_{HC}(t_j)) + U(t_{k+1}, R_{HC}^p(t_{k+1})) \right), \\
I_{MC}(t_{k+1}) - I_{MC}(0) &= \frac{h^\omega}{\Gamma(\omega + 2)} \left(\sum_{j=0}^k u_{j,k+1} U(t_j, I_{MC}(t_j)) + V(t_{k+1}, I_{MC}^p(t_{k+1})) \right), \\
S_v(t_{k+1}) - S_v(0) &= \frac{h^\omega}{\Gamma(\omega + 2)} \left(\sum_{j=0}^k u_{j,k+1} P(t_j, S_v(t_j)) + W(t_{k+1}, S_v^p(t_{k+1})) \right), \\
I_{VM}(t_{k+1}) - I_{VM}(0) &= \frac{h^\omega}{\Gamma(\omega + 2)} \left(\sum_{j=0}^k u_{j,k+1} W(t_j, I_{VM}(t_j)) + V(t_{k+1}, I_{VM}^p(t_{k+1})) \right),
\end{aligned} \tag{28}$$

where the weight

$$u_{j,k+1} = \begin{cases} k^{\omega+1} - (k - \omega)(k + 1)^\omega, & j = 0, \\ (k - j + 2)^{\omega+1} + (k - j)^{\omega+1} - 2(k - j + 1)^{\omega+1}, & 1 \leq j \leq k, \\ 1, & j = k + 1. \end{cases}$$

From the one-step Adams-Bashforth method, the predictor formula is presented as

$$\begin{aligned}
S_H^p(t_{k+1}) - S_H(0) &= \frac{1}{\Gamma(\omega)} \sum_{j=0}^k v_{j,k+1} K(t_j, S_H(t_j)), \\
V_{HC}^p(t_{k+1}) - V_{HC}(0) &= \frac{1}{\Gamma(\omega)} \sum_{j=0}^k v_{j,k+1} Q(t_j, V_{HC}(t_j)), \\
I_{HM}^p(t_{k+1}) - I_{HM}(0) &= \frac{1}{\Gamma(\omega)} \sum_{j=0}^k v_{j,k+1} V(t_j, I_{HM}(t_j)),
\end{aligned}$$

$$\begin{aligned}
 R_{\text{HM}}^p(t_{k+1}) - R_{\text{HM}}(0) &= \frac{1}{\Gamma(\omega)} \sum_{j=0}^k v_{j,k+1} F(t_j, R_{\text{HM}}(t_j)), \\
 I_{\text{HC}}^p(t_{k+1}) - I_{\text{HC}}(0) &= \frac{1}{\Gamma(\omega)} \sum_{j=0}^k v_{j,k+1} H(t_j, I_{\text{HC}}(t_j)), \\
 R_{\text{HC}}^p(t_{k+1}) - R_{\text{HC}}(0) &= \frac{1}{\Gamma(\omega)} \sum_{j=0}^k v_{j,k+1} G(t_j, R_{\text{HC}}(t_j)), \\
 I_{\text{MC}}^p(t_{k+1}) - I_{\text{MC}}(0) &= \frac{1}{\Gamma(\omega)} \sum_{j=0}^k v_{j,k+1} U(t_j, I_{\text{MC}}(t_j)), \\
 S_v^p(t_{k+1}) - S_v(0) &= \frac{1}{\Gamma(\omega)} \sum_{j=0}^k v_{j,k+1} P(t_j, S_v(t_j)), \\
 I_{\text{VM}}^p(t_{k+1}) - I_{\text{VM}}(0) &= \frac{1}{\Gamma(\omega)} \sum_{j=0}^k v_{j,k+1} W(t_j, I_{\text{VM}}(t_j)),
 \end{aligned} \tag{29}$$

where the weight

$$v_{j,k+1} = \omega^{-1} h^\omega ((k-j+1)^\omega - (k-j)^\omega).$$

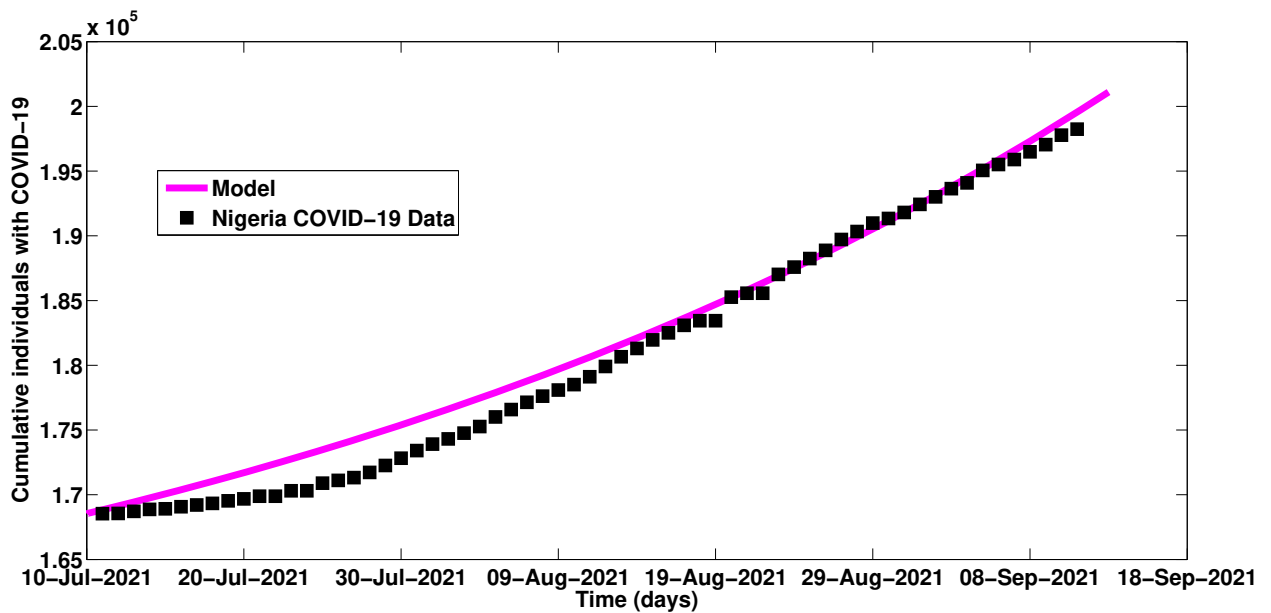


Figure 2. Fitting the cumulative number of COVID-19 reported cases

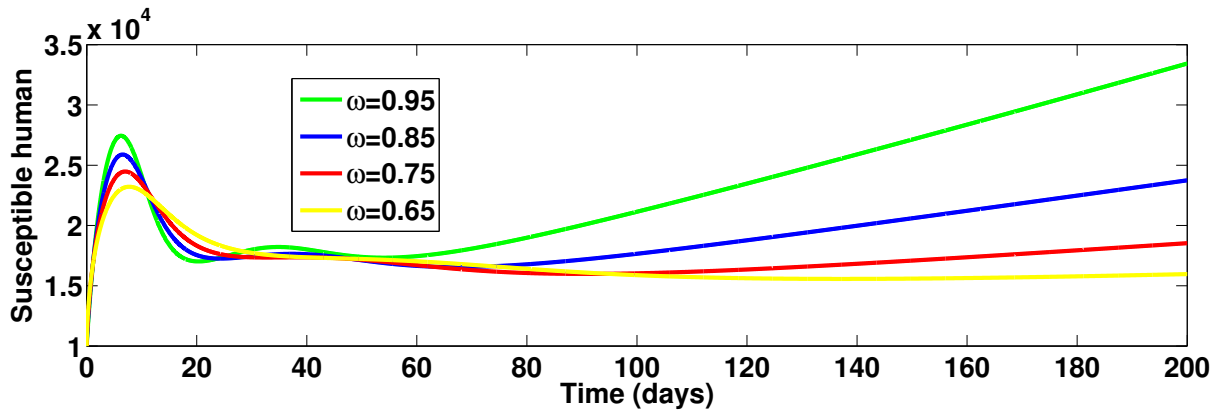


Figure 3. Simulation for susceptible human at different fractional order values

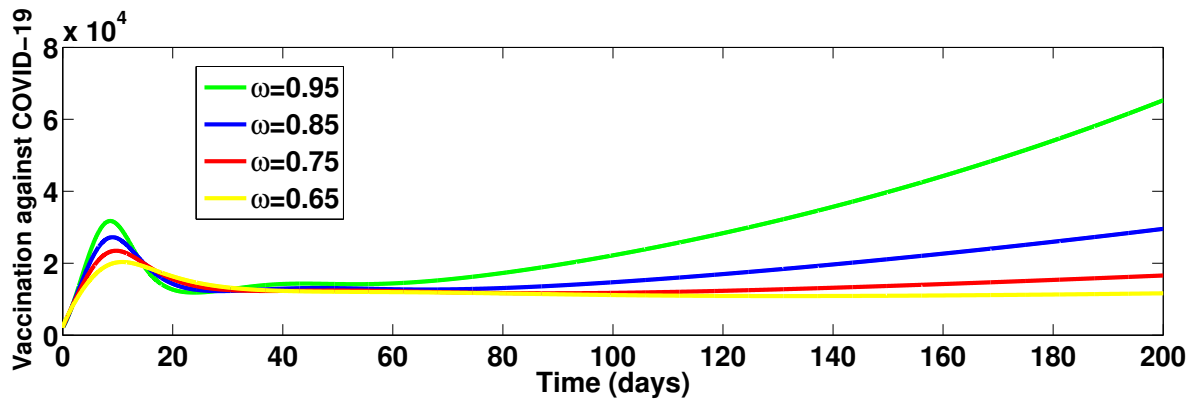


Figure 4. Simulation for vaccinated individuals against COVID-19 at different fractional order values

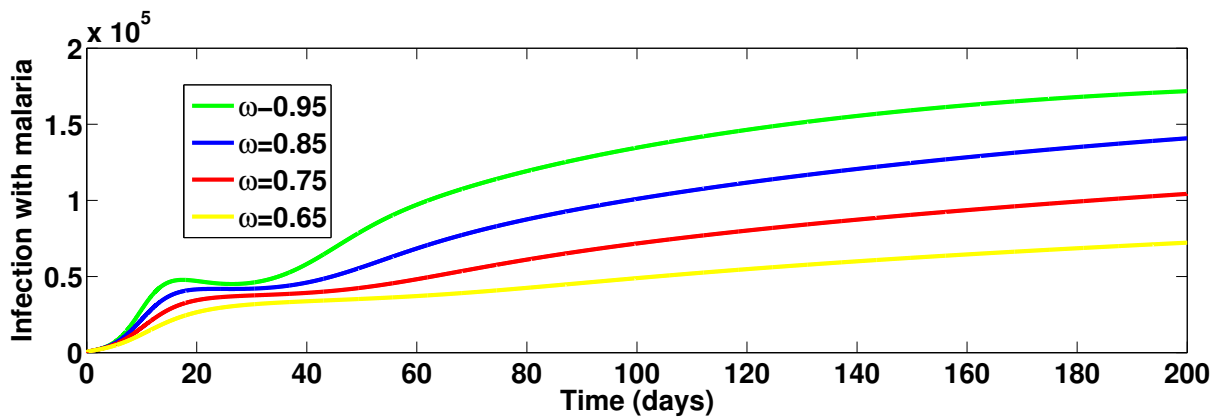


Figure 5. Simulation for individuals infected with malaria at different fractional order values

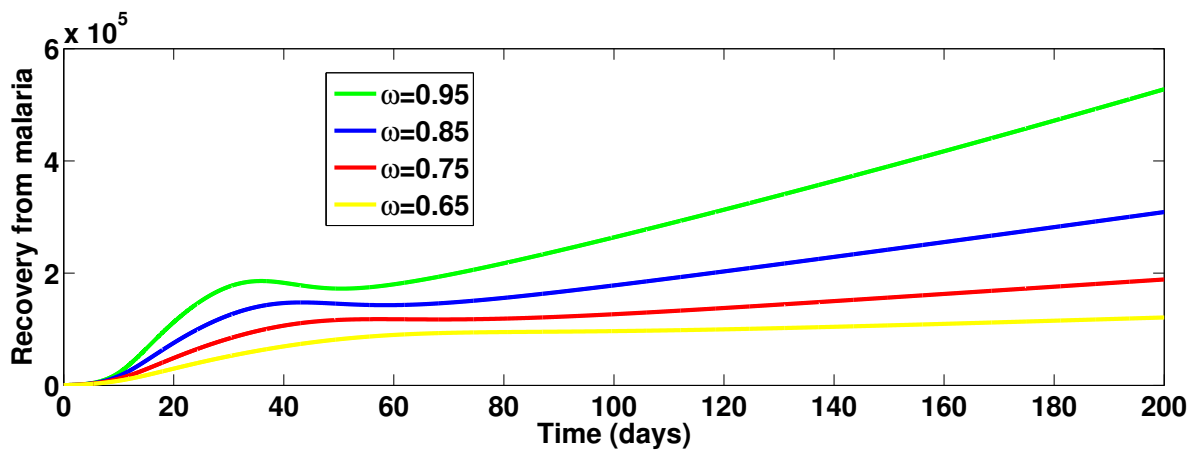


Figure 6. Simulation for individuals who recovered from malaria at different fractional order values

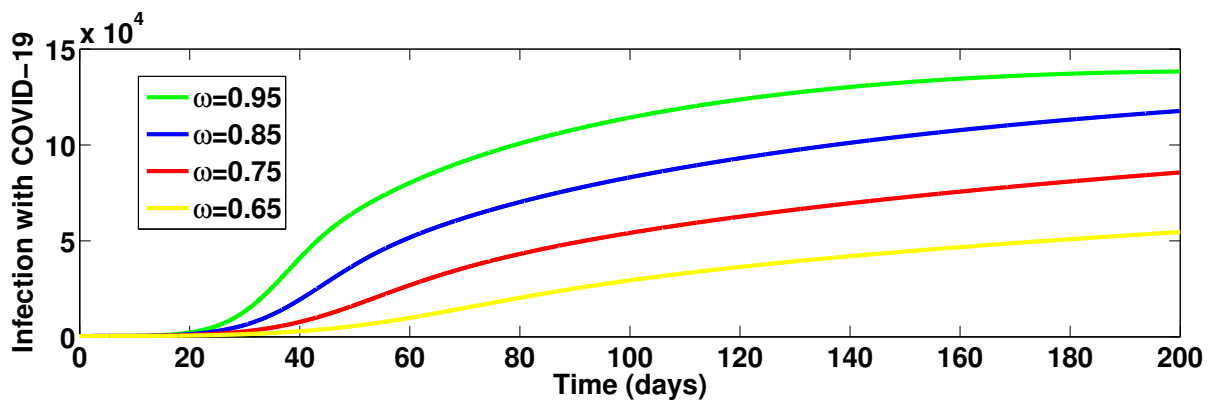


Figure 7. Simulation for individuals infected with COVID-19 at different fractional order values

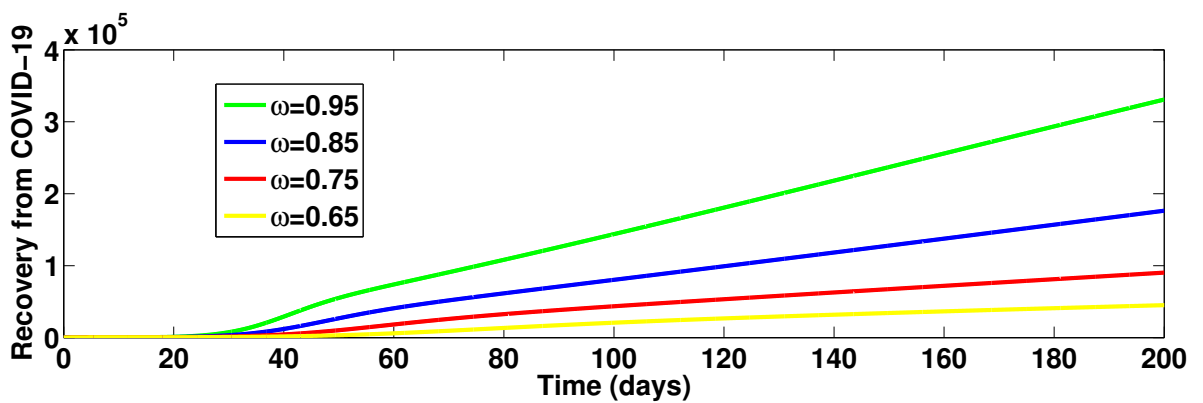


Figure 8. Simulation for individuals who recovered from COVID-19 at different fractional order values

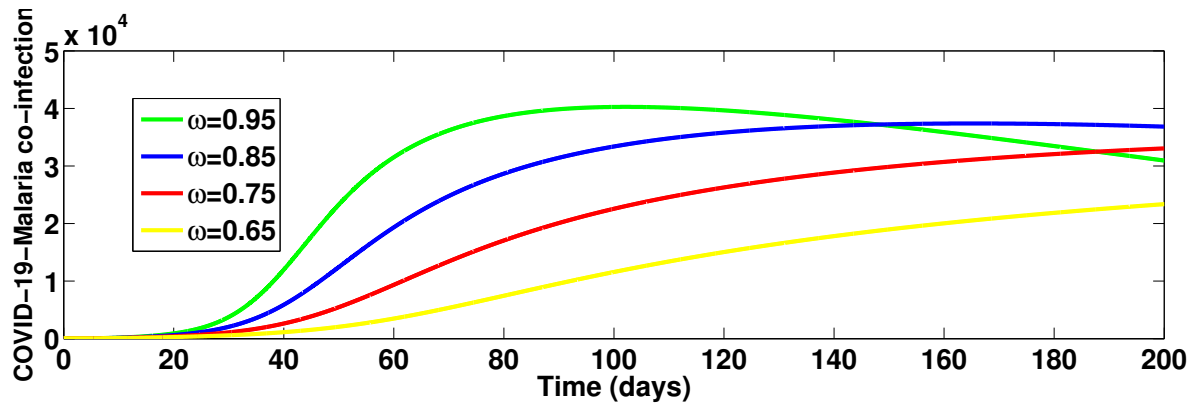


Figure 9. Simulation for individuals co-infected with COVID-19 and Malaria at different fractional order values

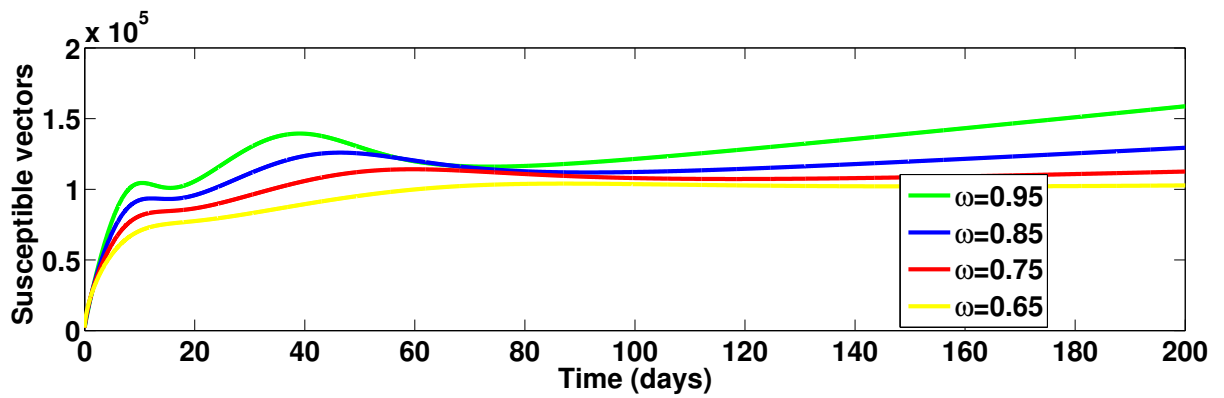


Figure 10. Simulation for susceptible vectors at different fractional order values

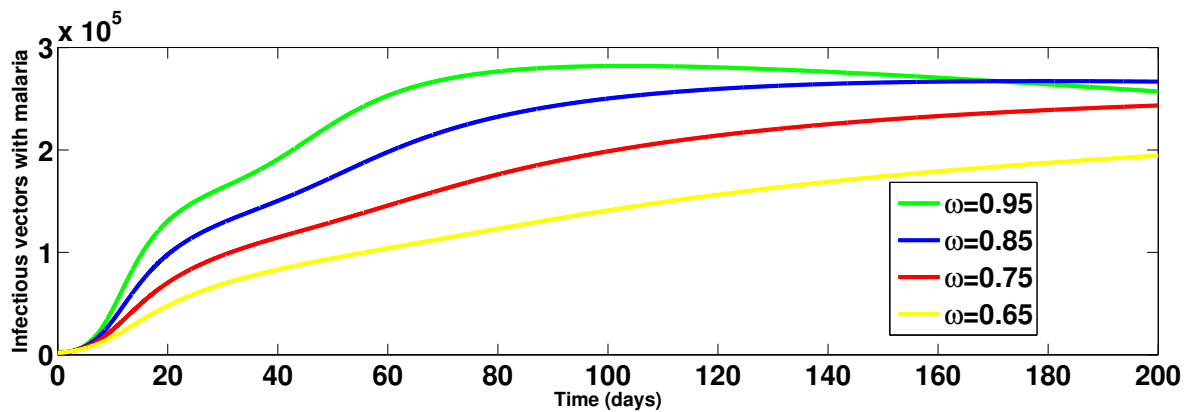


Figure 11. Simulation for infectious vectors with malaria at different fractional order values

Discussion of results

Figure 1 is the model flow diagram showing migration from one compartment to the other. Fitting of our model is presented in Figure 2 where the cumulative reported cases were used to fit the model to data from Nigeria. The figure showed that the co-infection model fits well with the Nigerian COVID-19 data for daily cumulative reported cases.

The various simulations carried out on each compartment produce distinct results of the epidemic as illustrated in the behavior of the figures. Figure 3, Figure 4, Figure 5, Figure 6, Figure 7, Figure 8, Figure 9, Figure 10 and Figure 11 are results of the compartments generated at different fractional order, $\omega = 0.95, 0.85, 0.75$ and 0.65 using parameters values from Table 1. In Figure 3, we plot the total susceptible population over time at different fractional order. It is observed that for the first 17 days, the fractional order is directly proportional to the total population; increasing the fractional order causes an increase in the susceptible population, and decreasing the fractional order reduces the population, indicating the absence of disease in the population. Between the 18th and 79th days, we experience a rapid swap in the behaviour which demonstrates the susceptibility of the human population. Figure 4 presents the simulations of individuals vaccinated against COVID-19 over time in different fractional order. It is observed that as we increase the fractional order, the number of individuals vaccinated against COVID-19 increases for the first 17 days, after which we observe a stable behaviour in the next 22 days due to the effect of vaccination on the population class. Figure 5 shows the total infectious individuals with malaria over time at different fractional order. It is observed that malaria infection causes a rapid increase in the population as fractional order increases from day one. We plot the number of individuals who have recovered from malaria over time at different fractional order in Figure 6. There is a migration from the infections class to the recovered class as shown in the population of individuals from the first day. Figure 7 presents the simulations of infectious individuals with COVID-19 over time. It is observed that fractional order has no effect on individuals with COVID-19 for the first 23 days. After 23 days, an increase in the fractional derivative order leads to an increase in the number of infectious individuals with COVID-19 and a decrease in the fractional order decreases the number of infectious individuals with COVID-19, too.

It is not until after the first 25 days that we noticed an effect due to fractional order on the number of individuals who have recovered from COVID-19 as presented in Figure 8. Accordingly, an increase in the fractional order causes an increase in the number of individuals who have recovered from COVID-19 and a decrease in the fractional directly decreases the number of individuals who have recovered from COVID-19. In Figure 9 we present the simulation of infectious individuals co-infected with malaria and COVID-19 over time in different fractional order. It is observed that the infectious population co-infected with malaria and COVID-19 is directly proportional to the fractional order after the first 24 days; an increase in the fractional order causes an increase in the co-infectious population and a decrease in population implies a decrease in the fractional order too. Figure 10 presents the simulations of susceptible vectors over time. It is observed that an increase in fractional order causes a sharp increase in the susceptible vectors and a decrease in the population of vectors implies a decrease in fractional order. In Figure 11, we plot infectious vectors with malaria over time at different fractional order. It noticed that an increase in the fractional order increases the infectious vectors with malaria and decreasing the fractional order reduces the number of infectious vectors with malaria.

Discussion of results on simulations of modification parameter on co-infection

Figure 12 presents simulations of the total co-infection class at different modification rates d_1 of 0.5, 1.0, 1.5, and 2.0 of susceptibility of malaria-infected individuals to COVID-19 over time. It has

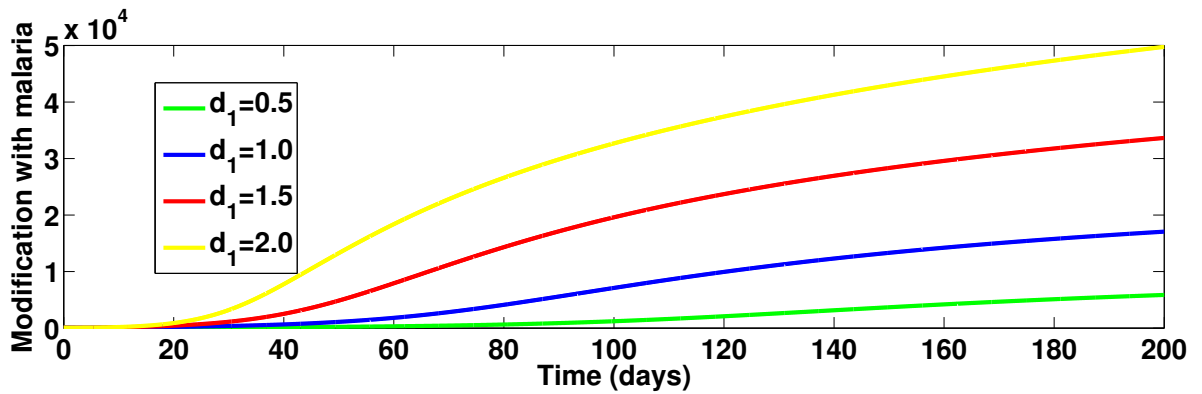


Figure 12. Modification parameter for malaria on co-infection class at different values

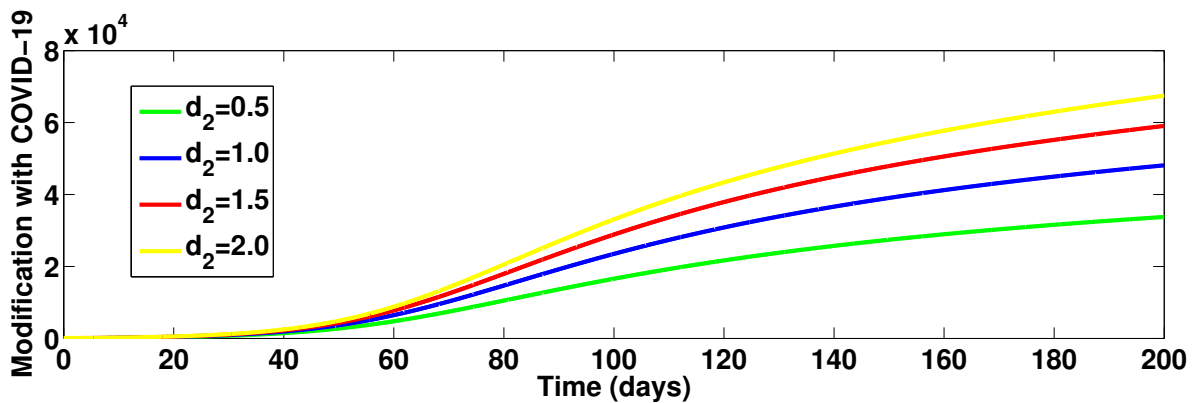


Figure 13. Modification parameter for COVID-19 on co-infection class at different values

clearly shown that, the co-infection class increases among those already infected with malaria as time increases. A clear indication that a single infection with malaria does not guarantee immunity to COVID-19. In Figure 13 we plot the simulations of the total co-infection class at different modification rates d_2 of 0.5, 1.0, 1.5, and 2.0 of susceptibility of COVID-19-infection to malaria over time. The result shows clearly that the co-infection class increases among those already infected with COVID-19. Singly infection with COVID-19 does not guarantee immunity to malaria, thereby allowing co-infection.

5 Conclusion

In this paper, we have developed a novel mathematical model for COVID-19 and Malaria and analyzed using fractional derivatives. In the results, we have shown how control measures such as vaccination and other preventive measures for either disease could help to curtail the co-infection of both diseases under an endemic scenario. The mathematical analysis of the model such as the positivity and boundedness of the equilibrium of solutions are also proven with the help of Laplace transform. We computed the basic reproduction number \mathcal{R}_0 and found that the COVID-19-malaria model is locally asymptotically stable when $\mathcal{R}_0 < 1$. The fractional model fits well to Nigeria's situation after fitting the model to data related to the dynamics of the co-infection disease in Nigeria. To further explain our earlier results, we simulated the model numerically and obtained several graphical results. Results of the simulation showed a good agreement between theoretical and numerical results; fractional order ω has effects on all the compartments over time and the co-infection class indicates that a single infection with malaria does not guarantee immunity to COVID-19 and infection with COVID-19 alone does not also guarantee immunity to malaria. A careful look at the findings in this work will give a better understanding of COVID-19 pandemic

and how it can be managed alongside malaria.

Based on our findings, there is a need for more awareness of the dangers of the widespread COVID-19 and the continual adherence to safety measures of malaria despite the COVID-19 lockdown. The use of face masks, maintaining social distance in gatherings, routine washing of hands, minimal travels, awareness programs, and timely hospitalization of infected individuals with mild and severe cases among other safety measures put in place to control the spread of COVID-19 need to be encouraged. For malaria cases, the use of insecticide-treated bed nets, protecting doors and windows with nets, clearing of stagnant water, drainages and bushes to avoid nurturing mosquitoes, and other routine malaria prevention strategies should be continued despite subsequent COVID-19 lock-down or restrictions. This step will go a long way in checking co-infection. The results obtained from the different simulations also explain more accurately, the various methods of prevention of infection from the two diseases. In future research, we recommend that researchers investigate the Hopf bifurcation of the delayed fractional-order COVID-19 model. See the papers [71–73] for more information.

Declarations

Use of AI tools

The authors declare that they have not used Artificial Intelligence (AI) tools in the creation of this article.

Data availability statement

All data generated or analyzed during this study are included in this article.

Ethical approval

The authors state that this research complies with ethical standards. This research does not involve either human participants or animals.

Consent for publication

Not applicable

Conflicts of interest

The authors declare that they have no conflict of interest.

Funding

Not applicable

Author's contributions

L.L.I.: Conceptualization, Formal Analysis, Software, Validation, Data Curation, Writing-Original Draft. A.O.: Methodology, Supervision and Editing. S.C.I.: Supervision and Review. The authors have read and agreed to the published version of the manuscript.

Acknowledgements

Not applicable

References

- [1] Cowman, A.F., Healer, J., Marapana, D. and Marsh, K. Malaria: biology and disease. *Cell*, 167(3), 610-624, (2016). [[CrossRef](#)]
- [2] Centers for Disease Control and Prevention (CDC), The History of Malaria, an Ancient Disease, (2018). <https://stacks.cdc.gov/view/cdc/135582>
- [3] Mandal, S., Sarkar, R.R. and Sinha, S. Mathematical models of Malaria-a review. *Malaria Journal*, 10, 202, (2011). [[CrossRef](#)]
- [4] World Health Organization (WHO), World Malaria Report 2015, (2015). <https://iris.who.int/handle/10665/200018>, <https://www.pmi.gov/press-release-world-malaria-report-2015-released-today>
- [5] World Health Organization (WHO), Malaria key facts, (2023). <https://www.who.int/news-room/fact-sheets/detail/malaria>
- [6] World Health Organization (WHO), Malaria, (2021). <https://www.afro.who.int/health-topics/malaria>
- [7] World Health Organization (WHO), World Malaria Report 2019, (2019). <https://www.who.int/publications/i/item/9789241565721>
- [8] Nigeria Malaria Indicator Survey (MIS) 2015, pp.96-99, (2015). <https://dhsprogram.com/pubs/pdf/mis20/mis20.pdf>
- [9] USAID, U.S. President's Malaria Initiative Nigeria Malaria Operational Plan FY 2020, (2020). <https://d1u4sg1s9ptc4z.cloudfront.net/uploads/2021/03/fy-2020-nigeria-malaria-operational-plan.pdf>
- [10] Abdu, E.M. and Mariamenatu, A.H. Biological property of novel coronavirus SARS-CoV-2 (2019-nCoV). *International Journal of Applied Sciences and Biotechnology*, 9(1), 16-22, (2021). [[CrossRef](#)]
- [11] Mohan, B.S. and Nambier, V. COVID-19: an insight into SARS-CoV-2 pandemic originated at Wuhan City in Hubei Province of China. *Infectious Diseases and Epidemiology*, 6(4), 146, (2020). [[CrossRef](#)]
- [12] Salahshoori, I., Mobaraki-Asl, N., Seyfaee, A., Mirzaei Nasirabad, N., Dehghan, Z., Faraji, M. et al. Overview of COVID-19 disease: virology, epidemiology, prevention diagnosis, treatment, and vaccines. *Biologics*, 1(1), 2-40, (2021). [[CrossRef](#)]
- [13] Adhikari, S.P., Meng, S., Wu, Y.J., Mao, Y.P., Ye, R.X., Wang, Q.Z. et al. Epidemiology, causes, clinical manifestation and diagnosis, prevention and control of coronavirus disease (COVID-19) during the early outbreak period: a scoping review. *Infectious Diseases of Poverty*, 9, 29, (2020). [[CrossRef](#)]
- [14] United States Food and Drug Administration: FDA Briefing Document. Pfizer-BioNTech COVID-19 vaccine, (2020). <https://www.fda.gov/media/144245/download>
- [15] Park, M., Cook, A.R., Lim, J.T., Sun, Y. and Dickens, B.L. A systematic review of COVID-19 epidemiology based on current evidence. *Journal of Clinical Medicine*, 9(4), 967, (2020). [[CrossRef](#)]
- [16] WHO, Corona Virus Disease 2019 (COVID-19) Situation Report-97. Surveillance, (2020). <https://www.who.int/docs/default-source/coronaviruse/situation-reports/20200426-sitrep-97-covid-19.pdf>
- [17] World Health Organization (WHO), WHO COVID-19 Dashboard, (2024). <https://data.who>

[int/dashboards/covid19/cases](https://reliefweb.int/dashboards/covid19/cases)

- [18] Reliefweb, World Malaria Report 2021, (2021). <https://reliefweb.int/report/world/world-malaria-report-2021>
- [19] Hussain, S., Madi, E.N., Khan, H., Gulzar, H., Etemad, S., Rezapour, S. et al. On the stochastic modeling of COVID-19 under the environmental white noise. *Journal of Function Spaces*, 2022, 4320865, (2022). [[CrossRef](#)]
- [20] Ahmed, K.M., Haroun, M.S.E.H., Hussien, A. and Omer, M.E.A. COVID-19 and Malaria Co-infection; same coin but different faces?. *Available at SSRN*, (2021). [[CrossRef](#)]
- [21] Boukhouima, A., Lotfi, E.M., Mahrouf, M., Rosa, S., Torres, D.F. and Yousfi, N. Stability analysis and optimal control of a fractional HIV-AIDS epidemic model with memory and general incidence rate. *The European Physical Journal Plus*, 136, 103, (2021). [[CrossRef](#)]
- [22] Traoré, B., Sangaré, B. and Traoré, S. A mathematical model of Malaria transmission with structured vector population and seasonality. *Journal of Applied Mathematics*, 2017, 6754097, (2017). [[CrossRef](#)]
- [23] Chiyaka, C., Tchuenche, J.M., Garira, W. and Dube, S. A mathematical analysis of the effects of control strategies on the transmission dynamics of malaria. *Applied Mathematics and Computation*, 195(2), 641-662, (2008). [[CrossRef](#)]
- [24] Macdonald, G. *The Epidemiology and Control of Malaria*. Oxford University Press: London, UK, (1957).
- [25] Egeonu, K.U., Omame, A. and Inyama, S.C. A co-infection model for two-strain malaria and cholera with optimal control. *International Journal of Dynamics and Control*, 9, 1612-1632, (2021). [[CrossRef](#)]
- [26] Ross, R. *The Prevention of Malaria*. John Murray: London, UK, (1911).
- [27] Tchoumi, S.Y., Diagne, M.L., Rwezaura, H. and Tchuenche, J.M. Malaria and COVID-19 co-dynamics: A mathematical model and optimal control. *Applied Mathematical Modelling*, 99, 294-327, (2021). [[CrossRef](#)]
- [28] Musa, S.S., Qureshi, S., Zhao, S., Yusuf, A., Mustapha, U.T. and He, D. Mathematical modeling of COVID-19 epidemic with effect of awareness programs. *Infectious Disease Modelling*, 6, 448-460, (2021). [[CrossRef](#)]
- [29] Daniel, D.O. Mathematical model for the transmission of COVID-19 with nonlinear forces of infection and the need for prevention measure in Nigeria. *Journal of Infectious Diseases and Epidemiology*, 6(5), 158, (2020). [[CrossRef](#)]
- [30] Omame, A., Nnanna, C.U. and Inyama, S.C. Optimal control and cost-effectiveness analysis of an HPV-Chlamydia trachomatis co-infection model. *Acta Biotheoretica*, 69, 185-223, (2021). [[CrossRef](#)]
- [31] Omame, A. and Okuonghae, D. A co-infection model for oncogenic Human papillomavirus and tuberculosis with optimal control and cost-effectiveness analysis. *Optimal Control Applications and Methods*, 42(4), 1081-1101, (2021). [[CrossRef](#)]
- [32] Mtisi, E., Rwezaura, H. and Tchuenche, J.M. A mathematical analysis of malaria and tuberculosis co-dynamics. *Discrete and Continuous Dynamical Systems-B*, 12(4), 827-864, (2009). [[CrossRef](#)]
- [33] Iwa, L.L., Nwajeri, U.K., Atede, A.O., Panle, A.B. and Egeonu, K.U. Malaria and cholera co-dynamic model analysis furnished with fractional-order differential equations. *Mathematical*

Modelling and Numerical Simulation with Applications, 3(1), 33-57, (2023). [[CrossRef](#)]

- [34] Thabet, S.T.M., Abdo, M.S. and Shah, K. Theoretical and numerical analysis for transmission dynamics of COVID-19 mathematical model involving Caputo–Fabrizio derivative. *Advances in Difference Equations*, 2021, 184, (2021). [[CrossRef](#)]
- [35] Uçar, E., Uçar, S., Evirgen, F. and Özdemir, N. A fractional SAIDR model in the frame of Atangana–Baleanu derivative. *Fractal and Fractional*, 5(2), 32, (2021). [[CrossRef](#)]
- [36] Mohammadi, H., Kumar, S., Rezapour, S. and Etemad, S. A theoretical study of the Caputo–Fabrizio fractional modeling for hearing loss due to Mumps virus with optimal control. *Chaos, Solitons & Fractals*, 144, 110668, (2021). [[CrossRef](#)]
- [37] Najafi, H., Etemad, S., Patanarapeelert, N., Asamoah, J.K.K., Rezapour, S. and Sitthiwirattam, T. A study on dynamics of CD4⁺ T-cells under the effect of HIV-1 infection based on a mathematical fractal-fractional model via the Adams-Bashforth scheme and Newton polynomials. *Mathematics*, 10(9), 1366, (2022). [[CrossRef](#)]
- [38] Batiha, I.M., Momani, S., Ouannas, A., Momani, Z. and Hadid, S.B. Fractional-order COVID-19 pandemic outbreak: Modeling and stability analysis. *International Journal of Biomathematics*, 15(01), 2150090, (2022). [[CrossRef](#)]
- [39] Badshah, N. and Akbar, H. Stability analysis of fractional order SEIR model for malaria disease in Khyber Pakhtunkhwa. *Demonstratio Mathematica*, 54(1), 326-334, (2021). [[CrossRef](#)]
- [40] Uçar, S. Analysis of hepatitis B disease with fractal–fractional Caputo derivative using real data from Turkey. *Journal of Computational and Applied Mathematics*, 419, 114692, (2023). [[Cross-Ref](#)]
- [41] Nwajeri, U.K., Panle, A.B., Omame, A., Obi, M.C. and Onyenegecha, C.P. On the fractional order model for HPV and Syphilis using non–singular kernel. *Results in Physics*, 37, 105463, (2022). [[CrossRef](#)]
- [42] Rezapour, S., Etemad, S. and Mohammadi, H. A mathematical analysis of a system of Caputo–Fabrizio fractional differential equations for the anthrax disease model in animals. *Advances in Difference Equations*, 2020, 481, (2020). [[CrossRef](#)]
- [43] Matar, M.M., Abbas, M.I., Alzabut, J., Kaabar, M.K.A., Etemad, S. and Rezapour, S. Investigation of the p-Laplacian nonperiodic nonlinear boundary value problem via generalized Caputo fractional derivatives. *Advances in Difference Equations*, 2021, 68, (2021). [[CrossRef](#)]
- [44] Etemad, S. and Rezapour, S. On the existence of solutions for fractional boundary value problems on the ethane graph. *Advances in Difference Equations*, 2020, 276, (2020). [[CrossRef](#)]
- [45] Özköse, F. and Yavuz, M. Investigation of interactions between COVID-19 and diabetes with hereditary traits using real data: A case study in Turkey. *Computers in Biology and Medicine*, 141, 105044, (2022). [[CrossRef](#)]
- [46] Agarwal, P., Ramadan, M.A., Rageh, A.A. and Hadhoud, A.R. A fractional-order mathematical model for analyzing the pandemic trend of COVID-19. *Mathematical Methods in the Applied Sciences*, 45(8), 4625-4642, (2022). [[CrossRef](#)]
- [47] Wu, Y., Ahmad, S., Ullah, A. and Shah, K. Study of the fractional-order HIV-1 infection model with uncertainty in initial data. *Mathematical Problems in Engineering*, 2022, 7286460, (2022). [[CrossRef](#)]
- [48] Ogunrinde, R.B., Nwajeri, U.K., Fadugba, S.E., Ogunrinde, R.R. and Oshinubi, K.I. Dynamic model of COVID-19 and citizens reaction using fractional derivative. *Alexandria Engineering Journal*, 60(2), 2001-2012, (2021). [[CrossRef](#)]

- [49] Nwajeri, U.K., Omame, A. and Onyenegha, C.P. Analysis of a fractional order model for HPV and CT co-infection. *Results in Physics*, 28, 104643, (2021). [[CrossRef](#)]
- [50] Ul Rehman, A., Singh, R. and Agarwal, P. Modeling, analysis and prediction of new variants of COVID-19 and dengue co-dynamics on complex networks. *Chaos, Solitons & Fractals*, 150, 111008, (2021). [[CrossRef](#)]
- [51] Djenina, N., Ouannas, A., Batiha, I.M., Grassi, G., Oussaeif, T.E. and Momani, S. A novel fractional-order discrete SIR model for predicting COVID-19 behavior. *Mathematics*, 10(13), 2224, (2022). [[CrossRef](#)]
- [52] Abioye, A.I., Peter, O.J., Ogunseye, H.A., Oguntolu, F.A., Ayoola, T.A. and Oladapo, A.O. A fractional-order mathematical model for malaria and COVID-19 co-infection dynamics. *Healthcare Analytics*, 4, 100210, (2023). [[CrossRef](#)]
- [53] Hussein, R., Guedes, M., Ibraheim, N., Ali, M.M., El-Tahir, A., Allam, N. et al. Impact of COVID-19 and malaria coinfection on clinical outcomes: a retrospective cohort study. *Clinical Microbiology and Infection*, 28(8), 1152.e1-1152.e6, (2022). [[CrossRef](#)]
- [54] Khan, M.A. and Atangana, A. Modeling the dynamics of novel coronavirus (2019-nCov) with fractional derivative. *Alexandria Engineering Journal*, 59(4), 2379-2389, (2020). [[CrossRef](#)]
- [55] Gorenflo, R. and Mainardi, F. Fractional calculus. In *Fractals and Fractional Calculus in Continuum Mechanics* (Vol. 378) (pp. 223-276). Vienna, Austria: Springer, (1997). [[CrossRef](#)]
- [56] Buonomo, B. Analysis of a malaria model with mosquito host choice and bed-net control. *International Journal of Biomathematics*, 8(06), 1550077, (2015). [[CrossRef](#)]
- [57] Augusto, F.B. Optimal isolation control strategies and cost-effectiveness analysis of a two-strain avian influenza model. *Biosystems*, 113(3), 155-164, (2013). [[CrossRef](#)]
- [58] Zio, S., Tougri, I. and Lamien, B. Propagation du COVID19 au burkina faso, modelisation bayesienne et quantification des incertitudes: premiere approche. *Ecole Polytechnique de Ouagadougou (EPO) Ouagadougou*, (2020).
- [59] Our World in Data, Coronavirus (COVID-19) Vaccinations, (2022). <https://ourworldindata.org/covid-vaccinations>
- [60] Liu, Z., Magal, P., Seydi, O. and Webb, G. A COVID-19 epidemic model with latency period. *Infectious Disease Modelling*, 5, 323-337, (2020). [[CrossRef](#)]
- [61] Chitnis, N., Hyman, J.M. and Cushing, J.M. Determining important parameters in the spread of malaria through the sensitivity analysis of a mathematical model. *Bulletin of Mathematical Biology*, 70, 1272-1296, (2008). [[CrossRef](#)]
- [62] Ngonghala, C.N., Iboi, E., Eikenberry, S., Scotch, M., MacIntyre, C.R., Bonds, M.H. and Gumel, A.B. Mathematical assessment of the impact of non-pharmaceutical interventions on curtailing the 2019 novel coronavirus. *Mathematical Biosciences*, 325, 108364, (2020). [[CrossRef](#)]
- [63] Okuonghae, D. and Omame, A. Analysis of a mathematical model for COVID-19 population dynamics in Lagos, Nigeria. *Chaos, Solitons & Fractals*, 139, 110032, (2020). [[CrossRef](#)]
- [64] Zhang, Z., Zeb, A., Egbelowo, O.F. and Erturk, V.S. Dynamics of a fractional order mathematical model for COVID-19 epidemic. *Advances in Difference Equations*, 2020, 420, (2020). [[CrossRef](#)]
- [65] Van den Driessche, P. and Watmough, J. Reproduction numbers and sub-threshold endemic equilibria for compartmental models of disease transmission. *Mathematical Biosciences*, 180(1-2), 29-48, (2002). [[CrossRef](#)]

- [66] Sene, N. SIR epidemic model with Mittag–Leffler fractional derivative. *Chaos, Solitons & Fractals*, 137, 109833, (2020). [[CrossRef](#)]
- [67] Demirci, E. and Ozalp, N. A method for solving differential equations of fractional order. *Journal of Computational and Applied Mathematics*, 236(11), 2754-2762, (2012). [[CrossRef](#)]
- [68] Diethelm, K., Ford, N.J. and Freed, A.D. A predictor-corrector approach for the numerical solution of fractional differential equations. *Nonlinear Dynamics*, 29, 3-22, (2002). [[CrossRef](#)]
- [69] Lin, W. Global existence theory and chaos control of fractional differential equations. *Journal of Mathematical Analysis and Applications*, 332(1), 709-726, (2007). [[CrossRef](#)]
- [70] Liu, K., Feckan, M. and Wang, J. Hyers–Ulam stability and existence of solutions to the generalized Liouville–Caputo fractional differential equations. *Symmetry*, 12(6), 955, (2020). [[CrossRef](#)]
- [71] Huang, C., Wang, J., Chen, X. and Cao, J. Bifurcations in a fractional-order BAM neural network with four different delays. *Neural Networks*, 141, 344-354, (2021). [[CrossRef](#)]
- [72] Xu, C., Mu, D., Liu, Z., Pang, Y., Liao, M. and Aouiti, C. New insight into bifurcation of fractional-order 4D neural networks incorporating two different time delays. *Communications in Nonlinear Science and Numerical Simulation*, 118, 107043, (2023). [[CrossRef](#)]
- [73] Xu, C., Zhang, W., Aouiti, C., Liu, Z. and Yao, L. Bifurcation insight for a fractional-order stage-structured predator–prey system incorporating mixed time delays. *Mathematical Methods in the Applied Sciences*, 46(8), 9103-9118, (2023). [[CrossRef](#)]

Bulletin of Biomathematics (BBM)
(<https://bulletinbiomath.org>)



Copyright: © 2024 by the authors. This work is licensed under a Creative Commons Attribution 4.0 (CC BY) International License. The authors retain ownership of the copyright for their article, but they allow anyone to download, reuse, reprint, modify, distribute, and/or copy articles in *BBM*, so long as the original authors and source are credited. To see the complete license contents, please visit (<http://creativecommons.org/licenses/by/4.0/>).

How to cite this article: Iwa, L.L., Oname, A. & Inyama, S.C. (2024). A fractional-order model of COVID-19 and Malaria co-infection. *Bulletin of Biomathematics*, 2(2), 133-161. <https://doi.org/10.59292/bulletinbiomath.2024006>



RESEARCH PAPER

A stochastic approach to tumor modeling incorporating macrophages

Sümeyra Uçar^{1,‡}, İlknur Koca^{2,‡}, Necati Özdemir^{1,*,‡} and Tarık İnci^{3,‡}

¹Department of Mathematics, Faculty of Science and Arts, Balıkesir University, 10145 Balıkesir, Türkiye, ²Department of Economics and Finance, Fethiye Business Faculty, Muğla Sıtkı Koçman University, 48300 Muğla, Türkiye, ³Department of Internal Medicine, Faculty of Medicine, Ege University, 35040 İzmir, Türkiye

* Corresponding Author

‡ sumeyraucar@balikesir.edu.tr (Sümeyra Uçar); ilknurkoca@mu.edu.tr (İlknur Koca); nozdemir@balikesir.edu.tr (Necati Özdemir); tarik.inci@ege.edu.tr (Tarık İnci)

Abstract

Macrophages are essential components of the immune system's response to tumors, engaging in intricate interactions shaped by factors such as tumor type, progression, and the surrounding microenvironment. These dynamic relationships between macrophages and cancer cells have become a focal point of research, as scientists seek innovative ways to harness the immune system, including macrophages, for cancer immunotherapy. In this study, we introduce a novel model that examines the interaction between tumor and macrophage cells. We provide an in-depth analysis of the equilibrium points and their stability, as well as a thorough investigation into the solution properties of the model. Moreover, by incorporating a stochastic approach, we account for inherent randomness and fluctuations within the system, offering a more comprehensive understanding of tumor-immune dynamics. Numerical simulations further validate the model, providing key insights into how stochastic elements may influence tumor progression and immune response.

Keywords: Stochastic differential equations; numerical approximations; tumor model; stability analysis

AMS 2020 Classification: 26A33; 34A34

1 Introduction

Tumor is the Latin word for swelling and is currently used to describe cancer. Cancer is a disease in which the body's own cells can grow uncontrollably, invade tissues, and cause specific problems. There are two subgroups of tumors called benign and malignant. Malignant tumors, widely

known as cancer, affect millions of people each year [1], and treatment regimens have diversified over decades. Yet, cancer and its treatments must be addressed to overcome this disease.

The healthy body is capable of defending against cancer cells. Our immune system is well-equipped to find and destroy cancerous cells before they progress to cancer. However, cancer cells acquire functions to evade the immune system, surviving and eventually leading to neoplastic or cancer growth in the body. Our immunity is composed of two different lines of defense. The first line of defense is the innate immune system, which takes action if a germ or unknown antigen is encountered in the body. Examples of the innate immune system include phagocytosis of bacteria, acid secretion in the stomach, skin resistance, neutrophils, macrophages, and natural killer cells [2–4].

Our tumor model introduces a significant advancement by capturing the complex interactions between tumor and macrophage cells. This model's novelty lies in its incorporation of stochastic differential equations, which account for biological variability and offer a more nuanced understanding of these interactions. By integrating these stochastic elements, our model provides a more realistic representation of the dynamic and often unpredictable nature of tumor growth and immune response, enhancing the accuracy and applicability of predictive simulations.

On the other hand, adaptive immunity takes over the process if the innate immune system cannot destroy the invaders. Acquired immunity is the process of generating a specific response to individual invading agents such as bacteria, viruses, toxins, foreign tissues, etc. In the case of reinfection with the same agents, this system generates quick responses. This system consists of B and T lymphocytes. B lymphocytes secrete small proteins called immunoglobulins, which can bind to and inactivate circulating antigens—substances found in foreign particles or germs that trigger an immune response. This is called B-cell-mediated immunity or humoral immunity. The other side of adaptive immunity is cell-mediated immunity, which is mediated by T lymphocytes. T lymphocytes continuously scan the body to find and eliminate emerging malignant cells [2, 5, 6]. One of the pathways cancerous cells use to evade the immune system is expressing the PD-L1 receptors on their surface. PD-L1 is a ligand found on cancer cells that binds to receptors on immune cells to inactivate them. It is one of the treatment options now in use for novel anticancer therapy. In Contrary to this phenomenon, cytotoxic T cells are proliferated by IL-10, despite its tumor-promoting effects. It is known that IL-10 has properties of both tumor-inhibiting and promoting effects through various mechanisms [7–9].

There have been few mathematical tools and concepts used to predict real-world problems in the last couple of decades, including classical differential and integral operators, fractional differential and integral operators, and stochastic differential equations. For classical mechanical problems with no memory, differentiation, and integration are used as a method of modeling. In fact, these two mathematical operators have been used to simulate many real-world phenomena with some limitations. Fractional calculus was introduced to replicate complex problems following power law processes, exponential decay rule, and memory effects. The concepts have been applied in particular to the modeling of real-life structures for example, understanding the dynamics of financial systems, ecosystems, population dynamics, the spread of diseases and many more [10–25].

A mathematical model that integrates uncertainty into its structure is called a stochastic system. The system's inherent complexity or external variables like noise may be the source of this uncertainty. The presence of random variables and probability distributions, which show the likelihood that various events will occur, are frequently characteristics of stochastic systems such as bacterial growth, electrical flows fluctuating due to thermal noise, or gas particles' moments. Stochastic activities can be used to model and understand a wide variety of phenomena, from chemical reactions to economics. They are also used to develop algorithms for predicting the

behavior of complex systems. For the study of stochastic techniques, one needs mathematical knowledge in probability, calculus, linear algebra, set theory, and topology, as well as branches of mathematical analysis such as real analysis and measure theory [26–30].

Ambient noise in the real world unavoidably affects the population system. The model’s parameters might not be strictly constant and instead might vary within certain bounds. Environmental noise is thus an excellent way to describe these phenomena in disease models. In addition, stochastic differential equation models are a crucial type of model when considering population dynamics since they are more realistic than other models. There has been considerable research on biological and epidemiological stochastic models. These models provide insight into the spread of diseases and can help simulate clinical trials and other medical research [31–36].

The purpose of this work is to delve into a novel tumor model, a type of stochastic order model which, for the first time, was put forward in employing classical derivative to aim at a tumor model, based on more favorable stochastic theories. In [37], the authors present a system which generates anti-PD-L1 variables, IL-10, CD8+T cells, and cancer cell and demonstrate the critical role that IL-10 and anti-PD-L1 play in inactivating cancer cells, and the mechanism by which cancer cells are eliminated during the single-dose administration of these two medications. Motivated by this nice paper and, as explained above, macrophages and cancer cells are very closely related, herein, we give the following model in order to see the macrophage effects. The integer order differential equation the system that puts forth the tumor model can be seen below:

$$\begin{aligned}
 \frac{dT(t)}{dt} &= a + bI(t)C(t)T(t)\left(1 - \frac{T(t)}{p}\right) - cT(t), \\
 \frac{dC(t)}{dt} &= kC(t)\left(1 - \frac{C(t)}{q}\right) - eC(t)T(t)I(t) - zC(t)T(t)Z(t) - \tilde{m}M(t)C(t), \\
 \frac{dI(t)}{dt} &= -fI(t), \\
 \frac{dZ(t)}{dt} &= -\gamma Z(t), \\
 \frac{dM(t)}{dt} &= r_M\left(1 - \frac{M(t)}{k_M}\right)M(t) + \tilde{p}C(t)M(t) - \tilde{d}M(t).
 \end{aligned} \tag{1}$$

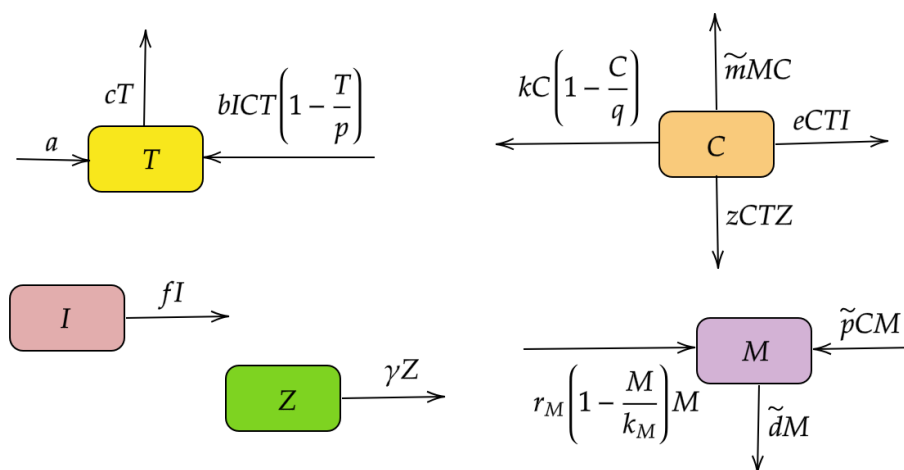


Figure 1. The transfer diagram of the tumor model

The variable factors concerning the model alter at time t as follows: $T(t)$, $C(t)$, $I(t)$, $Z(t)$, $M(t)$ characterize CD8+T lymphocytes, cancer cells, IL-10 cytokine, anti-PD-L1, makrophages in the order given. \tilde{p} is recruitment rate of macrophages, a is the initial density of CD8+T cells, b the reproduction rate of CD8+T cells under the influence of IL-10, \tilde{d} shows death rate of macrophages, k_M display carrying capacity of macrophages, k is the tumor growth ratio, z the death rate of cancer cells under the influence of anti-PD-L1, f is the decay rate of IL-10, q present the carrying capacity of cancer cells, r_M show proliferation ratios of macrophages, γ is the decay ratios anti-PD-L1, \tilde{m} is tumor killing rate by $M(t)$, c refers to the carrying capacity of CD8+T cells, e is the death ratio of cancer cells under the influence of IL-10, p displays the carrying capacity of CD8+T cells.

The article is further structured with subdivisions specified below: The equilibrium points and their stability analysis are introduced in Section 2. Section 3 substantiates the existence and uniqueness of the solution for our novel model while we again rake through the model by means of the stochastic theory in Section 4. In Section 5, this model is depicted with respect to numerically so as to look over the entire effect. As a final step, we discuss our acquired outcomes and conclude our study.

2 Equilibrium points and stability analysis

Understanding equilibrium points helps analyze and predict the behavior of systems (physical, mathematical, or engineering). The stability of equilibrium points is an important consideration in determining the long-term behavior of a system. So in this section, we focus on the equilibrium points of the system. The equilibrium points are the solutions of the model as follows:

$$\begin{aligned} a + bI(t)C(t)T(t)\left(1 - \frac{T(t)}{p}\right) - cT(t) &= 0, \\ kC(t)\left(1 - \frac{C(t)}{q}\right) - eC(t)T(t)I(t) - zC(t)T(t)Z(t) - \tilde{m}M(t)C(t) &= 0, \\ -fI(t) &= 0, \\ -\gamma Z(t) &= 0, \\ r_M\left(1 - \frac{M(t)}{k_M}\right)M(t) + \tilde{p}C(t)M(t) - \tilde{d}M(t) &= 0. \end{aligned}$$

The disease-free equilibrium point

$$E^* = (T^*, C^*, I^*, Z^*, M^*) = \left(\frac{a}{c}, 0, 0, 0, \frac{k_M(r_M - \tilde{d})}{r_M}\right),$$

and the endemic equilibrium point

$$E^{**} = (T^{**}, C^{**}, I^{**}, Z^{**}, M^{**}) = \left(\frac{a}{c}, \frac{q(\tilde{d}k_M\tilde{m} + kr_M - k_M\tilde{m}r_M)}{k_M\tilde{m}\tilde{p}q + kr_M}, 0, 0, \frac{dk_M(\tilde{p}q + r_M - \tilde{d})}{k_M\tilde{m}\tilde{p}q + kr_M}\right).$$

Theorem 1 *The disease-free equilibrium point $E^* = \left(\frac{a}{c}, 0, 0, 0, \frac{k_M(r_M - \tilde{d})}{r_M}\right)$ is locally asymptotically stable if $\tilde{d} < r_M$ and $\frac{k_M\tilde{m}(\tilde{d} - r_M)}{r_M} + k < 0$.*

Proof The Jacobian matrix at the disease-free equilibrium point E^* is

$$J(E^*) = \begin{pmatrix} -c & 0 & 0 & 0 & 0 \\ 0 & k + \frac{\tilde{m}k_M(\tilde{d}-r_M)}{r_M} & 0 & 0 & 0 \\ 0 & 0 & -f & 0 & 0 \\ 0 & 0 & 0 & -\gamma & 0 \\ 0 & \frac{\tilde{p}k_M(r_M-\tilde{d})}{r_M} & 0 & 0 & -r_M + r_M \left(1 + \frac{\tilde{d}-r_M}{r_M}\right) \end{pmatrix}.$$

The eigenvalues of this Jacobian matrix $J(E^*)$ are

$$\begin{aligned} \lambda_1 &= -f, \\ \lambda_2 &= \tilde{d} - r_M, \\ \lambda_3 &= \frac{k_M\tilde{m}(\tilde{d} - r_M)}{r_M} + k, \\ \lambda_4 &= -c, \\ \lambda_5 &= -\gamma. \end{aligned}$$

If $\tilde{d} < r_M$ and $\frac{k_M\tilde{m}(\tilde{d}-r_M)}{r_M} + k < 0$, then all eigenvalues are negative. So, from [38], the disease-free equilibrium point $E^* = \left(\frac{a}{c}, 0, 0, 0, \frac{k_M(r_M-\tilde{d})}{r_M}\right)$ is locally asymptotically stable.

Theorem 2 The endemic equilibrium point $E^{**} = \left(\frac{a}{c}, \frac{q(\tilde{d}k_M\tilde{m}+dr_M-k_M\tilde{m}r_M)}{k_M\tilde{m}\tilde{p}q+dr_M}, 0, 0, \frac{kk_M(\tilde{p}q+r_M-\tilde{d})}{k_M\tilde{m}\tilde{p}q+kr_M}\right)$ is locally asymptotically stable if $N^{\frac{1}{2}} < M$.

Proof The Jacobian matrix at the endemic equilibrium point E^{**} is

$$J(E^{**}) = \begin{pmatrix} -c & 0 & \frac{bq(\tilde{d}k_M\tilde{m}-k_M\tilde{m}r_M+kr_M)a\left(1-\frac{a}{cp}\right)}{(k_M\tilde{m}\tilde{p}q+kr_M)c} \\ 0 & \frac{k(-\tilde{d}\tilde{m}k_M+\tilde{m}k_Mr_M-dr_M)}{k_M\tilde{m}\tilde{p}q+kr_M} & -\frac{eqa(\tilde{d}k_M\tilde{m}-k_M\tilde{m}r_M+kr_M)}{(k_M\tilde{m}\tilde{p}q+kr_M)c} \\ 0 & 0 & -f \\ 0 & 0 & 0 \\ 0 & \frac{\tilde{p}kk_M(-\tilde{p}q+\tilde{d}-r_M)}{k_M\tilde{m}\tilde{p}q+kr_M} & 0 \\ 0 & 0 & 0 \\ -\frac{zqa(\tilde{d}k_M\tilde{m}-k_M\tilde{m}r_M+kr_M)}{(k_M\tilde{m}\tilde{p}q+kr_M)c} & 0 & -\frac{\tilde{m}q(\tilde{d}k_M\tilde{m}-k_M\tilde{m}r_M+kr_M)}{k_M\tilde{m}\tilde{p}q+kr_M} \\ 0 & 0 & 0 \\ -\gamma & 0 & 0 \\ 0 & \frac{r_M(\tilde{p}\tilde{m}k_Mq-k\tilde{p}q+k\tilde{d}-\tilde{p}qk_M\tilde{m}r_M+\tilde{p}qkr_M-k\tilde{d}r_M)}{k_M\tilde{m}\tilde{p}q+kr_M} & 0 \end{pmatrix}.$$

If we make the following assumptions:

$$\begin{aligned} L &= \frac{1}{2(k_M\tilde{m}\tilde{p}q + dr_M)}, \\ M &= -k\tilde{d}k_M\tilde{m} + k k_M\tilde{m}r_M - k\tilde{p}kr_M - k^2r_M + k\tilde{d}r_M - kr_M^2, \end{aligned}$$

$$N = \left(\begin{array}{c} -4k\tilde{d}k_M^2\tilde{m}^2\tilde{p}^2q^2 + 4kk_M^2\tilde{m}^2\tilde{p}^2q^2r_M - 4k^2k_M\tilde{m}\tilde{p}^2q^2r_M \\ + 4k\tilde{d}^2k_M^2\tilde{m}^2\tilde{p}q - 8k\tilde{d}k_M^2\tilde{m}^2\tilde{p}qr_M + 4kk_M^2\tilde{m}^2\tilde{p}qr_M^2 \\ + k^2\tilde{d}^2k_M^2\tilde{m}^2 - 2k^2\tilde{d}k_M^2\tilde{m}^2r_M + 2k^2\tilde{d}k_M\tilde{m}\tilde{p}qr_M \\ + k^2k_M^2\tilde{m}^2r_M^2 - 2k^2k_M\tilde{m}\tilde{p}qr_M^2 + k^2\tilde{p}^2q^2r_M^2 \\ + 2k^3\tilde{d}k_M\tilde{m}r_M - 2k^3k_M\tilde{m}r_M^2 - 2k^3\tilde{p}qr_M^2 \\ + 2k^2\tilde{d}^2k_M\tilde{m}r_M - 4k^2\tilde{d}k_M\tilde{m}r_M^2 - 2k^2\tilde{d}\tilde{p}qr_M^2 \\ + 2k^2k_M\tilde{m}r_M^3 + 2k^2\tilde{p}qr_M^3 + k^4r_M^2 + 2k^3\tilde{d}r_M^2 \\ - 2k^3r_M^3 + k^2\tilde{d}^2r_M^2 - 2k^2\tilde{d}r_M^3 + k^2r_M^4 \end{array} \right)^{\frac{1}{2}},$$

then, the eigenvalues of this Jacobian matrix $J(E^{**})$ are

$$\begin{aligned} \lambda_1 &= -a \left(M + N^{\frac{1}{2}} \right), \\ \lambda_2 &= -a \left(M - N^{\frac{1}{2}} \right), \\ \lambda_3 &= -f, \\ \lambda_4 &= -c, \\ \lambda_5 &= -\gamma. \end{aligned}$$

If $M > N^{\frac{1}{2}}$, then all eigenvalues are negative. So, from [38], the endemic equilibrium point $E^{**} = \left(\frac{a}{c}, \frac{q(\tilde{d}k_M\tilde{m}+kr_M-k_M\tilde{m}r_M)}{k_M\tilde{m}\tilde{p}q+kr_M}, 0, 0, \frac{kk_M(\tilde{p}q+r_M-\tilde{d})}{k_M\tilde{m}\tilde{p}q+kr_M} \right)$ is locally asymptotically stable.

3 Existence and uniqueness analysis of tumor model

In this section, we give the existence and uniqueness theorems to guarantee the existence of solutions and we will present the conditions of existence and uniqueness for our model. Let us consider our model as taking the right side like below:

$$\begin{aligned} \frac{dT(t)}{dt} &= T_1(t, T), \\ \frac{dC(t)}{dt} &= T_2(t, C), \\ \frac{dI(t)}{dt} &= T_3(t, I), \\ \frac{dZ(t)}{dt} &= T_4(t, Z), \\ \frac{dM(t)}{dt} &= T_5(t, M). \end{aligned}$$

Here we consider

$$\begin{aligned} T_1(t, T) &= a + bI(t)C(t)T(t) \left(1 - \frac{T(t)}{p} \right) - cT(t), \\ T_2(t, C) &= kC(t) \left(1 - \frac{C(t)}{q} \right) - eC(t)T(t)I(t) - zC(t)T(t)Z(t) - \tilde{m}M(t)C(t), \\ T_3(t, I) &= -fI(t), \\ T_4(t, Z) &= -\gamma Z(t), \end{aligned}$$

$$T_5(t, M) = r_M \left(1 - \frac{M(t)}{k_M} \right) M(t) + \tilde{p}C(t)M(t) - \tilde{d}M(t).$$

For the existence and uniqueness of the model, we consider the following theorem [39]:

Theorem 3 Assume that there are five positive constants t_1, t_2, t_3, t_4, t_5 and $\bar{t}_1, \bar{t}_2, \bar{t}_3, \bar{t}_4, \bar{t}_5$ such that

i)

$$\begin{aligned} |T_1(t, T) - T_1(t, T_1)|^2 &\leq t_1 |T - T_1|^2, \\ |T_2(t, C) - T_2(t, C_1)|^2 &\leq t_2 |C - C_1|^2, \\ |T_3(t, I) - T_3(t, I_1)|^2 &\leq t_3 |I - I_1|^2, \\ |T_4(t, Z) - T_4(t, Z_1)|^2 &\leq t_4 |Z - Z_1|^2, \\ |T_5(t, M) - T_5(t, M_1)|^2 &\leq t_5 |M - M_1|^2. \end{aligned}$$

ii)

$$\begin{aligned} |T_1(t, T)|^2 &\leq \bar{t}_1(1 + |T|^2), \\ |T_2(t, C)|^2 &\leq \bar{t}_2(1 + |C|^2), \\ |T_3(t, I)|^2 &\leq \bar{t}_3(1 + |I|^2), \\ |T_4(t, Z)|^2 &\leq \bar{t}_4(1 + |Z|^2), \\ |T_5(t, M)|^2 &\leq \bar{t}_5(1 + |M|^2). \end{aligned}$$

Then, there exists a unique solution if the above conditions are verified. We start with the first equation of model $T_1(t, T)$. Then we verify first condition for equation $T_1(t, T)$ like below:

$$|T_1(t, T) - T_1(t, T_1)|^2 \leq t_1 |T - T_1|^2.$$

Before we start the proof, let us define the following norm: $\|T\|_\infty = \sup_{t \in D_t} |T(t)|$, then we have

$T, T_1 \in R^2$ and $t \in [0, T]$,

$$\begin{aligned} |T_1(t, T) - T_1(t, T_1)|^2 &= \left| \frac{(bI(t)C(t) - \frac{bI(t)C(t)}{p}(T(t) + T_1(t))) (T(t) - T_1(t))}{-c(T(t) - T_1(t))} \right|^2 \\ &\leq \left| \left((bI(t)C(t)) \left(1 - \frac{T(t) + T_1(t)}{p} \right) - c \right) (T(t) - T_1(t)) \right|^2 \\ &\leq \left(2b^2 |I(t)|^2 |C(t)|^2 \left(1 + \frac{|T(t)|^2 + |T_1(t)|^2}{p} \right) + 2c^2 \right) |T(t) - T_1(t)|^2 \\ &\leq \left(2b^2 \sup_{t \in D_I} |I(t)|^2 \sup_{t \in D_C} |C(t)|^2 \left(1 + \frac{\sup_{t \in D_T} |T(t)|^2 + \sup_{t \in D_{T_1}} |T_1(t)|^2}{p} \right) + 2c^2 \right) \\ &\times |T(t) - T_1(t)|^2 \end{aligned}$$

$$\begin{aligned} &\leq \left(2b^2 \|I\|_\infty^2 \|C\|_\infty^2 \left(1 + \frac{\|T\|_\infty^2 + \|T_1\|_\infty^2}{p} \right) + 2c^2 \right) |T(t) - T_1(t)|^2 \\ &\leq t_1 |T - T_1|^2, \end{aligned}$$

where

$$t_1 = \left(2b^2 \|I\|_\infty^2 \|C\|_\infty^2 \left(1 + \frac{\|T\|_\infty^2 + \|T_1\|_\infty^2}{p} \right) + 2c^2 \right).$$

Now we proceed to show the second equation. If we have $C, C_1 \in R^2$ and $t \in [0, T]$, then

$$\begin{aligned} |T_2(t, C) - T_2(t, C_1)|^2 &= \left| (k - eT(t)I(t) - zT(t)Z(t) - \tilde{m}M(t))(C(t) - C_1(t)) - \frac{k}{q}(C^2(t) - C_1^2(t)) \right|^2 \\ &= \left| \left((k - eT(t)I(t) - zT(t)Z(t) - \tilde{m}M(t)) - \frac{k}{q}(C(t) + C_1(t)) \right) \right. \\ &\quad \left. \times (C(t) - C_1(t)) \right|^2 \\ &\leq \left(2(k^2 + e^2|T(t)|^2|I(t)|^2 + z^2|T(t)|^2|Z(t)|^2 + \tilde{m}|M(t)|^2) \right. \\ &\quad \left. + \frac{2k^2}{q^2}(|C(t)|^2 + |C_1(t)|^2) \right) \times |C(t) - C_1(t)|^2 \\ &\leq \left(2 \left(k^2 + e^2 \sup_{t \in D_T} |T(t)|^2 \sup_{t \in D_I} |I(t)|^2 + z^2 \sup_{t \in D_T} |T(t)|^2 \sup_{t \in D_Z} |Z(t)|^2 \right) \right. \\ &\quad \left. + 2\tilde{m} \sup_{t \in D_M} |M(t)|^2 + \frac{2d^2}{q^2} \left(\sup_{t \in D_C} |C(t)|^2 + \sup_{t \in D_{C_1}} |C_1(t)|^2 \right) \right) \\ &\quad \times |C(t) - C_1(t)|^2 \\ &\leq \left(2(k^2 + e^2\|T\|_\infty^2\|I\|_\infty^2 + z^2\|T\|_\infty^2\|Z\|_\infty^2 + \tilde{m}\|M\|_\infty^2) + \frac{2k^2}{q^2}(\|C\|_\infty^2 + \|C_1\|_\infty^2) \right) \\ &\quad \times |C(t) - C_1(t)|^2 \\ &\leq t_2 |C - C_1|^2, \end{aligned}$$

where

$$t_2 = \left(2(k^2 + e^2\|T\|_\infty^2\|I\|_\infty^2 + z^2\|T\|_\infty^2\|Z\|_\infty^2 + \tilde{m}\|M\|_\infty^2) + \frac{2k^2}{q^2}(\|C\|_\infty^2 + \|C_1\|_\infty^2) \right).$$

We take two positive constants $I, I_1 \in R^2$ and $t \in [0, T]$, then

$$\begin{aligned} |T_3(t, I) - T_3(t, I_1)|^2 &= |-fI(t) + fI_1(t)|^2 \\ &\leq f^2 |I(t) - I_1(t)|^2 \\ &\leq t_3 |I - I_1|^2, \end{aligned}$$

where

$$t_3 = f^2.$$

We take two positive constants $Z, Z_1 \in R^2$ and $t \in [0, T]$, then

$$\begin{aligned} |T_4(t, Z) - T_4(t, Z_1)|^2 &= |-\gamma Z(t) + \gamma Z_1(t)|^2 \leq \gamma^2 |Z(t) - Z_1(t)|^2 \\ &\leq t_4 |Z - Z_1|^2, \end{aligned}$$

where

$$t_4 = \gamma^2.$$

Finally, if we take two positive constants $M, M_1 \in R^2$ and $t \in [0, T]$, then

$$\begin{aligned} |T_5(t, M) - T_5(t, M_1)|^2 &= \left| \left(r_M + \tilde{p}C(t) - \tilde{d} \right) (M(t) - M_1(t)) - \frac{r_M}{k_M} (M^2(t) - M_1^2(t)) \right|^2 \\ &= \left| \left(\left(r_M + \tilde{p}C(t) - \tilde{d} \right) - \frac{r_M}{k_M} (M(t) + M_1(t)) \right) (M(t) - M_1(t)) \right|^2 \\ &\leq \left(2 \left(r_M^2 + \tilde{p}^2 |C(t)|^2 + \tilde{d}^2 \right) + \frac{2r_M^2}{k_M^2} (|M(t)|^2 + |M_1(t)|^2) \right) \\ &\quad \times |M(t) - M_1(t)|^2 \\ &\leq \left(2 \left(r_M^2 + \tilde{p}^2 \sup_{t \in D_C} |C(t)|^2 + \tilde{d}^2 \right) + \frac{2r_M^2}{k_M^2} \left(\sup_{t \in D_M} |M(t)|^2 + \sup_{t \in D_{M_1}} |M_1(t)|^2 \right) \right) \\ &\quad \times |M(t) - M_1(t)|^2 \\ &\leq \left(2 \left(r_M^2 + \tilde{p}^2 \|C\|_\infty^2 + \tilde{d}^2 \right) + \frac{2r_M^2}{k_M^2} (\|M\|_\infty^2 + \|M_1\|_\infty^2) \right) |M(t) - M_1(t)|^2 \\ &\leq t_5 |M - M_1|^2, \end{aligned}$$

where

$$t_5 = \left(2 \left(r_M^2 + \tilde{p}^2 \|C\|_\infty^2 + \tilde{d}^2 \right) + \frac{2r_M^2}{k_M^2} (\|M\|_\infty^2 + \|M_1\|_\infty^2) \right).$$

So condition (i) is satisfied.

Now we prove the second condition for the tumor model via the following condition:

$\forall (t, T) \in R^2 \times [t_0, T]$ then we will show that

$$\begin{aligned} |T_1(t, T)|^2 &= \left| a + bI(t)C(t)T(t) \left(1 - \frac{T(t)}{p} \right) - cT(t) \right|^2 \\ &\leq 4a^2 + 4b^2 |I(t)|^2 |C(t)|^2 |T(t)|^2 + 4b^2 |I(t)|^2 |C(t)|^2 \frac{|T^2(t)|^2}{p^2} + 4c^2 |T(t)|^2 \\ &\leq 4a^2 + 4b^2 \sup_{t \in D_I} |I(t)|^2 \sup_{t \in D_C} |C(t)|^2 |T(t)|^2 + 4b^2 \sup_{t \in D_I} |I(t)|^2 \sup_{t \in D_C} |C(t)|^2 \frac{\sup_{t \in D_T} |T^2(t)|^2}{p^2} \\ &\quad + 4c^2 |T(t)|^2 \end{aligned}$$

$$\begin{aligned} &\leq 4a^2 + \frac{4b^2}{p^2} \|I\|_\infty^2 \|C\|_\infty^2 \|T^2\|_\infty^2 + \left(4b^2 \|I\|_\infty^2 \|C\|_\infty^2 + 4c^2\right) |T|^2 \\ &\leq \left(4a^2 + \frac{4b^2}{p^2} \|I\|_\infty^2 \|C\|_\infty^2 \|T^2\|_\infty^2\right) \left(1 + \frac{4b^2 \|I\|_\infty^2 \|C\|_\infty^2 + 4c^2}{4a^2 + \frac{4b^2}{p^2} \|I\|_\infty^2 \|C\|_\infty^2 \|T^2\|_\infty^2} |T|^2\right) \\ &\leq \bar{t}_1(1 + |T|^2), \end{aligned}$$

where

$$\bar{t}_1 = \left(4a^2 + \frac{4b^2}{p^2} \|I\|_\infty^2 \|C\|_\infty^2 \|T^2\|_\infty^2\right),$$

and with under condition

$$\frac{4b^2 \|I\|_\infty^2 \|C\|_\infty^2 + 4c^2}{4a^2 + \frac{4b^2}{p^2} \|I\|_\infty^2 \|C\|_\infty^2 \|T^2\|_\infty^2} < 1.$$

Now we continue with the second equation.

$\forall(t, C) \in R^2 \times [t_0, T]$ then we will show that

$$\begin{aligned} |T_2(t, C)|^2 &= \left|kC(t) \left(1 - \frac{C(t)}{q}\right) - eC(t) T(t) I(t) - zC(t) T(t) Z(t) - \tilde{m}M(t) C(t)\right|^2 \\ &\leq 2 \left(k^2 + e^2 |T(t)|^2 |I(t)|^2 + z^2 |T(t)|^2 |Z(t)|^2 + \tilde{m}^2 |M(t)|^2\right) |C(t)|^2 + 2\frac{k^2}{q^2} |C^2(t)|^2 \\ &\leq 2 \left(k^2 + e^2 \sup_{t \in D_T} |T(t)|^2 \sup_{t \in D_I} |I(t)|^2 + z^2 \sup_{t \in D_T} |T(t)|^2 \sup_{t \in D_Z} |Z(t)|^2 + \tilde{m}^2 \sup_{t \in D_M} |M(t)|^2\right) |C(t)|^2 \\ &\quad + 2\frac{k^2}{q^2} \sup_{t \in D_C} |C^2(t)|^2 \\ &\leq 2 \left(k^2 + e^2 \|T\|_\infty^2 \|I\|_\infty^2 + z^2 \|T\|_\infty^2 \|Z\|_\infty^2 + \tilde{m}^2 \|M\|_\infty^2\right) |C|^2 + 2\frac{k^2}{q^2} \|C^2\|_\infty^2 \\ &\leq 2\frac{k^2}{q^2} \|C^2\|_\infty^2 \left(1 + \frac{2 \left(k^2 + e^2 \|T\|_\infty^2 \|I\|_\infty^2 + z^2 \|T\|_\infty^2 \|Z\|_\infty^2 + \tilde{m}^2 \|M\|_\infty^2\right) |C|^2}{2\frac{k^2}{q^2} \|C^2\|_\infty^2}\right) \\ &\leq \bar{t}_2(1 + |C|^2), \end{aligned}$$

where

$$\bar{t}_2 = 2\frac{k^2}{q^2} \|C^2\|_\infty^2,$$

and with under condition

$$\frac{2 \left(k^2 + e^2 \|T\|_\infty^2 \|I\|_\infty^2 + z^2 \|T\|_\infty^2 \|Z\|_\infty^2 + \tilde{m}^2 \|M\|_\infty^2\right)}{2\frac{k^2}{q^2} \|C^2\|_\infty^2} < 1.$$

$$\forall (t, I) \in R^2 \times [t_0, T]$$

$$\begin{aligned} |T_3(t, I)|^2 &= |-fI(t)|^2 \leq 1 + f^2 |I(t)|^2 \\ &\leq \bar{t}_3(1 + |I|^2), \end{aligned}$$

where

$$\bar{t}_3 > 0,$$

and with under condition

$$f^2 < 1.$$

$$\forall (t, Z) \in R^2 \times [t_0, T]$$

$$\begin{aligned} |T_4(t, Z)|^2 &= |-\gamma Z(t)|^2 \leq 1 + \gamma^2 |Z(t)|^2 \\ &\leq \bar{t}_4(1 + |Z|^2), \end{aligned}$$

where

$$\bar{t}_4 > 0,$$

and with under condition

$$\gamma^2 < 1.$$

$$\forall (t, M) \in R^2 \times [t_0, T]$$

$$\begin{aligned} |T_5(t, M)|^2 &= \left| r_M \left(1 - \frac{M(t)}{k_M} \right) M(t) + \tilde{p}C(t)M(t) - \tilde{d}M(t) \right|^2 \\ &\leq 4r_M^2 |M(t)|^2 + 4\frac{r_M^2}{k_M^2} \left| M^2(t) \right|^2 + 4\tilde{p}^2 |C(t)|^2 |M(t)|^2 + 4\tilde{d}^2 |M(t)|^2 \\ &\leq \left(4r_M^2 + 4\tilde{p}^2 |C(t)|^2 + 4\tilde{d}^2 \right) |M(t)|^2 + 4\frac{r_M^2}{k_M^2} \left| M^2(t) \right|^2 \\ &\leq \left(4r_M^2 + 4\tilde{p}^2 \sup_{t \in D_C} |C(t)|^2 + 4\tilde{d}^2 \right) |M(t)|^2 + 4\frac{r_M^2}{k_M^2} \sup_{t \in D_M} \left| M^2(t) \right|^2 \\ &\leq \left(4r_M^2 + 4\tilde{p}^2 \|C\|_\infty^2 + 4\tilde{d}^2 \right) |M(t)|^2 + 4\frac{r_M^2}{k_M^2} \|M^2\|_\infty^2 \\ &\leq 4\frac{r_M^2}{k_M^2} \|M^2\|_\infty^2 \left(1 + \frac{4r_M^2 + 4\tilde{p}^2 \|C\|_\infty^2 + 4\tilde{d}^2}{4\frac{r_M^2}{k_M^2} \|M^2\|_\infty^2} |M|^2 \right) \\ &\leq \bar{t}_5(1 + |M|^2), \end{aligned}$$

where

$$\bar{t}_5 = 4 \frac{r_M^2}{k_M^2} \|M^2\|_\infty^2,$$

and with under condition

$$\frac{4r_M^2 + 4\tilde{p}^2 \|C\|_\infty^2 + 4\tilde{d}^2}{4 \frac{r_M^2}{k_M^2} \|M^2\|_\infty^2} < 1.$$

So, if the conditions below are satisfied, then the model has a unique solution

$$\max \left\{ \begin{array}{l} \frac{4b^2 \|I\|_\infty^2 \|C\|_\infty^2 + 4c^2}{4a^2 + \frac{4b^2}{p^2} \|I\|_\infty^2 \|C\|_\infty^2 \|T^2\|_\infty^2}, \\ \frac{2(k^2 + e^2 \|T\|_\infty^2 \|I\|_\infty^2 + z^2 \|T\|_\infty^2 \|Z\|_\infty^2 + \tilde{m}^2 \|M\|_\infty^2)}{2 \frac{k^2}{q^2} \|C^2\|_\infty^2}, \\ f^2, \\ \gamma^2, \\ \frac{4r_M^2 + 4\tilde{p}^2 \|C\|_\infty^2 + 4\tilde{d}^2}{4 \frac{r_M^2}{k_M^2} \|M^2\|_\infty^2}, \end{array} \right\} < 1.$$

By the above theorem, we can say that the model has a unique solution.

4 Stochastic model

In this section, we add to the model under investigation some environmental noise. The idea was suggested by Atangana, where randomness was added to some models [40]. In this section, we convert the deterministic model to the following stochastic system:

$$\begin{aligned} dT(t) &= \left(a + bI(t)C(t)T(t) \left(1 - \frac{T(t)}{p} \right) - cT(t) \right) + \sigma_1 T(t) dB_1(t), \\ dC(t) &= \left(kC(t) \left(1 - \frac{C(t)}{q} \right) - eC(t)T(t)I(t) \right. \\ &\quad \left. - zC(t)T(t)Z(t) - \tilde{m}M(t)C(t) \right) + \sigma_2 C(t) dB_2(t), \\ dI(t) &= (-fI(t)) + \sigma_3 I(t) dB_3(t), \\ dZ(t) &= (-\gamma Z(t)) + \sigma_4 Z(t) dB_4(t), \\ dM(t) &= \left(r_M \left(1 - \frac{M(t)}{k_M} \right) M(t) + \tilde{p}C(t)M(t) - \tilde{d}M(t) \right) + \sigma_5 M(t) dB_5(t), \\ T(0) &= T_0, C(0) = C_0, I(0) = I_0, Z(0) = Z_0 \text{ and } M(0) = M_0. \end{aligned}$$

The existence of a unique solution to a general equation has been presented. Besides this, we have presented the conditions under which the deterministic model admits a unique system of solutions. Now we can present a numerical solution of the model by converting the stochastic model into an integral system below:

$$T(t) - T(0) = \int_0^t T_1(T, C, I, Z, M, \tau) d\tau + \sigma_1 \int_0^t T_{11}(T, \tau) dB_1(\tau),$$

$$\begin{aligned}
C(t) - C(0) &= \int_0^t T_2(T, C, I, Z, M, \tau) d\tau + \sigma_2 \int_0^t T_{21}(C, \tau) dB_2(\tau), \\
I(t) - I(0) &= \int_0^t T_3(T, C, I, Z, M, \tau) d\tau + \sigma_3 \int_0^t T_{31}(I, \tau) dB_3(\tau), \\
Z(t) - Z(0) &= \int_0^t T_4(T, C, I, Z, M, \tau) d\tau + \sigma_4 \int_0^t T_{41}(Z, \tau) dB_4(\tau), \\
M(t) - M(0) &= \int_0^t T_5(T, C, I, Z, M, \tau) d\tau + \sigma_5 \int_0^t T_{51}(M, \tau) dB_5(\tau).
\end{aligned}$$

If we choose to apply the classical Adams-Bashforth to the first component of the system, we have

$$\begin{aligned}
T_{n+1} &= T_n + \frac{3}{2}\Delta t T_1(T_n, C_n, I_n, Z_n, M_n, t_n) \\
&\quad - \frac{\Delta t}{2} T_1(T_{n-1}, C_{n-1}, I_{n-1}, Z_{n-1}, M_{n-1}, t_{n-1}) + \sigma_1 \int_{t_n}^{t_{n+1}} T_{11}(T, \tau) dB_1(\tau), \\
C_{n+1} &= C_n + \frac{3}{2}\Delta t T_2(T_n, C_n, I_n, Z_n, M_n, t_n) \\
&\quad - \frac{\Delta t}{2} T_2(T_{n-1}, C_{n-1}, I_{n-1}, Z_{n-1}, M_{n-1}, t_{n-1}) + \sigma_2 \int_{t_n}^{t_{n+1}} T_{21}(C, \tau) dB_2(\tau), \\
I_{n+1} &= I_n + \frac{3}{2}\Delta t T_3(T_n, C_n, I_n, Z_n, M_n, t_n) \\
&\quad - \frac{\Delta t}{2} T_3(T_{n-1}, C_{n-1}, I_{n-1}, Z_{n-1}, M_{n-1}, t_{n-1}) + \sigma_3 \int_{t_n}^{t_{n+1}} T_{31}(I, \tau) dB_3(\tau), \\
Z_{n+1} &= Z_n + \frac{3}{2}\Delta t T_4(T_n, C_n, I_n, Z_n, M_n, t_n) \\
&\quad - \frac{\Delta t}{2} T_4(T_{n-1}, C_{n-1}, I_{n-1}, Z_{n-1}, M_{n-1}, t_{n-1}) + \sigma_4 \int_{t_n}^{t_{n+1}} T_{41}(Z, \tau) dB_4(\tau), \\
M_{n+1} &= M_n + \frac{3}{2}\Delta t T_5(T_n, C_n, I_n, Z_n, M_n, t_n) \\
&\quad - \frac{\Delta t}{2} T_5(T_{n-1}, C_{n-1}, I_{n-1}, Z_{n-1}, M_{n-1}, t_{n-1}) + \sigma_5 \int_{t_n}^{t_{n+1}} T_{51}(M, \tau) dB_5(\tau).
\end{aligned}$$

Using a sequence of partition of the interval $[t_n, t_{n+1}]$, the last integrals can be approximated to

$$\begin{aligned}
T_{n+1} &= T_n + \frac{3}{2}\Delta t T_1(T_n, C_n, I_n, Z_n, M_n, t_n) \\
&\quad - \frac{\Delta t}{2} T_1(T_{n-1}, C_{n-1}, I_{n-1}, Z_{n-1}, M_{n-1}, t_{n-1}) + \sigma_1 \sum_{i=n-1}^n T_{11}(T_i, c_i) [B_1(t_{i+1}) - B_1(t_i)],
\end{aligned}$$

$$\begin{aligned}
 C_{n+1} &= C_n + \frac{3}{2}\Delta t T_2(T_n, C_n, I_n, Z_n, M_n, t_n) \\
 &\quad - \frac{\Delta t}{2} T_2(T_{n-1}, C_{n-1}, I_{n-1}, Z_{n-1}, M_{n-1}, t_{n-1}) + \sigma_2 \sum_{i=n-1}^n T_{21}(C_i, c_i) [B_2(t_{i+1}) - B_2(t_i)], \\
 I_{n+1} &= I_n + \frac{3}{2}\Delta t T_3(T_n, C_n, I_n, Z_n, M_n, t_n) \\
 &\quad - \frac{\Delta t}{2} T_3(T_{n-1}, C_{n-1}, I_{n-1}, Z_{n-1}, M_{n-1}, t_{n-1}) + \sigma_3 \sum_{i=n-1}^n T_{31}(I_i, c_i) [B_3(t_{i+1}) - B_3(t_i)], \\
 Z_{n+1} &= Z_n + \frac{3}{2}\Delta t T_4(T_n, C_n, I_n, Z_n, M_n, t_n) \\
 &\quad - \frac{\Delta t}{2} T_4(T_{n-1}, C_{n-1}, I_{n-1}, Z_{n-1}, M_{n-1}, t_{n-1}) + \sigma_4 \sum_{i=n-1}^n T_{41}(Z_i, c_i) [B_4(t_{i+1}) - B_4(t_i)], \\
 M_{n+1} &= M_n + \frac{3}{2}\Delta t T_5(T_n, C_n, I_n, Z_n, M_n, t_n) \\
 &\quad - \frac{\Delta t}{2} T_5(T_{n-1}, C_{n-1}, I_{n-1}, Z_{n-1}, M_{n-1}, t_{n-1}) + \sigma_5 \sum_{i=n-1}^n T_{51}(M_i, c_i) [B_5(t_{i+1}) - B_5(t_i)],
 \end{aligned}$$

where $c_i \in (t_n, t_{n+1})$.

5 Numerical simulations

Deterministic and stochastic modeling are two different approaches used in mathematical modeling to represent and analyze systems. Stochastic modeling of tumors provides insight into the inherent uncertainties and complexities associated with cancer biology. It allows researchers to better understand the range of possible outcomes so in this section, we show the numerical simulations for the considered stochastic tumor model which is given by

$$\begin{aligned}
 dT(t) &= \left(a + bI(t)C(t)T(t) \left(1 - \frac{T(t)}{p} \right) - cT(t) \right) + \sigma_1 T(t) dB_1(t), \\
 dC(t) &= \left(kC(t) \left(1 - \frac{C(t)}{q} \right) - eC(t)T(t)I(t) \right. \\
 &\quad \left. - zC(t)T(t)Z(t) - \tilde{m}M(t)C(t) \right) + \sigma_2 C(t) dB_2(t), \\
 dI(t) &= (-fI(t)) + \sigma_3 I(t) dB_3(t), \\
 dZ(t) &= (-\gamma Z(t)) + \sigma_4 Z(t) dB_4(t), \\
 dM(t) &= \left(r_M \left(1 - \frac{M(t)}{k_M} \right) M(t) + \tilde{p}C(t)M(t) - \tilde{d}M(t) \right) + \sigma_5 M(t) dB_5(t), \\
 T(0) &= T_0, C(0) = C_0, I(0) = I_0, Z(0) = Z_0 \text{ and } M(0) = M_0.
 \end{aligned}$$

For the numerical simulations of the system, we consider the values of the parameters as follows:

$$a = 10^{-4}, b = 0.175, c = 5 * 10^{-3}, k = 0.02, e = 0.15, f = 0.01, p = 1, q = 1, z = 1, \gamma = 0.001925, r_M = 0.64, k_M = 3.39, \tilde{p} = 4.5 * 10^{-9}, \tilde{d} = 0.55, \tilde{m} = 1.8 * 10^{-5}.$$

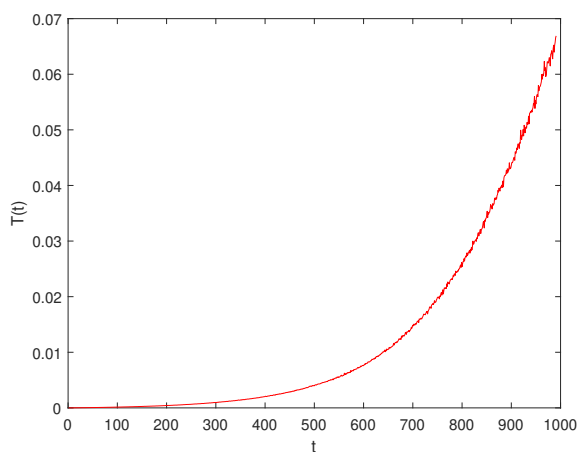
The initial conditions are given as follows:

$$T(0) = 0, C(0) = 1, I(0) = 4, Z(0) = 2 \text{ and } M(0) = 3.$$

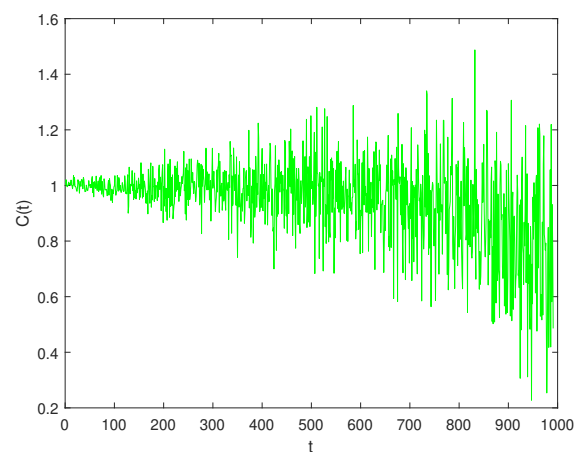
In the model, the densities of randomness values are given as figures

$$\sigma_1 = 0.001, \sigma_2 = 0.015, \sigma_3 = 0.012, \sigma_4 = 0.013, \sigma_5 = 0.014.$$

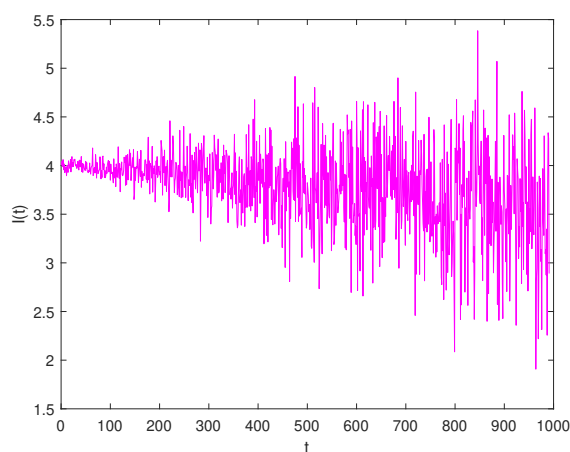
Tumors are influenced by a multitude of factors that exhibit probabilistic behavior. It is now strongly believed that even micro-biota have a role in cancer development and treatment. Chemotherapy, radiotherapy, and targeted drug therapy along with surgery are used to treat cancer caused by factors such as the likelihood of benefit from treatment, stage of cancer, cytogenetic of tumor, comorbidities and patients' performance status. Considering these complex behaviours of tumors, we observe that a more accurate depiction of the model's complexity arises when we examine the densities of randomness in the stochastic tumor model. These models assist researchers and clinicians in understanding the variety of tumor characteristics and developing strategies for tailored and adaptive cancer therapy by simulating a range of potential outcomes. Tumors are influenced by a multitude of factors that exhibit probabilistic behavior. Chemotherapy, radiotherapy, and drug therapy are used to treat cancer caused by factors such as genetics, environmental factors, lack of exercise, and stress. Cancer is a complex and dynamic system influenced by a multitude of factors so stochastic modeling provides a more realistic representation of these processes.



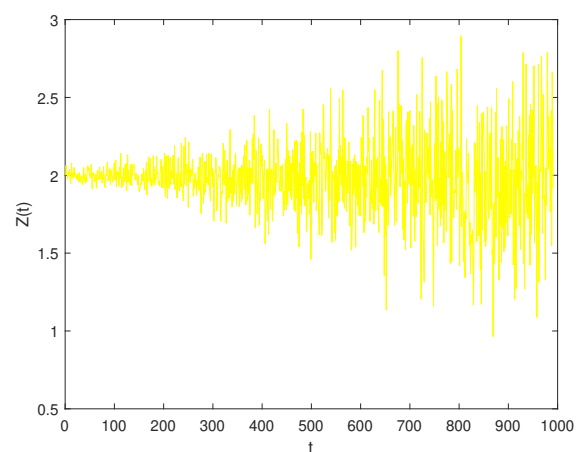
(a) Numerical simulation for CD8+T lymphocytes $T(t)$



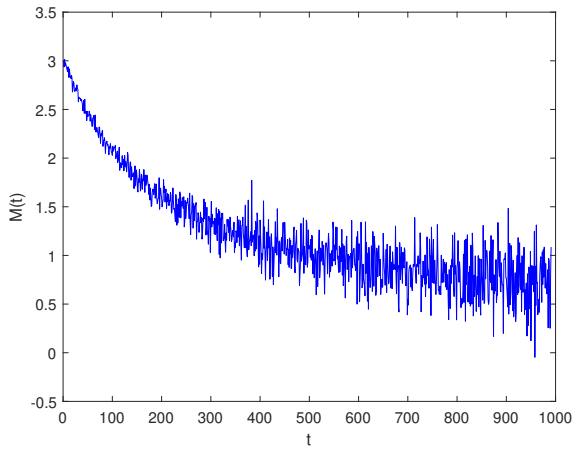
(b) Numerical simulation for cancer cells $C(t)$



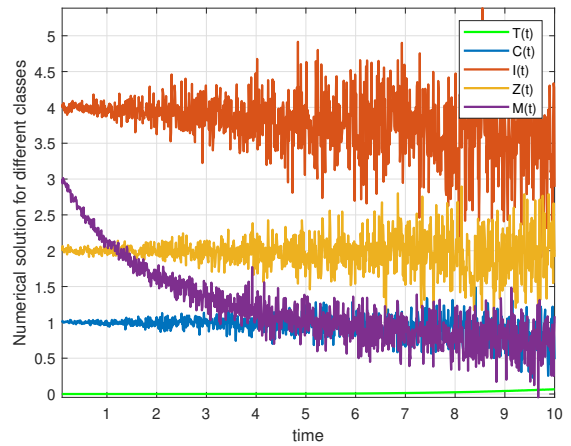
(c) Numerical simulation for IL-10 cytokine $I(t)$



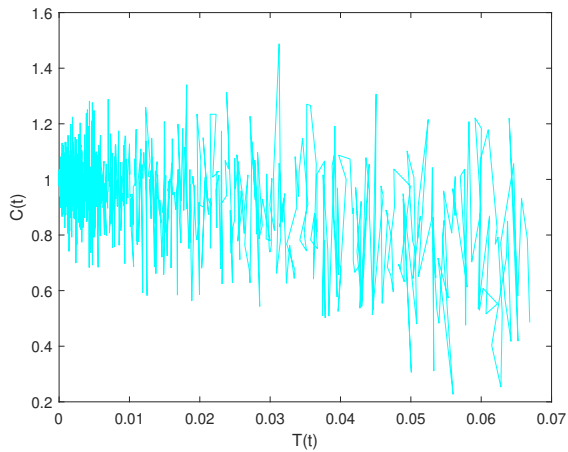
(d) Numerical simulation for anti-PD-L1 $Z(t)$



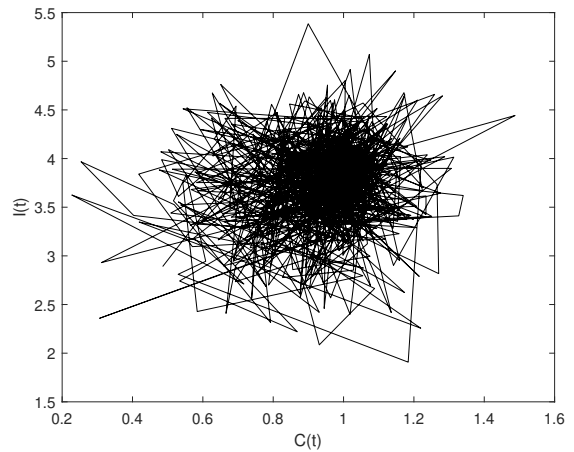
(e) Numerical simulation for makrophages $M(t)$



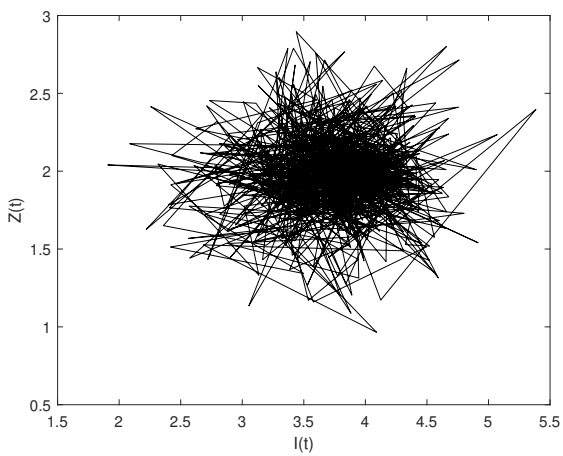
(f) Numerical simulation results of system for all classes $T(t), C(t), I(t), Z(t), M(t)$



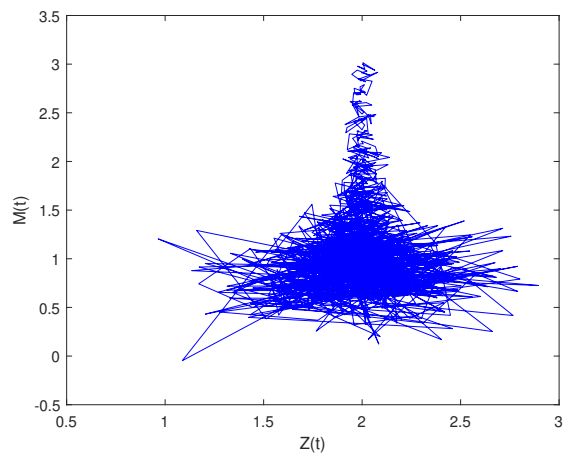
(g) Numerical simulation for $T - C$ phase



(h) Numerical simulation for $C - I$ phase



(i) Numerical simulation for $I - Z$ phase



(j) Numerical simulation for $Z - M$ phase

6 Conclusions

One important class of white blood cells in the immune system are macrophages. They are a component of the body's primary defense against diseases and foreign invaders which is the innate immune system. Also, macrophages are essential for both immune response and infection defense because they clear pathogens and detritus from the body and coordinate the intricate interactions between various immune system components. Given the importance of macrophage cells to the body, this study includes a discussion of a novel tumor model and monitored the propagation of the tumor model more comprehensively. The equilibrium points are produced and the conditions proving the solution's existence and exclusivity in relation to this tumor model become clear. Then, the model is scrutinized carefully in terms of stochastic theory. In the end, a number of numerical outputs for this model pertaining to the aforementioned stochastic model are presented here.

Declarations

Use of AI tools

The authors declare that they have not used Artificial Intelligence (AI) tools in the creation of this article.

Data availability statement

All data generated or analyzed during this study are included in this article.

Ethical approval

The authors state that this research complies with ethical standards. This research does not involve either human participants or animals.

Consent for publication

Not applicable

Conflicts of interest

The authors declare that they have no conflict of interest.

Funding

Not applicable

Author's contributions

N.Ö and İ.K.: Conceptualization, S.U. and T.İ.: Supervision, Investigation. N.Ö and İ.K.: Formal Analysis. İ.K.: Software. İ.K., S.U. and T.İ.: Validation. N.Ö., İ.K., S.U. and T.İ.: Writing-Review and Editing. The authors have read and agreed to the published version of the manuscript.

Acknowledgements

Not applicable

References

- [1] Global Cancer Observatory (GCO), Cancer Today, (2022). <https://gco.iarc.fr/today/data/factsheets/populations/900-world-fact-sheets>
- [2] Guyton, A.C. and Hall, J.E. *Textbook of Medical Physiology*. Elsevier: Pennsylvania, USA, (2006).

- [3] Hanahan, D. and Weinberg, R.A. Hallmarks of cancer: the next generation. *Cell*, 144(5), 646-674, (2011). [[CrossRef](#)]
- [4] Marsha, L., Conroy, K.R., Davis, J.L. and Embree, B.M. *Atlas Pathophysiology*. Lippincott Williams & Wilkins: Pennsylvania, USA, (2010).
- [5] Alberts, B., Johnson, A., Lewis, J., Raff, M., Roberts, K. and Walter, P. *Molecular Biology of the Cell*. Garland Science: New York, (2002).
- [6] Kumar, V., Abbas, A.K. and Aster, J.C. *Robbins Basic Pathology*. Elsevier: Netherlands, (2017).
- [7] Dennis, K.L., Blatner, N.R., Gounari, F. and Khazaie K. Current status of interleukin-10 and regulatory T-cells in cancer. *Current Opinion in Oncology*, 25(6), 637-645, (2013). [[CrossRef](#)]
- [8] Sheikhpour, E., Noorbakhsh, P., Foroughi, E., Farahnak, S., Nasiri, R. and Neamatzadeh, H. A Survey on the Role of Interleukin-10 in Breast Cancer: A Narrative. *Reports of Biochemistry and Molecular Biology*, 7(1), 30-37, (2018). [[CrossRef](#)]
- [9] Sheergojri, A.R., Iqbal, P., Agarwal, P. and Özdemir, N. Uncertainty-based Gompertz growth model for tumor population and its numerical analysis. *An International Journal of Optimization and Control: Theories & Applications*, 12(2), 137-150, (2022). [[CrossRef](#)]
- [10] Hammouch, Z., Yavuz, M. and Özdemir, N. Numerical solutions and synchronization of a variable-order fractional chaotic system. *Mathematical Modelling and Numerical Simulation with Applications*, 1(1), 11-23, (2021). [[CrossRef](#)]
- [11] Uçar, E. and Özdemir, N. New fractional cancer mathematical model via IL-10 cytokine and anti-PD-L1 inhibitor. *Fractal and Fractional*, 7(2), 151, (2023). [[CrossRef](#)]
- [12] Alla Hamou, A., Azroul, E., Diki, G. and Guedda, M. Effect of family and public health education in drug transmission: an epidemiological model with memory. *Modeling Earth Systems and Environment*, 9, 2809-2828, (2023). [[CrossRef](#)]
- [13] Evirgen, F. Transmission of Nipah virus dynamics under Caputo fractional derivative. *Journal of Computational and Applied Mathematics*, 418, 114654, (2023). [[CrossRef](#)]
- [14] Atede, A.O., Omame, A. and Inyama, S.C. A fractional order vaccination model for COVID-19 incorporating environmental transmission: a case study using Nigerian data. *Bulletin of Biomathematics*, 1(1), 78-110, (2023). [[CrossRef](#)]
- [15] Özdemir, N. and Uçar, E. Investigating of an immune system-cancer mathematical model with Mittag-Leffler kernel. *AIMS Mathematics*, 5(2), 1519-1531, (2020). [[CrossRef](#)]
- [16] Uçar, S., Evirgen, F., Özdemir, N. and Hammouch, Z. Mathematical analysis and simulation of a giving up smoking model within the scope of non-singular derivative. *Proceedings of the Institute of Mathematics and Mechanics*, 48, 84-99, (2022). [[CrossRef](#)]
- [17] Guo, Y., Fan, L. and Wang, X. Mathematical investigation of the role of re-polarisation of M2 in cancer therapy. *Discrete and Continuous Dynamical Systems - Series B*, 28(4), 2718-2744, (2023). [[CrossRef](#)]
- [18] Aguiar, M., Pinto C., Nieto, J.J. and Ribeiro, R.M. New trends on mathematical modeling and simulation of biological systems. *Chaos Solitons and Fractals*, 172, 113568, (2023). [[CrossRef](#)]
- [19] Yavuz, M., Ozdemir, N. and Okur, Y.Y. Generalized differential transform method for fractional partial differential equation from finance. In Proceedings, *International Conference on Fractional Differentiation and its Applications (ICFDA)*, pp. 778-785, Novi Sad, Serbia, (2016, July).
- [20] Ucar, E., Özdemir, N. and Altun, E. Fractional order model of immune cells influenced by

- cancer cells. *Mathematical Modelling of Natural Phenomena*, 14(3), 308, (2019). [[CrossRef](#)]
- [21] Paul, S., Mahata, A., Mukherjee, S., Das, M., Mali, P.C., Roy, B. et al. Study of fractional order SIR model with MH type treatment rate and its stability analysis. *Bulletin of Biomathematics*, 2(1), 85-113, (2024). [[CrossRef](#)]
- [22] Paul, S., Mahata, A., Karak, M., Mukherjee, S., Biswas, S. and Roy, B. A fractal-fractional order Susceptible-Exposed-Infected-Recovered (SEIR) model with Caputo sense. *Healthcare Analytics*, 5, 100317, (2024). [[CrossRef](#)]
- [23] Paul, S., Mahata, A., Mukherjee, S., Mali, P.C. and Roy, B. Dynamical behavior of fractional order SEIR epidemic model with multiple time delays and its stability analysis. *Examples and Counterexamples*, 4, 100128, (2023). [[CrossRef](#)]
- [24] Mahata, A., Roy, B., Mondal, S.P. and Alam, S. Application of ordinary differential equation in glucose-insulin regulatory system modeling in fuzzy environment. *Ecological Genetics and Genomics*, 3-5, 60-66, (2017). [[CrossRef](#)]
- [25] Evirgen, F. and Özdemir, N. A fractional order dynamical trajectory approach for optimization problem with HPM. In *Fractional Dynamics and Control* (pp. 145–155). New York: Springer, (2012). [[CrossRef](#)]
- [26] Ross, S.M. *Stochastic Processes*. Wiley: New York, (1996).
- [27] Burdzy, K. *Brownian Motion and its Applications to Mathematical Analysis*. Springer: Switzerland, (2014). [[CrossRef](#)]
- [28] Brown, R. XXVII. A brief account of microscopical observations made in the months of June, July and August 1827, on the particles contained in the pollen of plants; and on the general existence of active molecules in organic and inorganic bodies. *The Philosophical Magazine*, 4(21), 161-173, (1828). [[CrossRef](#)]
- [29] Ikram, R., Khan, A., Zahri, M., Saeed, A., Yavuz, M. and Kumam, P. Extinction and stationary distribution of a stochastic COVID-19 epidemic model with time-delay. *Computers in Biology and Medicine*, 141, 105115, (2022). [[CrossRef](#)]
- [30] Beghin L. and Caputo, M. Stochastic applications of Caputo-type convolution operators with nonsingular kernels. *Stochastic Analysis and Applications*, 41(2), 377-393, (2023). [[CrossRef](#)]
- [31] Koca, I. and Atangana, A. Theoretical and numerical analysis of a chaotic model with nonlocal and stochastic differential operators. *An International Journal of Optimization and Control: Theories & Applications*, 13(2), 181-192, (2023). [[CrossRef](#)]
- [32] Okuonghae, D. Analysis of a stochastic mathematical model for tuberculosis with case detection. *International Journal of Dynamics and Control*, 10, 734-747, (2022). [[CrossRef](#)]
- [33] Liping, C., Khan, M.A., Atangana, A. and Kumar, S. A new financial chaotic model in Atangana-Baleanu stochastic fractional differential equations. *Alexandria Engineering Journal*, 60(6), 5193-5204, (2021). [[CrossRef](#)]
- [34] Ali, I. and Khan, S.U. A dynamic competition analysis of stochastic fractional differential equation arising in finance via pseudospectral method. *Mathematics*, 11(6), 1328, (2023). [[CrossRef](#)]
- [35] Naim, M., Sabbar, Y. and Zeb, A. Stability characterization of a fractional-order viral system with the non-cytolytic immune assumption. *Mathematical Modelling and Numerical Simulation with Applications*, 2(3), 164-176, (2022). [[CrossRef](#)]
- [36] Tadmon, C. and Njike Tchaptchet, E.R. Impact of Financial Crisis on Economic Growth: A

- Stochastic Model. *Stochastics and Quality Control*, 37(1), 45-63, (2022). [[CrossRef](#)]
- [37] Uçar, E., Özdemir, N. and Altun, E. Qualitative analysis and numerical simulations of new model describing cancer. *Journal of Computational and Applied Mathematics*, 422, 114899, (2023). [[CrossRef](#)]
- [38] Ahmed, E., El-Sayed A.M.A. and El-Saka, H.A.A. Equilibrium points, stability and numerical solutions of fractional-order predator-prey and rabies models. *Journal of Mathematical Analysis and Applications*, 325(1), 542-553, (2007). [[CrossRef](#)]
- [39] Atangana, A. Mathematical model of survival of fractional calculus, critics and their impact: How singular is our world. *Advances in Difference Equations*, 2021(403), 1-59, (2021). [[CrossRef](#)]
- [40] Atangana, A. Extension of rate of change concept: From local to nonlocal operators with applications. *Results in Physics*, 19, 103515, (2020). [[CrossRef](#)]

Bulletin of Biomathematics (BBM)
(<https://bulletinbiomath.org>)



Copyright: © 2024 by the authors. This work is licensed under a Creative Commons Attribution 4.0 (CC BY) International License. The authors retain ownership of the copyright for their article, but they allow anyone to download, reuse, reprint, modify, distribute, and/or copy articles in *BBM*, so long as the original authors and source are credited. To see the complete license contents, please visit (<http://creativecommons.org/licenses/by/4.0/>).

How to cite this article: Uçar, S., Koca, İ., Özdemir, N. & İnci, T. (2024). A stochastic approach to tumor modeling incorporating macrophages. *Bulletin of Biomathematics*, 2(2), 162-181. <https://doi.org/10.59292/bulletinbiomath.2024007>



RESEARCH PAPER

Bifurcations on a discrete–time SIS–epidemic model with saturated infection rate

Hasan S. Panigoro ^{1,*}, Emli Rahmi ^{1,†}, Salmun K. Nasib ^{1,†}, Nur'ain Putri H. Gawa ^{1,†} and Olumuyiwa James Peter ^{2,†}

¹Biomathematics Research Group, Department of Mathematics, Universitas Negeri Gorontalo, Bone Bolango 96554, Indonesia, ²Department of Mathematical and Computer Sciences, University of Medical Sciences, Ondo City, Ondo State, Nigeria

* Corresponding Author

† hspanigoro@ung.ac.id (Hasan S. Panigoro); emlirahmi@ung.ac.id (Emli Rahmi); salmun@ung.ac.id (Salmun K. Nasib); aingawa0802@gmail.com (Nur'ain Putri H. Gawa); peterjames4real@gmail.com (Olumuyiwa James Peter)

Abstract

In this paper, we explore the complex dynamics of a discrete-time SIS (Susceptible-Infected-Susceptible)-epidemic model. The population is assumed to be divided into two compartments: susceptible and infected populations where the birth rate is constant, the infection rate is saturated, and each recovered population has a chance to become infected again. Two types of mathematical results are provided namely the analytical results which consist of the existence of fixed points and their dynamical behaviors, and the numerical results, which consist of the global sensitivity analysis, bifurcation diagrams, and the phase portraits. Two fixed points are obtained namely the disease-free and the endemic fixed points and their stability properties. Some numerical simulations are provided to present the global sensitivity analysis and the existence of some bifurcations. The occurrence of forward and period-doubling bifurcations has confirmed the complexity of the solutions.

Keywords: SIS-epidemic model; saturated infection rate; bifurcation

AMS 2020 Classification: 37N25; 92B05; 39A60; 92D25

1 Introduction

The mathematical modeling using a deterministic approach is a powerful tool to reduce the impact of the infectious disease [1–3]. In recent decades, two popular ways are used for the deterministic approaches namely the continuous-time and the discrete-time models. There are many epidemiological studies employing differential equations for the operator of the continuous time model. See [4–9] and references therein. For the discrete-time model, the difference equation is used and becomes popular due to the complexity of the dynamical behaviors in epidemiological

cases. Most of them propose the complexity of dynamical behaviors such as period-doubling and Neimark-Sacker bifurcations as well as the existence of chaotic solutions. See [10–17] and cited articles therein.

The classical epidemic model is given by Kermack and MacKendrick [18, 19] defined by

$$\frac{dS}{dt} = -\beta SI, \quad \frac{dI}{dt} = \beta SI - \rho I, \quad \frac{dR}{dt} = \rho I, \quad (1)$$

where S is the susceptible compartment, I is the infected compartment, R is the recovered compartment, β is the infection rate, and ρ is the recovery rate. Some modifications are applied to include the real phenomena in nature. For example, Federico et al. [20] include the optimal vaccination and the recovery rate to the susceptible compartment to model (1). In another way, Zhang and Qiao [21] focus on studying the bifurcation analysis of model (5) by assuming the infection rate is saturated and the population has a strong Allee effect. Interesting works were also given by Li and Eskandari [1] which focus on the analytical and numerical results of a discrete-time seasonally forced SIR epidemic model. On the other hand, Omame et al. [22] and Atede et al. [23] have focused on investigating the application of model (1) on COVID-19 transmission by involving the vaccination and the memory effect. Some of them have integrated deterministic and stochastic approaches to describe the dynamical behaviors in modelling [24–30]. Following those articles, in this work, we also focus on the mathematical results of a modified SIR model and do not specifically discuss an epidemiological case. The model is modified based on some assumptions as follows:

- (i) The constant birth rate is denoted by Λ .
- (ii) The population has a natural death rate denoted by δ_1 , δ_2 , and δ_3 which respectively define the natural death rate of susceptible, infected, and recovered compartments.
- (iii) The recovered individuals can be infected by disease again with the transfer rate to susceptible prey denoted by ω .
- (iv) The infection rate term βSI is replaced by the saturated infection rate term denoted by $\frac{\beta SI}{\eta + I}$. This infection rate term naturally occurs in the epidemic model since each population can protect itself from infection so that although the infection population increases, the infection rate will have a threshold [31–33].

Thus, model (1) becomes

$$\frac{dS}{dt} = \Lambda - \frac{\beta SI}{\eta + I} - \delta_1 S + \omega R, \quad \frac{dI}{dt} = \frac{\beta SI}{\eta + I} - \rho I - \delta_2 I, \quad \frac{dR}{dt} = \rho I - \delta_3 R - \omega R. \quad (2)$$

By assuming all recovered compartments can be infected again, we drop the recovered compartment R and hence the model (2) is simplified into

$$\begin{aligned} \frac{dS}{dt} &= \Lambda - \frac{\beta SI}{\eta + I} + \omega I - \delta_1 S, \\ \frac{dI}{dt} &= \frac{\beta SI}{\eta + I} - (\omega + \delta_2) I. \end{aligned} \quad (3)$$

Now, we adopt similar ways as in [34–36] to construct the discrete-time model using the forward

Euler scheme. We get

$$\begin{aligned}\frac{S_{n+1} - S_n}{h} &= \Lambda - \frac{\beta S_n I_n}{\eta + I_n} + \omega I_n - \delta_1 S_n, \\ \frac{I_{n+1} - I_n}{h} &= \frac{\beta S_n I_n}{\eta + I_n} - (\omega + \delta_2) I_n.\end{aligned}\tag{4}$$

From model (4), the simplification yields

$$\begin{aligned}S_{n+1} &= S_n + h \left(\Lambda - \frac{\beta S_n I_n}{\eta + I_n} + \omega I_n - \delta_1 S_n \right), \\ I_{n+1} &= I_n + h \left(\frac{\beta S_n I_n}{\eta + I_n} - (\omega + \delta_2) I_n \right).\end{aligned}\tag{5}$$

Based on the above description, we get the key contributions and the novelty of this research are given as follows:

- (i) The model is constructed using a saturated infection rate and all recovered individuals can be infected again. We also use the difference equation for the operator rather than the differential equation. According to our literature review, although the model is simple, we cannot find similar works as given by model (5).
- (ii) All possible dynamical behaviors of fixed point are analyzed namely sink, source, saddle, and non-hyperbolic.
- (iii) The most influential parameter concerning the basic reproduction number and the population density for each compartment is identified using the Partial Rank Correlation Coefficient (PRCC) along with Saltelli sampling to generate the data.
- (iv) More complex dynamics are provided numerically namely the forward and period-doubling bifurcations.

We organize this article as follows: In [Section 1](#), we give the introduction and model formulation. In [Section 2](#), we explore the dynamical behaviors of the model by identifying the feasible fixed points, the basic reproduction number, and their stability properties. In [Section 3](#), some numerical simulations are provided such as the global sensitivity analysis, forward, and period-doubling bifurcations by giving the PRCC bar chart, contour plots, PRCC time-series, bifurcation diagrams, and phase portraits around fixed points. We end this article by presenting a conclusion in [Section 4](#).

2 Analytical results and findings

We start investigating the feasible fixed point of model (5) by solving the following equation

$$\begin{aligned}S &= S + h \left(\Lambda - \frac{\beta S I}{\eta + I} + \omega I - \delta_1 S \right), \\ I &= I + h \left(\frac{\beta S I}{\eta + I} - (\omega + \delta_2) I \right).\end{aligned}\tag{6}$$

We find two fixed points on the axial and the interior of the model (5) which are discussed in the next subsections.

The disease-free fixed point

The first fixed point is given by the disease-free fixed point (DFF) denoted by

$$E_0 = \left(\frac{\Lambda}{\delta_1}, 0 \right),$$

which describes the condition when the disease disappears from the population. By following [37–41], we apply the next generation matrix to obtain the basic reproduction number (\mathcal{R}_0) which states the number of secondary infections caused by one primary infection in an entirely susceptible population. We get

$$\mathcal{R}_0 = \frac{\beta\Lambda}{(\omega + \delta_2) \delta_1 \eta}. \quad (7)$$

Now, we give the following theorem to present the dynamical behaviors of DFF.

Theorem 1 Let $h_a = \frac{2}{\delta_1}$ and $h_b = \frac{2\omega}{(1-\mathcal{R}_0)(\omega+\delta_2)}$. The DFF $E_0 = \left(\frac{\Lambda}{\delta_1}, 0 \right)$ is

- (i) a sink (locally asymptotically stable) if $\mathcal{R}_0 < 1$ and $h < \min\{h_a, h_b\}$; or
- (ii) a source if $\mathcal{R}_0 > 1$ and $h > h_a$; or if $\mathcal{R}_0 < 1$ and $h > \min\{h_a, h_b\}$; or
- (iii) a saddle if $h < h_b$ and $\mathcal{R}_0 > 1$; or if $h < h_a$ and $\mathcal{R}_0 < 1$ and $h > h_b$; or if $h > h_a$ and $\mathcal{R}_0 < 1$ and $h < h_b$; or
- (iv) a non-hyperbolic if $h = h_a$; or $\mathcal{R}_0 = 1$; or $\mathcal{R}_0 < 1$ and $h = h_b$.

Proof For DFF, we have the following Jacobian matrix:

$$J(S, I)|_{E_0} = \begin{bmatrix} 1 - \frac{2h}{h_a} & \frac{(\delta_1\omega\eta - \beta\Lambda)h}{\delta_1\omega\eta} \\ 0 & 1 - \frac{2h}{h_b} \end{bmatrix}.$$

Therefore, we obtain a pair of eigenvalues $\lambda_1 = 1 - \frac{2h}{h_a}$ and $\lambda_2 = 1 - \frac{2h}{h_b}$. By observing λ_1 , we have the following condition

- $|\lambda_1| < 1$ when $h < h_a$; and
- $|\lambda_1| = 1$ when $h = h_a$; and
- $|\lambda_1| > 1$ when $h > h_a$.

We also have the sign of λ_2 as follows.

- $|\lambda_2| < 1$ when $\mathcal{R}_0 < 1$ and $h < h_b$; and
- $|\lambda_2| = 1$ when $\mathcal{R}_0 = 1$ or; when $\mathcal{R}_0 < 1$ and $h = h_b$; and
- $|\lambda_2| > 1$ when $\mathcal{R}_0 > 1$; or when $\mathcal{R}_0 < 1$ and $h > h_b$.

Following Lemma 1 in [42], all statements given by **Theorem 1** are proven.

The endemic fixed point

The next fixed point is given by the endemic fixed point (EFP) defined by $\hat{E} = (\hat{S}, \hat{I})$ where $\hat{S} = \frac{(\omega+\delta_2)(\eta+\hat{I})}{\beta}$ and $\hat{I} = \frac{(\mathcal{R}_0-1)(\omega+\delta_2)\delta_1\eta}{\beta\delta_2+(\omega+\delta_2)\delta_1}$. The EFP describes the condition when the disease exists in the population where the existence condition is given by $\mathcal{R}_0 > 1$. To investigate the dynamics

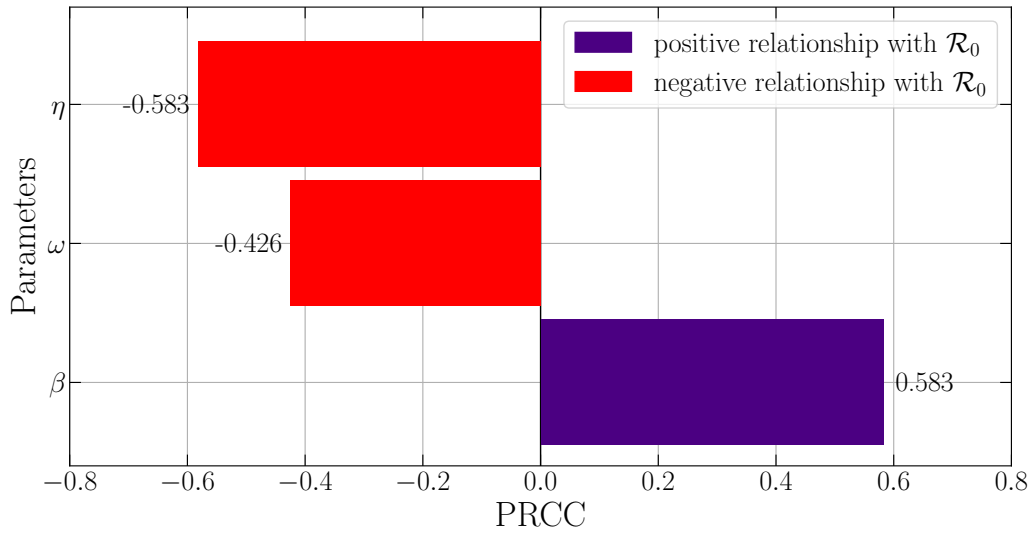


Figure 1. PRCC results with respect to the value of the basic reproduction number (\mathcal{R}_0). The infection rate (β) becomes the most influential parameter to the value of \mathcal{R}_0

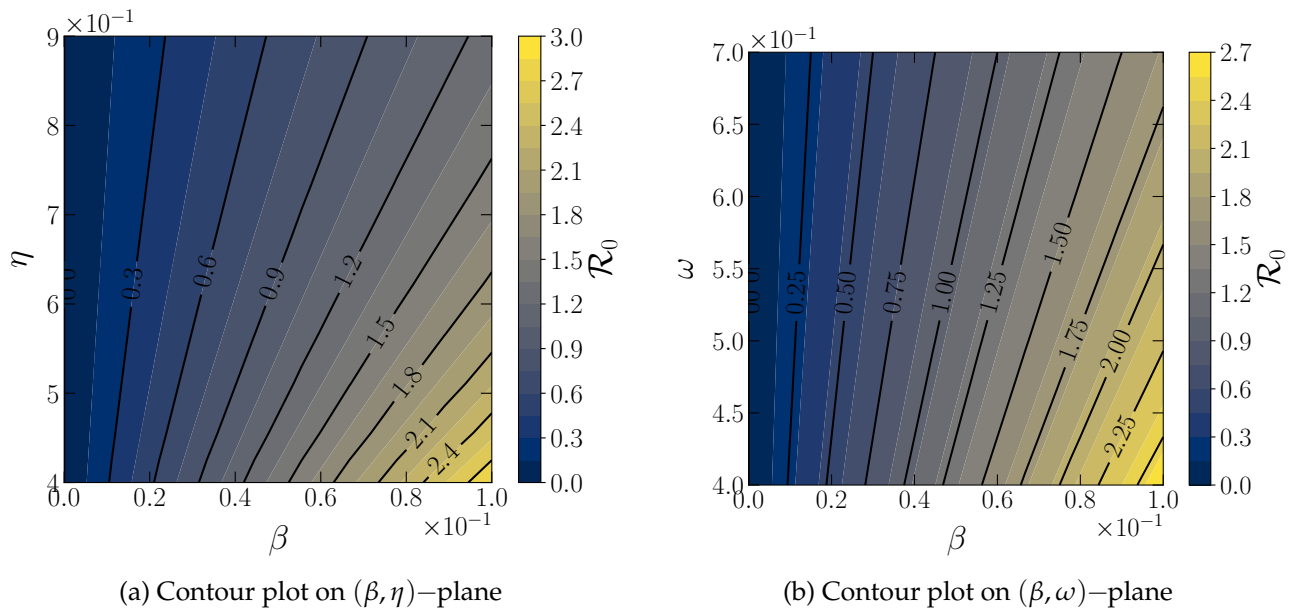


Figure 2. The contour plots of (a) (β, η) , and (b) (β, ω) respect to the values of \mathcal{R}_0 . The parameter β is directly proportional while η and ω is inversely proportional to \mathcal{R}_0

around EFP, we do linearization around EFP. The Jacobian matrix at EFP is given by

$$J(S, I)|_{\hat{E}} = \begin{bmatrix} 1 - h \left(\frac{(\beta + \delta_1)\hat{I} + \delta_1\eta}{\eta + \hat{I}} \right) & -h \left(\frac{\delta_2\eta - \omega\hat{I}}{\eta + \hat{I}} \right) \\ \frac{\beta\hat{I}h}{\eta + \hat{I}} & 1 - \frac{(\omega + \delta_2)\hat{I}h}{\eta + \hat{I}} \end{bmatrix},$$

and hence, we have eigenvalues

$$\lambda_{1,2} = \frac{1}{2} \left(\xi \pm \sqrt{\xi^2 - 4\zeta} \right), \tag{8}$$

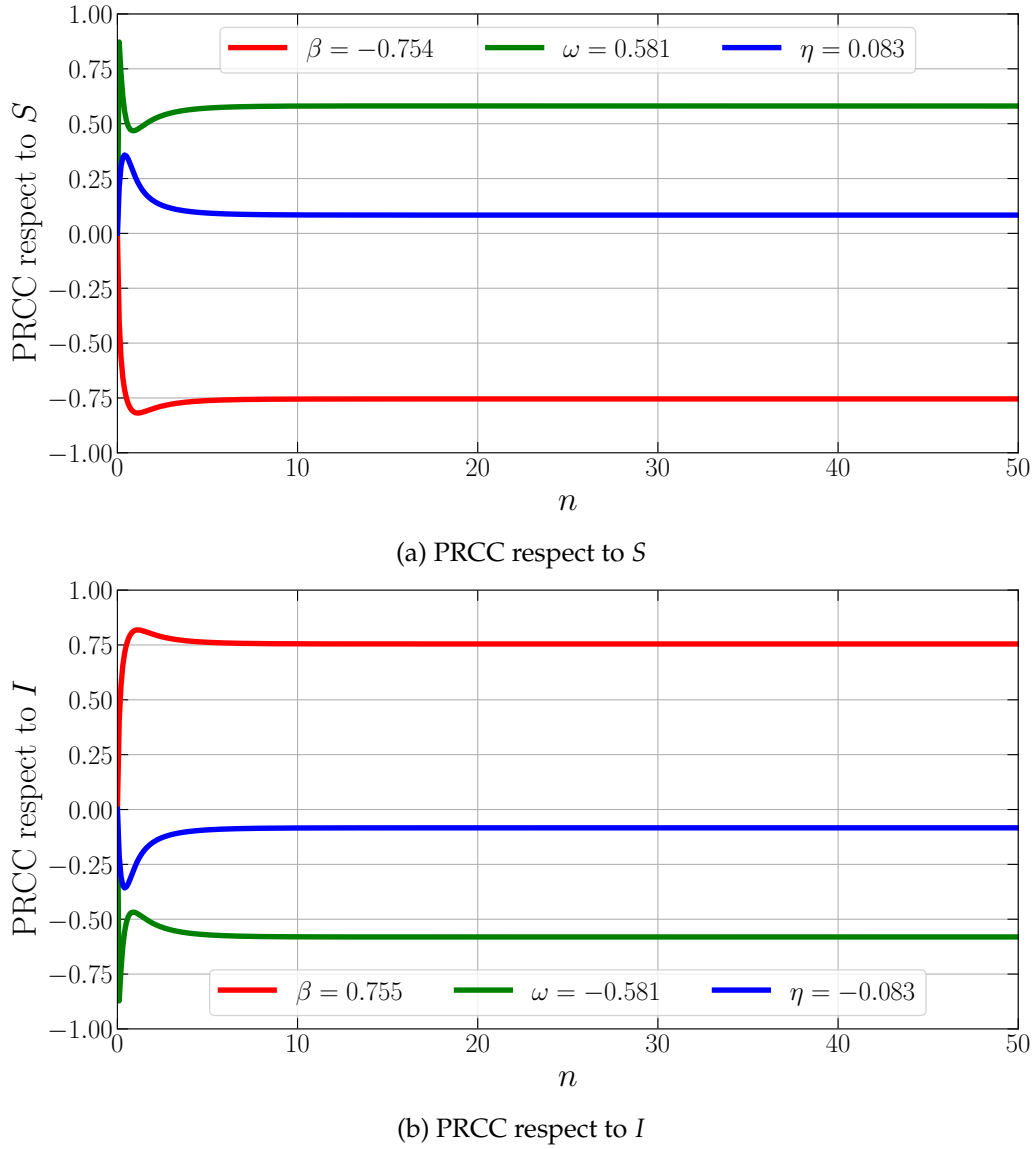


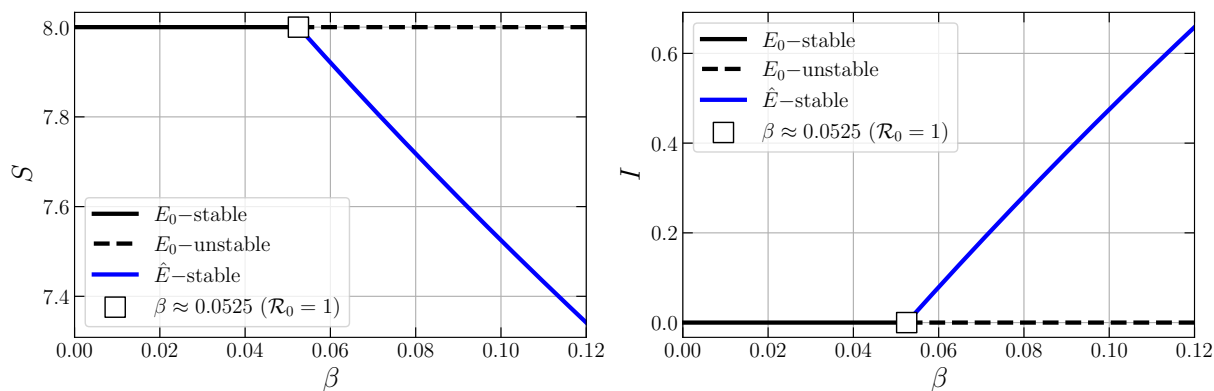
Figure 3. PRCC results respect to the density of susceptible individuals (S) and infected individuals (I). The parameter β is directly proportional to I and inversely proportional to S while η and ω are opposite to it

where

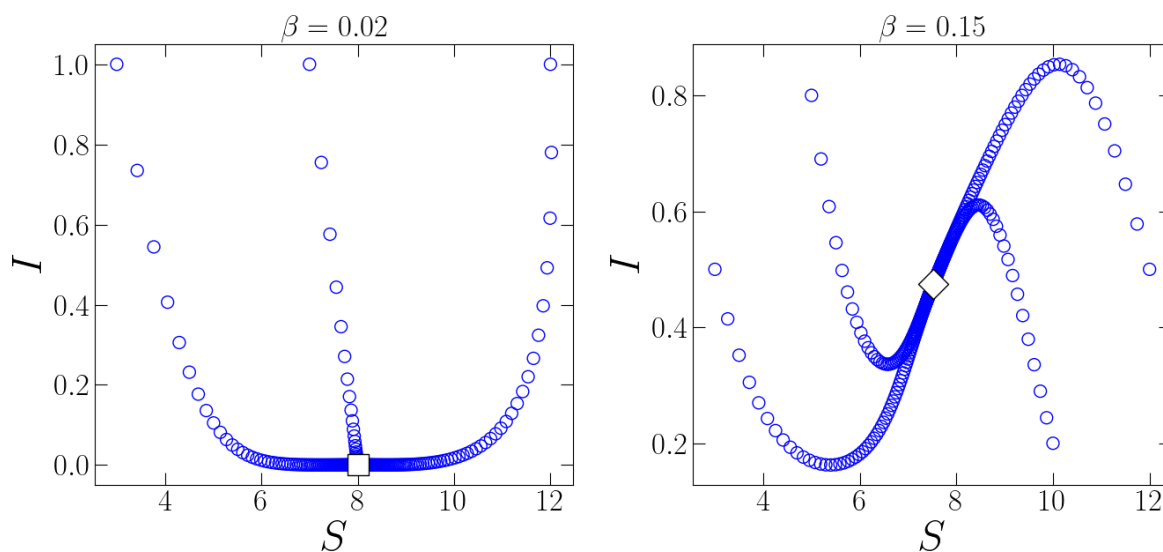
$$\begin{aligned}\xi &= 2 - \frac{h}{\eta + \hat{I}} [((\beta + \delta_1) - (\omega + \delta_2)) \hat{I} + \delta_1 \eta], \\ \zeta &= 1 - \frac{h}{\eta + \hat{I}} [((\omega + \delta_2) + (\beta + \delta_1)) \hat{I} + \delta_1 \eta] \\ &\quad + \frac{h^2 \hat{I}}{\eta + \hat{I}} [(\omega + \delta_2) \delta_1 + \beta \delta_2].\end{aligned}$$

Let $\Phi(\theta) = \theta^2 - \theta\xi + \zeta$. We have

$$\begin{aligned}\Phi(1) &= 1 - \xi + \zeta \\ &= [h((\omega + \delta_2) \delta_1 + \beta \delta_2) - 2(\omega + \delta_2)] \frac{h \hat{I}}{\eta + \hat{I}},\end{aligned}$$



(a) Bifurcation diagram driven by β



(b) Phase portrait for different values of β

Figure 4. Bifurcation diagrams and phase portraits of model (5) driven by β using parameter values: $\Lambda = 0.8$, $\eta = 0.6$, $\omega = 0.6$, $\delta_1 = 0.1$, $\delta_2 = 0.1$, and $h = 0.1$

which satisfies $\Phi(1) > 0$ when $h > \frac{2(\omega+\delta_2)}{(\omega+\delta_2)\delta_1+\beta\delta_2}$. We also achieve

$$\begin{aligned} \Phi(-1) &= 1 + \zeta + \zeta \\ &= 4 - \frac{2h}{\eta + \hat{I}} [(\beta + \delta_1) \hat{I} + \delta_1 \eta] + \frac{h^2 \hat{I}}{\eta + \hat{I}} [(\omega + \delta_2) \delta_1 + \beta \delta_2]. \end{aligned}$$

Following Lemmas 1 and 2 in [42], we have the following theorem as the results.

Theorem 2 Let $\mathcal{R}_0 > 1$ and $h > \frac{2(\omega+\delta_2)}{(\omega+\delta_2)\delta_1+\beta\delta_2}$. The EFP is

- (i) a sink if $\Phi(-1) > 0$ and $\zeta < 1$; or
- (ii) a source if $\Phi(-1) > 0$ and $\zeta > 1$; or
- (iii) a saddle if $\Phi(-1) < 0$; or
- (iv) a non-hyperbolic if $\Phi(-1) = 0$ and $\zeta \neq 0, 2$; or if $\zeta^2 < 4\zeta$ and $\zeta = 1$.

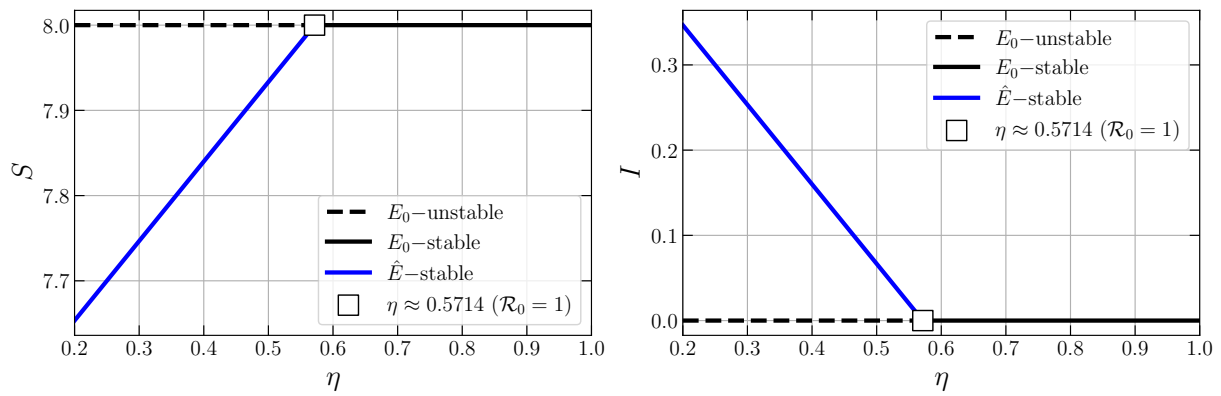
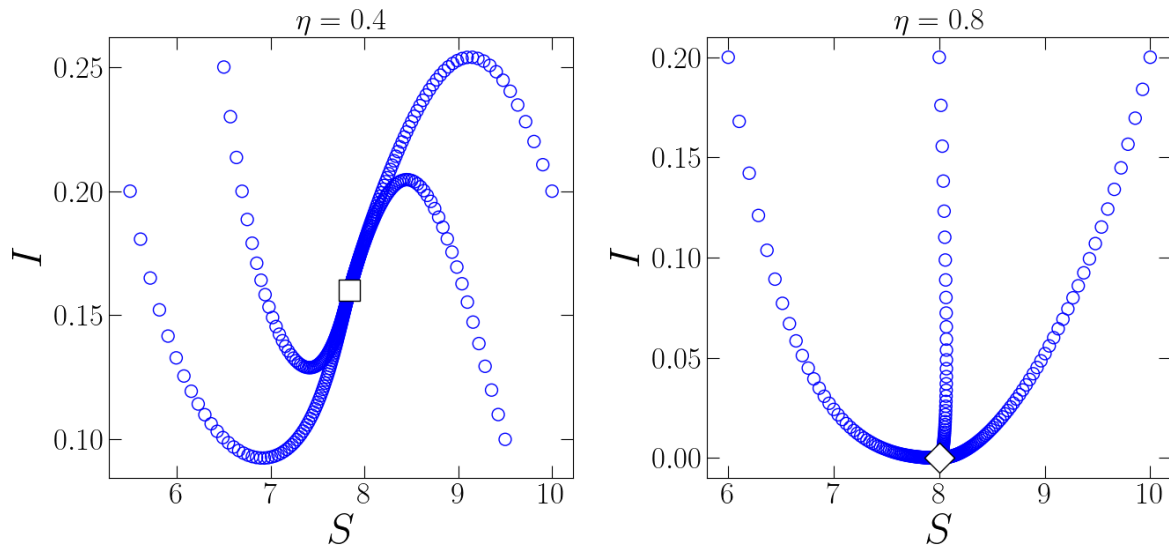
(a) Bifurcation diagram driven by η (b) Phase portrait for different values of η

Figure 5. Bifurcation diagrams and phase portraits of model (5) driven by η using parameter values: $\Lambda = 0.8$, $\beta = 0.05$, $\omega = 0.6$, $\delta_1 = 0.1$, $\delta_2 = 0.1$, and $h = 0.1$

3 Numerical results

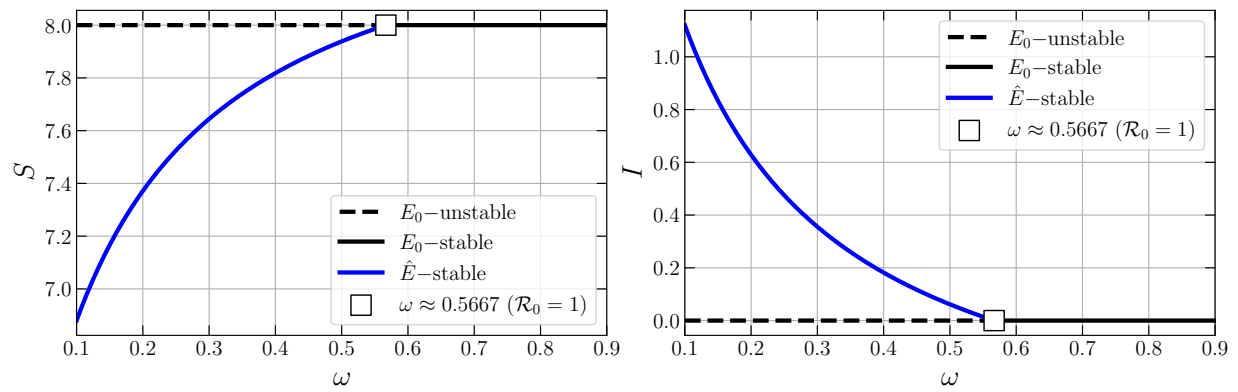
To explore the complexity of the dynamical behaviors, some numerical simulations are demonstrated. Since no one specific epidemiological case is related to the model, we use hypothetical parameter values for the simulations. We first set the parameter values as follows.

$$\Lambda = 0.8, \beta = 0.01, \eta = 0.6, \delta_1 = 0.1, \delta_2 = 0.1, \omega = 0.6, h = 0.5. \quad (9)$$

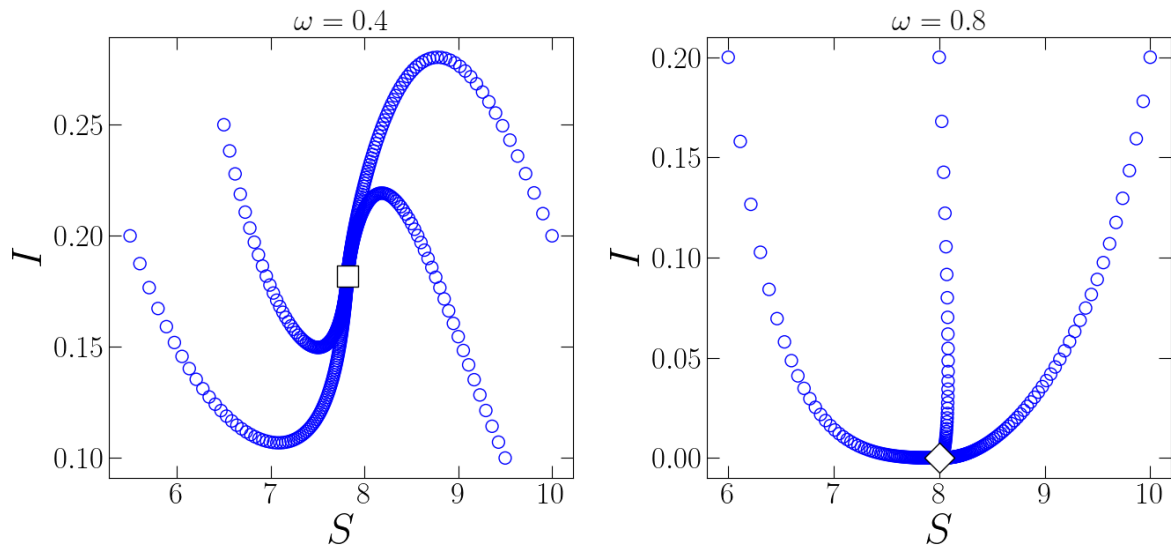
By using the parameter values (9), we give the following subsections to show the global sensitivity analysis, forward, and period-doubling bifurcations.

Global sensitivity analysis

To investigate the most influential parameter of model (5), we perform the global sensitivity analysis [43, 44]. The Partial Rank Correlation Coefficient (PRCC) [45] is employed for parameter ranking along with Saltelli sampling [46] to generate the sample data around the parameter values given by (9). We consider the basic reproduction number and the population densities for the



(a) Bifurcation diagram driven by η



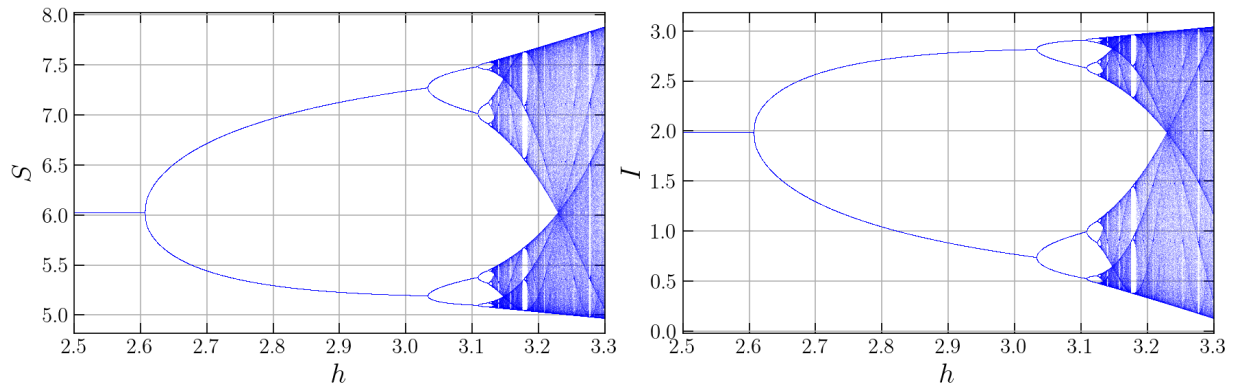
(b) Phase portrait for different values of ω

Figure 6. Bifurcation diagrams and phase portraits of model (5) driven by ω using parameter values: $\Lambda = 0.8$, $\beta = 0.05$, $\eta = 0.6$, $\delta_1 = 0.1$, $\delta_2 = 0.1$, and $h = 0.1$

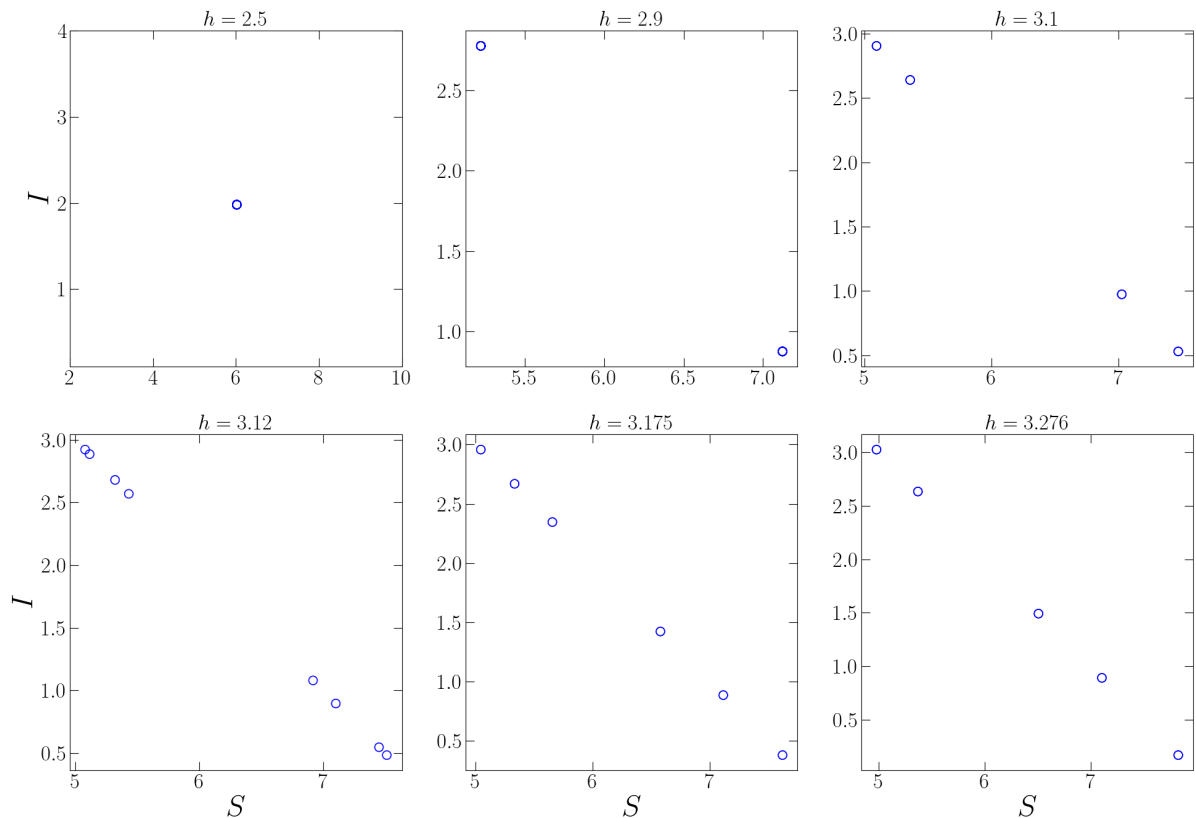
constraint function and the rank of the parameter as the objective function. Since the birth rate (Λ) and the natural death rate δ_i , $i = 1, 2, 3$ can be obtained directly if the real data exists, we only focus on the impact of the infection rate (β), the recovery rate (ω), and the half-saturation constant (η).

We first investigate the most influential parameter of model (5) concerning the value of the basic reproduction number (\mathcal{R}_0). As a result, we have the infection rate (β) become the most influential parameter with PRCC 0.583 while η and ω are respectively at the second and the third rank with PRCC -0.583 and -0.426 . See the bar chart of PRCC results in Figure 1. We also confirm that β has a positive relationship with \mathcal{R}_0 while η and ω have a negative relationship with \mathcal{R}_0 by observing the sign of the PRCC results. This means that if the value of β increases, then the value of \mathcal{R}_0 increases. If the value of η or ω increases, the value of \mathcal{R}_0 will decrease. We give the contour plot of these conditions in Figure 2.

Now, we investigate the most influential parameter concerning the density of the susceptible compartment (S) and the infected compartment (I). Again, by applying PRCC and Saltelli sampling as well as computing the PRCC value for n in range $[0, 50]$, we find β still becomes the most influential parameter to the density of S and I . See the numerical results in Figure 3.



(a) Bifurcation diagram



(b) Some periodic solutions

Figure 7. Bifurcation diagram and periodic solutions of model (5) driven by h using parameter values: $\Lambda = 0.8$, $\beta = 0.05$, $\eta = 0.6$, $\omega = 0.6$, $\delta_1 = 0.1$, $\delta_2 = 0.1$, and $h = 0.1$

From the sign of the PRCC values, we also verify that β has a negative relationship with S and a positive relationship with I , while η and ω have a positive relationship with S and a negative relationship with I . This means that when the infection rate increases, the density of the susceptible compartment decreases while the density of the infected compartment increases. When the recovery rate and the half-saturation constant increase, the density of the susceptible compartment increases, and the density of the infected compartment decreases.

Forward bifurcations

We then investigate the impact of the infection rate (β), the half-saturation constant (η), and the recovery rate (ω) on the dynamics of model (5). Let the parameter values as in (9). By varying

the value of β in the interval $[0, 0.12]$, we investigate the existence and stability condition for each fixed point. As a result, we have the bifurcation diagram as given in [Figure 4\(a\)](#) and phase portrait in [Figure 4\(b\)](#). When $\beta < \beta^*$ where $\beta^* \approx 0.0525$ (or $\mathcal{R}_0 \approx 1$), the nearby solution converges to DFF $E_0 = (8, 0)$ which indicate the DFF is a sink. When β crosses β^* , the DFF loses its stability followed by the occurrence of EFP \hat{E} where the DFF becomes a saddle and EFP is a sink. This phenomenon is called forward bifurcation where β is the bifurcation parameter and β^* is the bifurcation point. Similar dynamical behaviors are presented when the half saturation parameter (η) and the recovery rate (ω) is varied. Using (9) and varying η in interval $[0.2, 1]$, we have a forward bifurcation where η and $\eta^* \approx 0.5714$ (or $\mathcal{R}_0 \approx 1$) are respectively the bifurcation parameter and bifurcation point. The forward bifurcation also occurs when ω crosses $\omega^* \approx 0.5667$ which confirms that ω and ω^* respectively become the bifurcation parameter and bifurcation point. See [Figure 5](#) and [Figure 6](#) for the numerical simulations of the bifurcation diagrams and their corresponding phase portraits. At these phenomena, we conclude that β , η , and ω have impacts on the existence and stability of DFE and FEP. The disease in the population will become extinct or endemic when the infection rate, half saturation constant, and the recovery rate are varied.

Period-doubling bifurcation

In this subsection, we present the occurrence of the sequence of period-doubling bifurcation as well as the example of the period of the solutions when the step-size (h). The parameter values given by (9) are set and h is varied in $[2.5, 3.3]$. As a result, we have [Figure 7\(a\)](#) as the bifurcation diagram. We confirm that the sink EFP becomes unstable when crosses $h \approx 2.61$ and a period-2 solution occurs. Each branch of the periodic solution also split into the other period-2 solution and so forth. This indicates the existence of the sequence of period-doubling bifurcation. We give [Figure 7\(b\)](#) to show some of the periodic solutions such as a sink for $h = 2.5$, period-2 for $h = 2.9$, period-4 for $h = 3.1$, period-8 for $h = 3.12$, period-6 for $h = 3.175$, and period-5 for $h = 3.276$. This phenomenon shows that the endemic point may lose its stability when the step-size becomes larger. Therefore, if we have less data for some interval of time, the dynamical behaviors may change via period-doubling bifurcation and the forecasting will be wrong.

4 Conclusion

The discrete-time SIS-epidemic model with a saturated infection rate has been studied. Some analytical and numerical results have been investigated. Two fixed points have been identified namely disease-free and endemic fixed points as well as the basic reproduction number. We have shown that the existence and stability of each fixed point depend on the basic reproduction number. More information about the dynamics of the model has been explored numerically. The PRCC along with Saltelli sampling has been used to investigate the most influential parameter concerning the value of the basic reproduction number and the density of each compartment which shows that the infection rate becomes the most influenced one. The existence of some bifurcations is also demonstrated namely forward bifurcations and period-doubling bifurcation. We conclude that the infection rate, the half-saturation constant, and the recovery rate have an impact not only on the stability of the fixed points but also on the occurrence of forward bifurcation. Although the model is mathematically explored such as the stability condition, sensitivity analysis, and some bifurcation phenomena, this work has less epidemiological interpretation since we do not apply this model to any epidemiological cases. Moreover, the model also studies two compartments only, which means we can explore more by adding some compartments based on the real phenomena in nature. This limitation will become interesting to study further.

Declarations

Use of AI tools

The authors declare that they have not used Artificial Intelligence (AI) tools in the creation of this article.

Data availability statement

All data generated or analyzed during this study are included in this article.

Ethical approval

The authors state that this research complies with ethical standards. This research does not involve either human participants or animals.

Consent for publication

Not applicable

Conflicts of interest

The authors declare that they have no conflict of interest.

Funding

This research was funded by Lembaga Penelitian dan Pengabdian Kepada Masyarakat-Universitas Negeri Gorontalo via PNBP-UNG with DIPA-UNG No. SP DIPA-023.17.2.677521/2023/2023, under contract No. B/704/UN47.D1/PT.01.03/2023.

Author's contributions

H.S.P.: Conceptualization, Methodology, Validation, Writing - Review & Editing, Supervision, Project Administration, Funding Acquisition. E.R.: Conceptualization, Methodology, Validation, Resources, Writing - Original Draft, Visualization, Supervision, Project Administration, Funding Acquisition. S.K.N.: Conceptualization, Formal Analysis, Resources, Writing - Original Draft N.P.H.G.: Software, Formal Analysis, Investigation, Data Curation, Writing - Original Draft, Visualization O.J.P.: Software, Validation, Investigation, Writing - Review & Editing. All authors discussed the results and contributed to the final manuscript.

Acknowledgements

The authors express their profound gratitude to the specialists who willingly imparted their knowledge and insights, which greatly aided in the creation of this manuscript.

References

- [1] Li, B. and Eskandari, Z. Dynamical analysis of a discrete-time SIR epidemic model. *Journal of the Franklin Institute*, 360(12), 7989-8007, (2023). [[CrossRef](#)]
- [2] Phukan, J. and Dutta, H. Dynamic analysis of a fractional order SIR model with specific functional response and Holling type II treatment rate. *Chaos, Solitons & Fractals*, 175(1), 114005, (2023). [[CrossRef](#)]
- [3] Wu, P. and Feng, Z. Global dynamics of a space-age structured COVID-19 model coupling within-host infection and between-host transmission. *Communications in Nonlinear Science and Numerical Simulation*, 131, 107801, (2024). [[CrossRef](#)]

- [4] Peter, O.J., Panigoro, H.S., Ibrahim, M.A., Otunuga, O.M., Ayoola, T.A. and Oladapo, A.O. Analysis and dynamics of measles with control strategies: a mathematical modeling approach. *International Journal of Dynamics and Control*, 11, 2538-2552, (2023). [[CrossRef](#)]
- [5] Xu, C., Yu, Y., Ren, G., Sun, Y. and Si, X. Stability analysis and optimal control of a fractional-order generalized SEIR model for the COVID-19 pandemic. *Applied Mathematics and Computation*, 457, 128210, (2023). [[CrossRef](#)]
- [6] Sadki, M., Harroudi, S. and Allali, K. Fractional-order SIR epidemic model with treatment cure rate. *Partial Differential Equations in Applied Mathematics*, 8, 100593, (2023). [[CrossRef](#)]
- [7] Paul, A.K., Basak, N. and Kuddus, M.A. Mathematical analysis and simulation of COVID-19 model with booster dose vaccination strategy in Bangladesh. *Results in Engineering*, 21, 101741, (2024). [[CrossRef](#)]
- [8] Centres, P.M., Perez-Morelo, D.J., Guzman, R., Reinaudi, L. and Gimenez, M.C. Diffusion model for the spread of infectious diseases: SIR model with mobile agents. *Physica A: Statistical Mechanics and its Applications*, 633, 129399, (2024). [[CrossRef](#)]
- [9] Cui, W. and Zhao, Y. Saddle-node bifurcation and Bogdanov-Takens bifurcation of a SIRS epidemic model with nonlinear incidence rate. *Journal of Differential Equations*, 384, 252-278, (2024). [[CrossRef](#)]
- [10] Hu, Z., Teng, Z. and Jiang, H. Stability analysis in a class of discrete SIRS epidemic models. *Nonlinear Analysis: Real World Applications*, 13(5), 2017-2033, (2012). [[CrossRef](#)]
- [11] Din, Q. and Ishaque, W. Bifurcation analysis and chaos control in discrete-time eco-epidemiological models of pelicans at risk in the Salton Sea. *International Journal of Dynamics and Control*, 8, 132-148, (2020). [[CrossRef](#)]
- [12] Szabadváry, J.H. and Zhou, Y. On qualitative analysis of a discrete time SIR epidemical model. *Chaos, Solitons & Fractals: X*, 7, 100067, (2021). [[CrossRef](#)]
- [13] George, R., Gul, N., Zeb, A., Avazzadeh, Z., Djilali, S. and Rezapour, S. Bifurcations analysis of a discrete time SIR epidemic model with nonlinear incidence function. *Results in Physics*, 38, 105580, (2022). [[CrossRef](#)]
- [14] Al-Basyouni, K.S. and Khan, A.Q. Discrete-time COVID-19 epidemic model with chaos, stability and bifurcation. *Results in Physics*, 43, 106038, (2022). [[CrossRef](#)]
- [15] Ghosh, D., Santra, P.K., Mahapatra, G.S., Elsonbaty, A. and Elsadany, A.A. A discrete-time epidemic model for the analysis of transmission of COVID19 based upon data of epidemiological parameters. *European Physical Journal: Special Topics*, 231, 3461-3470, (2022). [[CrossRef](#)]
- [16] He, Z.Y., Abbes, A., Jahanshahi, H., Alotaibi, N.D. and Wang, Y. Fractional-order discrete-time SIR epidemic model with vaccination: chaos and complexity. *Mathematics*, 10(2), 1-18, (2022). [[CrossRef](#)]
- [17] Knopov, P.S. and Korkhin, A.S. Dynamic models of epidemiology in discrete time taking into account processes with lag. *International Journal of Dynamics and Control*, 11, 2193-2214, (2023). [[CrossRef](#)]
- [18] Kermack, W.O. and McKendrick, A.G. A contribution to the mathematical theory of epidemics. *Proceedings of the Royal Society of London. Series A, Containing Papers of a Mathematical and Physical Character*, 115(772), 700-721, (1927). [[CrossRef](#)]
- [19] Edelstein-Keshet, L. *Mathematical Models in Biology*. SIAM: Philadelphia, (2005). [[CrossRef](#)]
- [20] Federico, S., Ferrari, G. and Torrente, M.L. Optimal vaccination in a SIRS epidemic model.

Economic Theory, 77, 49-74, (2024). [[CrossRef](#)]

- [21] Zhang, J. and Qiao, Y. Bifurcation analysis of an SIR model with saturated incidence rate and strong Allee effect. *Journal of Biological Systems*, 32(01), 1-36, (2023). [[CrossRef](#)]
- [22] Omame, A. and Abbas, M. The stability analysis of a co-circulation model for COVID-19, dengue, and zika with nonlinear incidence rates and vaccination strategies. *Healthcare Analytics*, 3, 100151, (2023). [[CrossRef](#)]
- [23] Atede, A.O., Omame, A. and Inyama, S.C. A fractional order vaccination model for COVID-19 incorporating environmental transmission: a case study using Nigerian data. *Bulletin of Biomathematics*, 1(1), 78–110, (2023). [[CrossRef](#)]
- [24] Kiouach, D. and Boulaasair, L. Stationary distribution and dynamic behaviour of a stochastic SIVR epidemic model with imperfect vaccine. *Journal of Applied Mathematics*, 2018, 1291402, (2018). [[CrossRef](#)]
- [25] Coulibaly, B.D., Ghizlane, C. and El Khomssi, M. An approach to stochastic differential equations for long-term forecasting in the presence of α -stable noise: an application to gold prices. *Mathematical Modelling and Numerical Simulation with Applications*, 4(2), 165-192, (2024). [[CrossRef](#)]
- [26] Boulaasair, L., Bouzahir, H., Vargas, A.N. and Diop, M.A. Existence and uniqueness of solutions for stochastic urban-population growth model. *Frontiers in Applied Mathematics and Statistics*, 8, 960399, (2022). [[CrossRef](#)]
- [27] Aydın, N.S. A seismic-risk-based bi-objective stochastic optimization framework for the pre-disaster allocation of earthquake search and rescue units. *Mathematical Modelling and Numerical Simulation with Applications*, 4(3), 370-394, (2024). [[CrossRef](#)]
- [28] Yavuz, M., Coşar, F.Ö., Günay, F. and Özdemir, F.N. A new mathematical modeling of the COVID-19 pandemic including the vaccination campaign. *Open Journal of Modelling and Simulation*, 9(3), 299-321, (2021). [[CrossRef](#)]
- [29] Boulaasair, L. Threshold properties of a stochastic epidemic model with a variable vaccination rate. *Bulletin of Biomathematics*, 1(2), 177–191, (2023). [[CrossRef](#)]
- [30] Yavuz, M., Boulaasair, L., Bouzahir, H., Diop, M.A. and Benaid, B. The impact of two independent Gaussian white noises on the behavior of a stochastic epidemic model. *Journal of Applied Mathematics and Computational Mechanics*, 23(1), 121–134, (2024). [[CrossRef](#)]
- [31] Bentaleb, D., Harroudi, S., Amine, S. and Allali, K. Analysis and optimal control of a multi-strain SEIR epidemic model with saturated incidence rate and treatment. *Differential Equations and Dynamical Systems*, 31(4), 907-923, (2023). [[CrossRef](#)]
- [32] Sun, D., Li, Q. and Zhao, W. Stability and optimal control of a fractional SEQIR epidemic model with saturated incidence rate. *Fractal and Fractional*, 7(7), 533, (2023). [[CrossRef](#)]
- [33] Bounkaicha, C. and Allali, K. Modelling disease spread with spatio-temporal fractional derivative equations and saturated incidence rate. *Modeling Earth Systems and Environment*, 10, 259-271, (2024). [[CrossRef](#)]
- [34] Ahmed, R., Rafaqat, M., Siddique, I. and Arefin, M.A. Complex dynamics and chaos control of a discrete-time predator-prey model. *Discrete Dynamics in Nature and Society*, 2023, 8873611, (2023). [[CrossRef](#)]
- [35] Hamada, M.Y., El-Azab, T. and El-Metwally, H. Bifurcation analysis of a two-dimensional discrete-time predator–prey model. *Mathematical Methods in the Applied Sciences*, 46(4), 4815-4833, (2023). [[CrossRef](#)]

- [36] Panigoro, H.S., Resmawan, R., Rahmi, E., Beta, M.A. and Sidik, A.T.R. The existence of a limit-cycle of a discrete-time Lotka-Volterra model with fear effect and linear harvesting. In *Proceedings, E3S Web of Conferences* (Vol. 400), p. 03003, (2023, July). [[CrossRef](#)]
- [37] Anggriani, N., Tasman, H., Ndi, M.Z., Supriatna, A.K., Soewono, E. and Siregar, E. The effect of reinfection with the same serotype on dengue transmission dynamics. *Applied Mathematics and Computation*, 349, 62-80, (2019). [[CrossRef](#)]
- [38] Banni, E.M., Kleden, M.A., Lobo, M. and Ndi, M.Z. Estimasi reproduction number model matematika penyebaran malaria di Sumba Tengah, Indonesia. *Jambura Journal of Biomathematics (JJBM)*, 2(1), 13-19, (2021). [[CrossRef](#)]
- [39] Moya, E.M.D., Pietrus, A. and Oliva, S.M. Mathematical model with fractional order derivatives for Tuberculosis taking into account its relationship with HIV/AIDS and Diabetes. *Jambura Journal of Biomathematics (JJBM)*, 2(2), 80-95, (2021). [[CrossRef](#)]
- [40] Kumari, N., Kumar, S., Sharma, S., Singh, F. and Parshad, R. Basic reproduction number estimation and forecasting of COVID-19: A case study of India, Brazil and Peru. *Communications on Pure & Applied Analysis*, 22(2), 417-440, (2023). [[CrossRef](#)]
- [41] Muzembo, B.A., Kitahara, K., Mitra, D., Ntontolo, N.P., Ngatu, N.R., Ohno, A. et al. The basic reproduction number (R_0) of ebola virus disease: A systematic review and meta-analysis. *Travel Medicine and Infectious Disease*, 57, 102685, (2024). [[CrossRef](#)]
- [42] Panigoro, H.S., Rahmi, E., Achmad, N., Mahmud, S.L., Resmawan, R. and Nuha, A.R. A discrete-time fractional-order Rosenzweig-MacArthur predator-prey model involving prey refuge. *Communications in Mathematical Biology and Neuroscience*, 2021, 77, (2021). [[CrossRef](#)]
- [43] Nayeem, J., Podder, C.N. and Salek, M.A. Sensitivity analysis and impact of an imperfect vaccine of two strains of Hepatitis B virus infection. *Journal of Biological Systems*, 31(02), 437-458, (2023). [[CrossRef](#)]
- [44] Lu, X. and Borgonovo, E. Global sensitivity analysis in epidemiological modeling. *European Journal of Operational Research*, 304(1), 9-24, (2023). [[CrossRef](#)]
- [45] Marino, S., Hogue, I.B., Ray, C.J. and Kirschner, D.E. A methodology for performing global uncertainty and sensitivity analysis in systems biology. *Journal of Theoretical Biology*, 254(1), 178-196, (2008). [[CrossRef](#)]
- [46] Saltelli, A. Making best use of model evaluations to compute sensitivity indices. *Computer Physics Communications*, 145(2), 280-297, (2002). [[CrossRef](#)]

Bulletin of Biomathematics (BBM)
(<https://bulletinbiomath.org>)



Copyright: © 2024 by the authors. This work is licensed under a Creative Commons Attribution 4.0 (CC BY) International License. The authors retain ownership of the copyright for their article, but they allow anyone to download, reuse, reprint, modify, distribute, and/or copy articles in *BBM*, so long as the original authors and source are credited. To see the complete license contents, please visit (<http://creativecommons.org/licenses/by/4.0/>).

How to cite this article: Panigoro, H.S., Rahmi, E., Nasib, S.K., Gawa, N.P.H. & Peter, O.J. (2024). Bifurcations on a discrete-time SIS-epidemic model with saturated infection rate. *Bulletin of Biomathematics*, 2(2), 182-197. <https://doi.org/10.59292/bulletinbiomath.2024008>



RESEARCH PAPER

The effect of amyloid beta, membrane, and ER pathways on the fractional behavior of neuronal calcium

Brajesh Kumar Jha ^{1,*,\dagger}, Vora Hardagna Vatsal ^{1,\dagger} and Tajinder Pal Singh ^{1,\dagger}

¹Department of Mathematics, School of Technology, Pandit Deendayal Energy University, Gandhinagar, 382426 Gujarat, India

* Corresponding Author

^{\dagger} brajeshjha2881@gmail.com (Brajesh Kumar Jha); hardagna.vora@gmail.com (Vora Hardagna Vatsal); Tajinder.Singh@spt.pdpu.ac.in (Tajinder Pal Singh)

Abstract

Calcium signal transduction is essential for cellular activities such as gene transcription, death, and neuronal plasticity. Dynamical changes in the concentration of calcium have a profound effect on the intracellular activity of neurons. The Caputo fractional reaction-diffusion equation is a useful tool for modeling the intricate biological process involved in calcium concentration regulation. We include the Amyloid Beta, STIM-Orai mechanism, voltage-dependent calcium entry, inositol triphosphate receptor (IPR), endoplasmic reticulum (ER) flux, SERCA pump, and plasma membrane flux in our mathematical model. We use Green's function and Hankel and Laplace integral transforms to solve the membrane flux problem. Our simulations investigate the effects of various factors on the spatiotemporal behavior of calcium levels, with a simulation on the buffers in Alzheimer's disease-affected neurons. We also look at the effects of calcium-binding substances like the S100B protein and BAPTA and EGTA. Our results demonstrate how important the S100B protein Amyloid beta and the STIM-Orai mechanism are, and how important they are to consider when simulating the calcium signaling system. As such, our research indicates that a more realistic and complete model for modeling calcium dynamics may be obtained by using a generalized reaction-diffusion technique.

Keywords: Fractional-order derivative; calcium ions; neuron; Alzheimer's disease

AMS 2020 Classification: 35R11; 35A22; 35K57; 92C20

1 Introduction

Calcium ions Ca^{2+} serving as ubiquitous second messengers, play a crucial role in various cellular processes. These include cellular differentiation, excitability, apoptosis, gene transcription, and synaptic plasticity, all integral to maintaining cellular function and system regulation [1]. To regulate these diverse functions, cells employ multiple mechanisms to control intracellular

calcium levels. These mechanisms include the passive entry of calcium from the extracellular space through various voltage-gated and membrane ER pathways and diffusion within the cell, followed by sequestration by intracellular entities [2, 3]. Calcium enters the cell through voltage-operated calcium channels and certain exchangers. This diffusion triggers the immediate activation of physiological processes. A significant amount of calcium is buffered immediately, while the remainder undergoes further processing. The spatial and temporal dynamics of calcium inside neurons are essential for healthy cellular function, which can be analyzed by mathematical modeling.

The endoplasmic reticulum (ER) serves as a major internal calcium reservoir, playing a pivotal role in intracellular calcium signaling. The ER releases calcium, contributing to calcium waves that facilitate signaling cascades. Other factors, such as Plasma membrane calcium ATPase (PMCA), Orai channel, and mitochondria, are also actively involved in maintaining cytoplasmic calcium concentration.

Calcium diffuses within the cell through various pathways in cytosolic fluid and different organelles. This calcium homeostasis depending on various factors creates anomalous behavior of the previous concentration profile. To address this complexity, Caputo's differential framework is applied to the nonlocal nature of the reaction-diffusion model. Non-integer differential equation considered the previous memory to compute the current step, which gives a better realistic approach.

The calcium hypothesis has been studied and mathematically modeled over the past few decades. Smith et al. have analyzed the asymptotic behavior of calcium signaling using a steady-state analytical solution approach [4]. Dupont et al. have modeled calcium-induced calcium release of intracellular pools and verified their results with experimental data [5]. Dupont et al. developed a simplified model of the calcium kinase and its transductions [6]. Smith et al. examined several aspects of calcium kinetics, including oscillation patterns, buffer interactions, and receptor involvement [7]. Schmeitz et al. have investigated the time and space features of calcium signaling in *T* cells in a variety of experimental data systems [8]. The work of Friedhoff et al. was an analysis of the nature of calcium oscillations by means of stochastic methods [9]. The comprehensive study of bifurcation analysis of calcium oscillations was the focus of the work of Marko et al. [10]. In addition, Dave and Jha extended the studies by applying the models to Alzheimer's dementia and have shown aberrant calcium levels in nerve cells [11]. Manhas et al. have developed models for the evaluation of calcium bifurcation studies in acinar cells [12]. Naik and Pardasani worked out the finite element approach to calcium diffusion along with ER and the plasma membrane for the oocyte [13]. Jha et al. investigated the fractional calcium reaction-diffusion in nerve cells [14]. Joshi and Yavuz explored the bifurcation of calcium transients in hepatocyte cells [15]. Vora et al. developed one- and two-dimensional fractional calcium dynamics with Orai flow in neuronal cells [16, 17]. Joshi and Jha studied the mechanism of chaotic calcium behavior using the Hilfer operator on neuronal cells [18]. Vaishali and Adlakha studied the ATP-insulin- IP_3 regulating calcium homeostasis in pancreatic cells [19]. Luchko and Yamamoto developed the time-fractional diffusion wave model, which was solved using an analytical approach [20]. Pawar and Pardasani developed models to elucidate the dynamics of calcium, inositol triphosphate (IP_3), and amyloid-beta systems and shed light on cellular degeneration [21]. Lai et al. studied the regulation of calcium and buffer by calcium channels in cardiac myocytes [22]. Luchko et al. established the uniqueness and existence of the initial value and boundary fractional differential problem, which helps to derive the maximum principle [23]. Agarwal et al. studied the advection-diffusion process of calcium by using the Caputo-Fabrizio operator [24]. Tewari et al. have developed a computational model for the homeostasis of calcium and mitochondria [25]. Jagtap and Adlakha studied the dynamics of IP_3R and calcium in the hepatocyte [26]. Singh et al. studied the calcium signaling in the alpha

cells using a numerical approach [27]. Hardagna et al. studied the calcium diffusion in nerve cells in polar dimensions using fractional dynamics [28]. Jha et al. studied the fractional order investigation of the neuronal polar diffusion equation [29]. Joshi studied the COVID-19 dynamics with neuro-degeneration using memory impact [30]. Purohit et al. studied the fractional dynamics with the multi-order approach in physics [31]. Vaishali and Adlakha studied the system of calcium homeostasis in beta cells [32]. Naik et al. studied the flip bifurcation analysis of the chemical model in discrete time [33]. Manhas studied the IP_3 and calcium oscillations for mitochondria in non-excitable cells [34]. Kumar and Erturk studied the cholera disease by using the fractional differential numerical method [35]. Nakul et al. studied the calcium diffusion in cholangiocyte cells using the finite volume approach [36].

As of now, there is a dearth of comprehensive research exploring the collective impacts of the Membrane and the endoplasmic reticulum (ER) through mathematical modeling. This study seeks to bridge this gap by analyzing the combined effects of these parameters on calcium oscillations in neuronal cells.

2 Essential mathematical definitions

Definition 1 Let a function $f \in C((0, T) \times (0, R))$ is continuous and differentiable in space and time where $(r, t) \in (0, R), (0, T)$ [37–40].

Definition 2 Let $n > 0, n \in \mathbb{R}_+$ and Riemann–Liouville fractional integration defined by [37]

$$J^\alpha f(t) = \frac{1}{\Gamma(\alpha)} \int_0^t (t - \xi)^{(\alpha-1)} f(\xi) d\xi, \quad \alpha > 0, \alpha \in \mathbb{R}. \quad (1)$$

Definition 3 Caputo fractional integration and differentiation is defined by [37],

$${}_0^c D_t^\alpha f(t) = J^{m-\alpha} D^m f(t), \quad (2)$$

$${}_0^c D_t^\alpha f(t) = \frac{1}{\Gamma(m-\alpha)} \int_0^t (t - \xi)^{(m-\alpha-1)} f(\xi)^m d\xi, \quad \alpha > 0, \alpha \in \mathbb{R} +. \quad (3)$$

Definition 4 The Mittag-Leffler function is defined by a non-negative variable parameter α , a real number parameter β , and a complex plane variable p [37, 41],

$$E_\alpha(p) = \sum_{k=0}^{\infty} \frac{p^k}{\Gamma(\alpha k + 1)}, \quad (4)$$

$$E_{\alpha,\beta}(p) = \sum_{k=0}^{\infty} \frac{p^k}{\Gamma(\alpha k + \beta)}, \quad (5)$$

and transforming by Laplace definition [41],

$$\mathcal{L}\{E_{\alpha,\beta}(zt^\alpha)\} = \frac{s^{\alpha-1}}{s^\alpha \mp z}, \quad (6)$$

$$\mathcal{L}\{t^{\gamma-1} E_{\mu,\gamma}(\pm pt^\mu)\} = \frac{s^{\mu-\gamma}}{s^\mu \mp p}, \quad \text{Real}(s) > |p|^{1/\mu}, p \in \mathbb{C}, \quad (7)$$

$$\mathcal{L}\{{}_0^c D_t^\alpha f(t)\} = s^\alpha F(s) - \sum_{k=0}^{n-1} s^{\alpha-k-1} f^{(k)}(0), \quad n-1 < \alpha \leq n. \quad (8)$$

Definition 5 Wright’s function, which is defined by [37],

$$\phi(\alpha, \mu, p) = \sum_{k=0}^{\infty} \frac{p^k}{\Gamma(\alpha k + \mu)k!}, \quad \mu > -1, \mu \in \mathbb{C}, \tag{9}$$

and its Laplace transform is [41]

$$\mathcal{L}\{\phi(\alpha, \mu, -pt^\mu)\} = s^{-1}e^{s^\mu p}. \tag{10}$$

Definition 6 Mainardi’s function [41] is given by,

$$M_\alpha(p) = \sum_{k=0}^{\infty} \frac{-p^k}{\Gamma(-\alpha k + (1 - \alpha))k!}, \quad 0 < \alpha < 1. \tag{11}$$

Mainardi’s function Laplace transform is

$$\mathcal{L}\left\{t^{-\alpha} M_\alpha\left(\frac{p}{t^\alpha}\right)\right\} = s^{\alpha-1}e^{-s^\alpha p}. \tag{12}$$

3 Modeling and biological background

A fractional model has been created to examine the influence of the Amyloid beta, STIM-Orai channel in conjunction with important factors such as buffer concentration, VGCC, IP_3 receptors, and ER fluxes. Subsequently, these components’ responsibilities are examined to learn how they affect neuronal processes and diseases like Alzheimer’s disease.

Impact of protein

Calcium ions interact and combine with protein resulting in calcium-bound buffers, which is a necessary step in modeling the spatiotemporal behavior of calcium ions. Entry of neurotransmitters between nerve cells depends on this calcium buffer reaction. Errors in this buffering mechanism have the potential to cause cell death and play a role in the emergence of neurodegenerative illnesses like Parkinson’s and Alzheimer’s disease.

The buffer complex is described using a chemical reaction equation. The mathematical equation for the buffer complex and cytosolic calcium ions is as follows [42],



$[Ca^{2+}]$ represents calcium-free ions, whereas $[P]$ is a protein that binds to calcium ions and creates a calcium-bound protein molecule bound via the k_+ rate. This both-way process dissociates the bound from calcium molecules and the protein at a disassociation rate of k_- .

Impact of amyloid beta

The distortion of amyloid precursor protein (APP) results in the production of amyloid beta 42 ($A\beta_{42}$), which perforates the plasma membrane. Amyloid beta plaques and tangles build up as a result, inhibiting surrounding plasma membrane processes. $A\beta_{42}$ opens up a new channel for calcium ions, causing the concentration of calcium to rise quickly to unmanageable levels without

a sustained influx. For weak neurons, the accumulating calcium is harmful [43]. Then we have

$$J_{Am} = V_{Am} \frac{1}{1 + e^{(V-q_1)/q_2}}, \quad (14)$$

where V_{Am} is the rate of calcium ions entering through this pathway. q_1 and q_2 are voltage dependence of calcium ions and values are -30,23 mV.

Impact of STIM-Orai

The development of memory carrier spines in neurons is mediated by the STIM-Orai pathway. The calcium ions that stream from the nanodomain of the Orai channel are made easier by STIM insights, which control calcium activity through ER calcium concentration. Calcium ions help mature mushroom spines maintain their steady shape. Any disruption of channel clusters or erratic flow might lead to cognitive impairments [44, 45],

$$J_{Orai} = \phi \frac{I_{Orai}}{A_{OZF}}. \quad (15)$$

In this context, ϕ represents the probability of channel opening, I_{Orai} denotes the current flowing through the Orai channel.

Impact of IP_3R

The main intracellular calcium storage is located in the ER. IP_3 receptors (IP_3R) have the ability to release calcium, which is controlled by the biphasic connection between calcium and inositol 1,4,5-trisphosphate (IP_3). Intracellular calcium oscillations are induced by IP_3R flow and are necessary for processes such as synaptic modulation, learning, and neurite development. The intraorganellar network's calcium homeostasis can be both elevated and disrupted by mutations [11],

$$J_{IP_3R} = (C_{ER} - C)K_{IP_3R}O_{IP_3R}. \quad (16)$$

C_{ER} is the calcium level in ER, C is cytosolic calcium, and O_{IP_3R} is the opening rate of the IP_3R , which varies from zero to one.

Impact of SERCA

The Sarcoendoplasmic Reticulum Calcium ATPase (SERCA) pump is a component of the ER calcium store replenishment system that attenuates cytoplasmic calcium signal hyperactivity. Calcium sequestration systems may be severely overloaded by a modified SERCA pump [46],

$$J_{SERCA} = V_{SERCA} \frac{C^2}{C^2 + K_{SERCA}^2} \frac{1}{C_{ER}}. \quad (17)$$

V_{SERCA} is pump value, K_{SERCA} is the dissociation factor of pump.

Impact of channel and leak flux

Calcium moves passively from the endoplasm into the cytoplasm via channels and leaks made of different kinds of pores and proteins. Calcium homeostasis can be upset and the ER overloaded

by poor calcium control. The mathematical formulation of leak and channel flow is as follows [46],

$$J_{leak} = \frac{D_{leak}}{C_1}(1 + C_1) \left(\frac{C_0}{1 + C_1} - C \right), \tag{18}$$

$$J_{Ch} = \frac{D_{Chan}}{C_1}(1 + C_1) \left(\frac{C_0}{1 + C_1} - C \right), \tag{19}$$

where D_{leak} is leak constant, D_{Chan} is channel conductance.

Impact of PMCA flux

Via the high-energy, high-affinity PMCA pump, which the tau protein may block, the plasma membrane actively mediates calcium and dysregulates cytoplasmic calcium. This disturbance is quantitatively represented by the mathematical expression of PMCA flux [46],

$$J_{PMCA} = V_{PMCA} \frac{C^2}{C^2 + K_{PMCA}^2}. \tag{20}$$

Impact of voltage-dependent calcium channel

Calcium ion channels that are gated by voltage are present in neurons and other excitable cells. These ion channels allow the movement of ions, such as sodium, chloride, and calcium, into and out of the cells. VDCC plays a crucial role in the influx of calcium into cells, which then triggers various intracellular physiological processes [47, 48]. VDCCs are categorized into these subtypes *L*, *P/Q*, *N*, and *T* subtypes. *L*-type calcium channels are of particular importance in brain cells, initiating calcium-based activities and subsequent intracellular processes. This equation is expressed as follows [46, 49],

$$I_{VDCC} = P_V z^2 \frac{F^2 V_m}{RT} \frac{C - C_a \exp(-z \frac{F V_m}{RT})}{1 - \exp(-z \frac{F V_m}{RT})}, \tag{21}$$

calcium flux is given by,

$$\sigma_{Ca} = \frac{-I_{Ca}}{V_{neurons} z F}. \tag{22}$$

Table 1 shows all of the values for these parameters.

Modified model in Caputo sense

By combining channels, leaks, pumps, and buffer reactions, one may represent simplified neuronal calcium homeostasis by converting the time derivative into a Caputo fractional derivative. The following is how the suggested model is put forth:

$$\frac{\partial^u C}{\partial t^u} = D \left(\frac{\partial^2 C}{\partial r^2} + \frac{1}{r} \frac{\partial C}{\partial r} \right) - k_+[P][Ca^{2+}] + k_-[CaP] + J_{IPR} - J_{SERCA} + J_{leak} + J_{Ch}. \tag{23}$$

The other formulations, as is customary, represent the order of the Caputo derivative, u , which has a lower limit equal to zero and an upper limit equal to t .

The initial condition and boundary condition for the derivation of the above formula are as follows

$$C(r, 0) = g(r), \quad C(\infty, t) = 0. \tag{24}$$

As follows, the Neumann condition refers to the natural state of calcium diffusion in nerve cells

$$\frac{\partial[C]}{\partial n} = J_{Am} + J_{Orai} - J_{PMCA} + J_{VDCC}. \tag{25}$$

To handle simple multiplication of the nonlinearity in J_{SERCA} . Linearizing the equation by taking two different possible aspects [50]:

Case 1: For $C \ll K_{SERCA}$. Then

$$\frac{C^2}{C^2 + K_{SERCA}^2} \ll \frac{C^2}{K_{SERCA}^2} \ll \frac{C}{K_{SERCA}}. \tag{26}$$

Case 2: For $K_{SERCA} \ll C$. Let $K = \beta c$, for $0 < \beta < 1$,

$$\frac{C^2}{C^2 + K_{SERCA}^2} = \frac{1}{1 + \beta^2}. \tag{27}$$

Nondimensionalization for the term of the proposed model is as follows:

$$r^* = r/l, \quad t^* = t/T, \quad C^* = C/K, \quad C_\infty^* = C_\infty/K, \quad P_\infty^* = P_\infty/[P]_T.$$

To decrease the complexities of the following model, which is the proposed mathematical form, and let

$$a = k_+[P] - K_{IPR}O_{IPR} + \frac{K_{SERCA}}{V_{SERCA}} - \frac{1 + C_1}{C_1}(D_{leak} + D_{Chan}),$$

$$b = k_+[P]C_\infty + C_{ER}(K_{IPR}O_{IPR}) + k_+[P]C_\infty + (D_{leak} + D_{Chan})[C_0/C_1],$$

$${}_0^C D_t^\mu C = D_{Ca} \nabla^2 C - a_i C + b_i, \tag{28}$$

where $i = 1, 2$ for Case 1 and Case 2, respectively.

4 Main results

In this section, the solution of the calcium diffusion fractional dynamics is solved by using the hybrid transform method.

Theorem 1 For variables of the range, $0 \leq t < \infty, 0 \leq r < \infty, u = (0, 1]$, have the form as Eq. (28) and basic condition as Eq. (24), Neuronal calcium flow comes from various channels and receptors which are considered a non-homogeneous condition, (25), can be derived as the form,

$$G(r, t) = \frac{\sqrt{2}}{\sqrt{\pi}} \int_0^\infty E_u[(Dk^2 - a_i)t^\mu] J_0(kr) k dk + \frac{\sqrt{2}}{\sqrt{\pi}} (b_i + j_0) t^\mu \int_0^\infty E_{u, u+1}[(Dk^2 - a_i)t^\mu] J_0(kr) k dk. \tag{29}$$

Proof Using Eq. (28) as our foundational model.

Taking two cases for the SERCA pump, v . The Hankel transform is applied over the radius.

$${}_0^C D_t^u \dot{C} = Dk^2 \dot{C} - a_i \dot{C} + (b_i + j_0) \delta(k), \tag{30}$$

using the Laplace transform to apply temporal transformation

$$\ddot{C}(k, s) = \frac{s^{u-1} g(k)}{(s^u - Dk^2 + a_i)} + \frac{b_i + j_0 \delta(k)}{s(s^u - Dk^2 + a_i)} \delta(k), \tag{31}$$

where k is the Hankel transform variable.

The Laplace transform is now used by the formulas below in the solution

$$\begin{aligned} E_u(pt^u) \leftarrow L &\rightarrow \frac{s^{u-1}}{s^u - p'} \\ t^{\gamma-1} E_{u,\gamma}(pt^u) \leftarrow L &\rightarrow \frac{s^{\mu-1}}{s^\mu \mp p'} \end{aligned} \tag{32}$$

$$C(\dot{k}, t) = E_u[(Dk^2 - a_i)t^u] g(k) + (b_i + j_0)t^u E_{u,u+1}[(Dk^2 - a_i)t^u] \delta(k). \tag{33}$$

With the inverting transform, we obtain:

$$\begin{aligned} C(r, t) &= \frac{\sqrt{2}}{\sqrt{\pi}} \int_0^\infty E_u[(Dk^2 - a_i)t^u] g(k) J_0(kr) k dk \\ &\quad + \frac{(b_i + j_0)t^u \sqrt{2}}{\sqrt{\pi}} \int_0^\infty E_{u,u+1}[(Dk^2 - a_i)t^u] \delta(k) J_0(kr) k dk, \end{aligned} \tag{34}$$

$$\begin{aligned} C(r, t) &= \frac{\sqrt{2}}{\sqrt{\pi}} \int_0^\infty E_u[(Dk^2 - a_i)t^u] J_0(kr) k \int_0^\infty g(y) J_0(kr) k dy * dk \\ &\quad + \frac{(b_i + j_0)t^u \sqrt{2}}{\sqrt{\pi}} \int_0^\infty E_{u,u+1}[(Dk^2 - a_i)t^u] \int_0^\infty \delta(y) J_0(kr) k dy * dk, \end{aligned} \tag{35}$$

$$C(r, t) = \int_0^\infty G^1(r - y, t) g(y) dy + \int_0^\infty G^2(r - y, t) \delta(y) dy. \tag{36}$$

$$G_u^1(r, t) = \frac{\sqrt{2}}{\sqrt{\pi}} \int_0^\infty E_u[(Dk^2 - a_i)t^u] J_0(kr) k dk, \tag{37}$$

$$G_u^2(r, t) = (b_i + j_0)t^u \int_0^\infty E_{u,u+1}[(Dk^2 - a_i)t^u] J_0(kr) k dk, \tag{38}$$

$$\begin{aligned} G_u(r, t) &= \frac{\sqrt{2}}{\sqrt{\pi}} \int_0^\infty E_u[(Dk^2 - a_i)t^u] J_0(kr) k dk \\ &\quad + \frac{\sqrt{2}}{\sqrt{\pi}} (b_i + j_0)t^u \int_0^\infty E_{u,u+1}[(Dk^2 - a_i)t^u] J_0(kr) k dk. \end{aligned} \tag{39}$$

Hence proved.

Lemma 1 [38–40] An example of a function with an exponential combination is the Mittag-Leffler function family. When $Z \in C$, a complex field, has any value, $E_{(\mu,\gamma)}(x)$ converges. Eq. (40) is a Green's function

solution derived by a semi-analytical method for calcium diffusion in neuron cells. This analytical method, however, needs to be revised to provide closed-form answers.

5 Analysis

The essential solution was obtained by using Green’s function to describe the outcome of the integral transform. Below is the further analysis that was performed to get a closed-form answer.

Theorem 2 Taking $0 < u \leq 1$, $0 < r < \infty$, $0 \leq t < \infty$, the mathematical form is (40) from this closed-form solution obtained as,

$$G(r, t) = \frac{1}{2D\sqrt{t^u}} \int_0^\infty e^{\frac{-r^2}{4i^{u_k}} - a_i k t^u} k^{-\frac{1}{2}} M_u(k) dk + \frac{(b_i + j_o)t^{u/2}}{2D} \int_0^\infty e^{\frac{-r^2}{4i^{u_k}} - a_i k t^u} k^{-\frac{1}{2}} \phi(-u, 1; k) dk. \quad (40)$$

Proof Implementing the Hankel transform to a radial variable and using Eq. (40), we obtain,

$$G_u(r, t) = E_u[(Dk^2 - a_i)t^u] + (b_i + j_o)t^u E_{u, u+1}[(Dk^2 - a_i)t^u]. \quad (41)$$

Now using the Laplace to transform the temporal domain, we obtain,

$$G_{u,2}''(k, s) = \frac{s^{u-1}}{(s^u + Dk^2 + a_i)} + \frac{s^{-1}(b_i + j_o)}{(s^u + Dk^2 + a_i)}, \quad (42)$$

$$G_{u,2}''(k, s) = s^{u-1} \int_0^\infty e^{-p(s^u + Dk^2 + a_i)} dp + (b_i + j_o)s^{-1} \int_0^\infty e^{-p(s^u + Dk^2 + a_i)} dp. \quad (43)$$

Applying the inverse Laplace now, and utilizing the definitions,

$$G_{u,2}''(k, s) = \int_0^\infty e^{-p(Dk^2 + a_i)} t^{-u} M_u\left(\frac{p}{t^u}\right) dp + (b_i + j_o) \int_0^\infty e^{-p(Dk^2 + a_i)} \phi(-u, 1; -pt^u) dp. \quad (44)$$

Using the inverse Hankel transform, we get

$$G(r, t) = \frac{1}{2D\sqrt{t^u}} \int_0^\infty e^{\frac{-r^2}{4i^{u_k}} - a_i k t^u} k^{-\frac{1}{2}} M_u(k) dk + \frac{(b_i + j_o)t^{u/2}}{2D} \int_0^\infty e^{\frac{-r^2}{4i^{u_k}} - a_i k t^u} k^{-\frac{1}{2}} \phi(-u, 1; k) dk. \quad (45)$$

Hence the result.

Existence and uniqueness

Remark 1 [38, 39] The closed-form solution is gained by using Green’s function.

Let $\alpha, m > 0$, then for p , continuous function defined below

$$E_{(m,\alpha)}(p) = \sum_{k=0}^\infty p^k / (m(\mu k + \mu)), \quad (46)$$

is the convergent and let constant $M_i > 0$ as,

$$|E_{(m,\mu)}(z)| \leq M_i. \quad (47)$$

If $\alpha \geq 0$ and $\xi \in \mathbb{C}$, thus additions of the above series uniformly converge throughout an entire complex plane [39, 40].

For the uniqueness of the solution, let us take $c(r, t) = h(r, t) - \dot{h}(r, t)$. If a distinguished result exists of this nature with this physiological constraint then $c(r, t) \equiv 0 \rightarrow h(r_i, t_i) \equiv \dot{h}(r_i, t_i)$ which shows the uniqueness of the solution.

Theorem 3 $c \in C[[0, T] \times [0, R]]$ and states the Eq. (28), equality can be given as below,

$$\max_{\Omega} c = \max_{\Gamma} c, \tag{48}$$

where Γ is the boundary and Ω is the domain.

Proof This statement will be proven by contradiction.

Let us take into consideration

$$M = \max_{\Omega} c, \tag{49}$$

$$\ddot{M} = \max_{\Gamma} c, \tag{50}$$

concerning this $\ddot{M} \leq M$. Then M carries any arbitrary point (r_M, t_M) .

Using a function that can be expressed as $w : \Omega \rightarrow \mathbb{R}$ fulfills our assumption as well, having equivalent physiological values.

Now, we may proceed as follows

$${}_0^C D_t^u w - D \nabla^2 w + a_i w - b_i = 0, \tag{51}$$

considering the function as it is described here

$$w = c + (M - \ddot{M})t^{(-m)}. \tag{52}$$

In maximal attainment at a level of c . (r_M, t_M) above equation implies

$$w = \ddot{M} + (M - \ddot{M})\epsilon, w < M. \tag{53}$$

Also, $w \geq c$ in Ω and at maximum point

$$w = c(r_M, t_M) + M - \ddot{M}. \tag{54}$$

For the left-side equation

$${}_0^C D_t^u w - D \frac{\partial^2 w}{\partial r^2} + \frac{1}{r} \frac{\partial w}{\partial r} + a_i w - b_i + \frac{M - \ddot{M} \Gamma(1 - m)}{\Gamma(1 - m - u)} t^{-m-u} \leq \frac{M - \ddot{M} \Gamma(1 - n)}{\Gamma(1 - m - u)} t^{-m-u} > 0. \tag{55}$$

From above equation

$${}_0^C D_t^u c - D \nabla^2 c + a_i c - b_i > 0. \tag{56}$$

The positive output contradicts this

$$\max_{\Omega} c = \max_{\Gamma} c. \tag{57}$$

Hence proved.

Applicability of the model

A multitude of cerebral processes, including neurotransmitter release, synaptic plasticity, and gene transcription, are contingent upon calcium ions. To achieve physiological equivalence with in vivo neuronal calcium dynamics, the calcium amounts in our model were adjusted. This method ensures that the model accurately mimics the behavior of neuronal calcium.

A variety of brain processes, including neurotransmitter release, synaptic plasticity, and gene transcription, are critically dependent upon calcium ions. In order to achieve physiological equivalence with in vivo neuronal calcium dynamics, the calcium amounts in the model were adjusted. This ensures that the model accurately mimics the behavior of neuronal calcium [14, 18].

6 Results and interpretation

The results demonstrate the distribution of calcium within a neuron in terms of spatial and temporal dimensions. Table 1 provides the numerical values and accompanying descriptions of the input parameters utilized in the generation of these results.

In Figure 1, shows the calcium pattern for a $100\mu M$ buffer. This graphic depicts the creation of a calcium spike that is uniformly distributed in terms of temporal order transition for the cytosol. This hysteresis memory emphasizes the nonlocal character of neuronal calcium transport at a scale of $0.7\mu M$. Calcium ions diffuse across the cytosolic buffer, binding to the ER storage receptors and profoundly altering protein activity. Calcium ion concentration falls linearly as the radial distance from the plasma membrane increases. Buffer is very important in calcium homeostasis. We can observe the temporal impact on the calcium ions with differential order. Here EGTA buffer is taken for normal neuronal cells which are bound with the calcium ions.

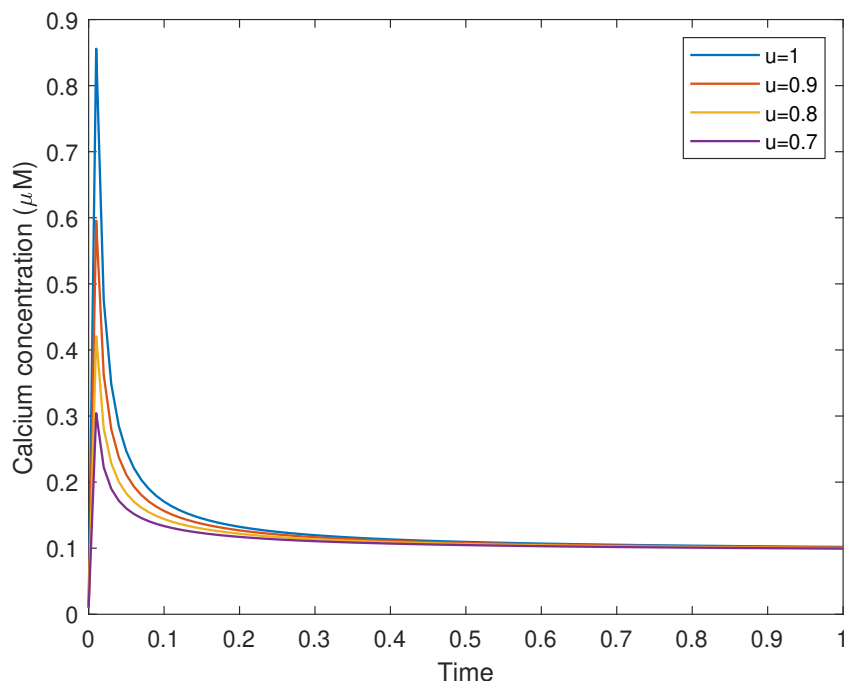


Figure 1. The time diffusion of calcium ions, as simulated by successive orders of the time derivative, when the buffer is $100\mu M$

In Figure 2, shows the radial distribution of calcium concentration at a buffer value of $100\mu M$ with a fractional order $u = 1, 0.9, 0.8, 0.7$. This illustration depicts the creation of a calcium spike

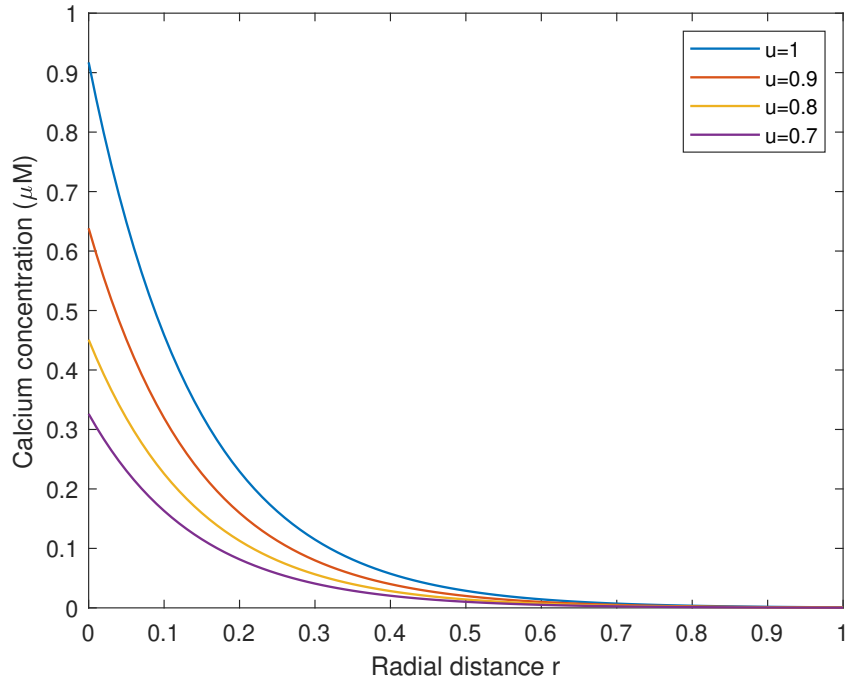


Figure 2. The radial distribution of calcium ions, as simulated by successive orders of the time derivative, when the buffer is $100 \mu\text{M}$

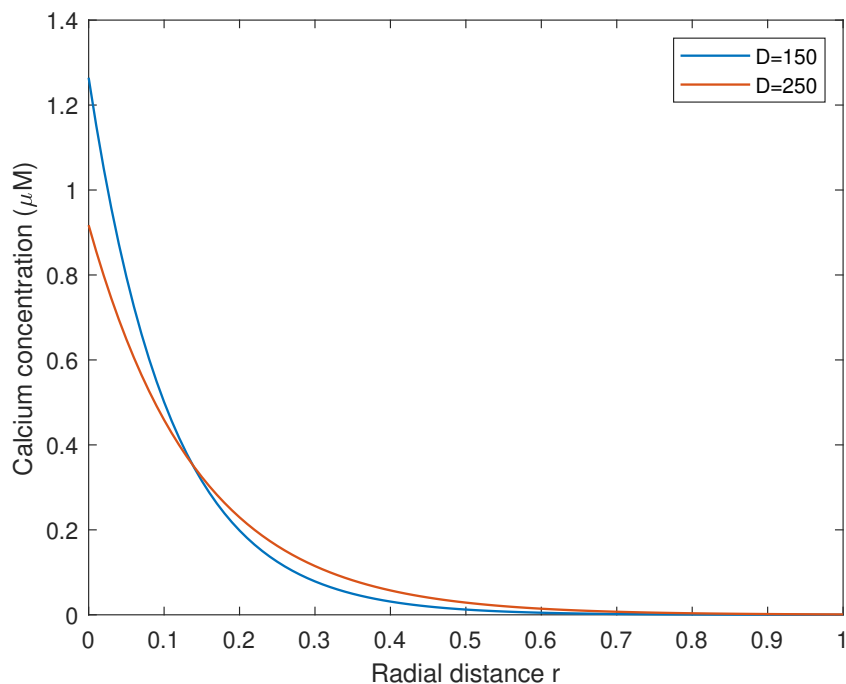


Figure 3. Radial distribution of free calcium ions for a diffusion coefficient 150 and 250 with temporal order $u = 1$

dispersed radially in the cytosolic free calcium concentration. At $u = 0.9$, the hysteresis memory has a lower nonlocal character than $u = 1.0$. The lower fractional order $u = 0.9$ results in a reduction in cytosolic free calcium ions, creating a subdiffusion impact on the spatial pattern. This order includes all prior states up to 0.9 of the reaction-diffusion process, recording the transition

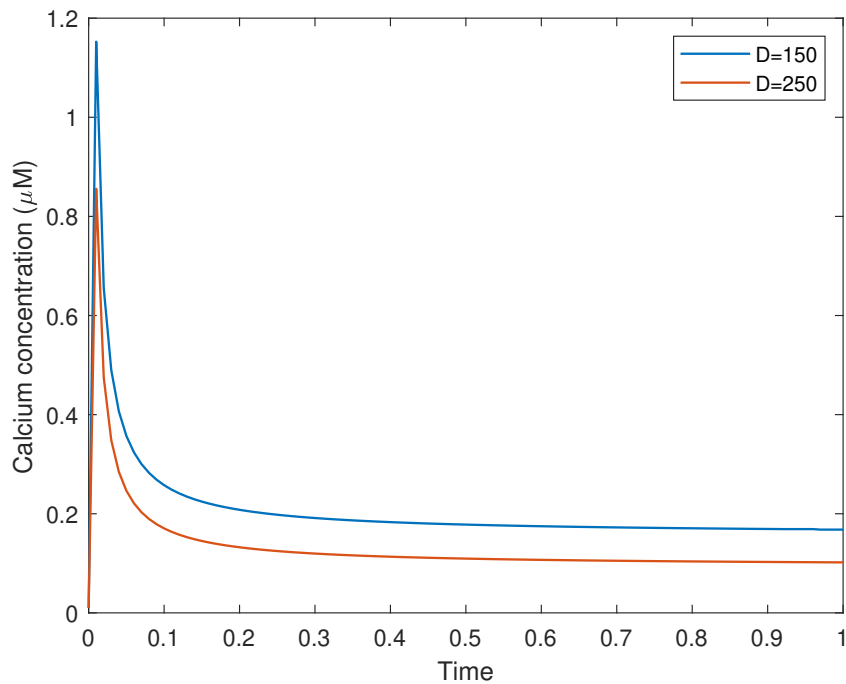


Figure 4. Temporal pattern of free calcium ions for a diffusion coefficient 150 and 250 with temporal order $u = 1$ of the differential order of calcium ions.

In [Figure 3](#), displays calcium concentration variations with a diffusion coefficient of $D = 150$ for this reaction-diffusion process with radial distance. $D = 250$ shows that calcium concentration increases with a reduced diffusion coefficient, signifying localized calcium signaling locations and probable calcium overload.

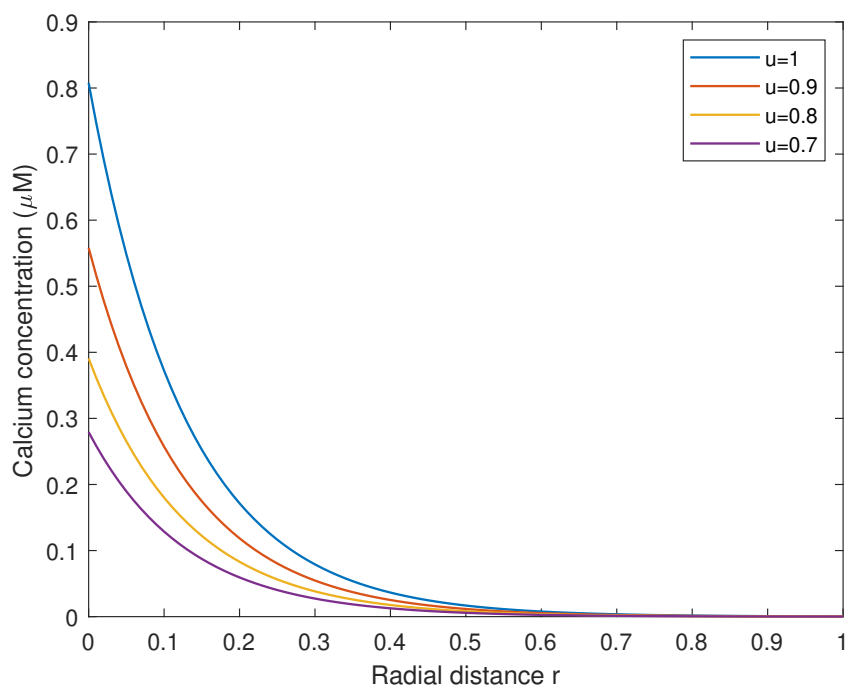


Figure 5. Radial diffusion of calcium ions with $[B] = 200\mu M$ for a different order of time derivative

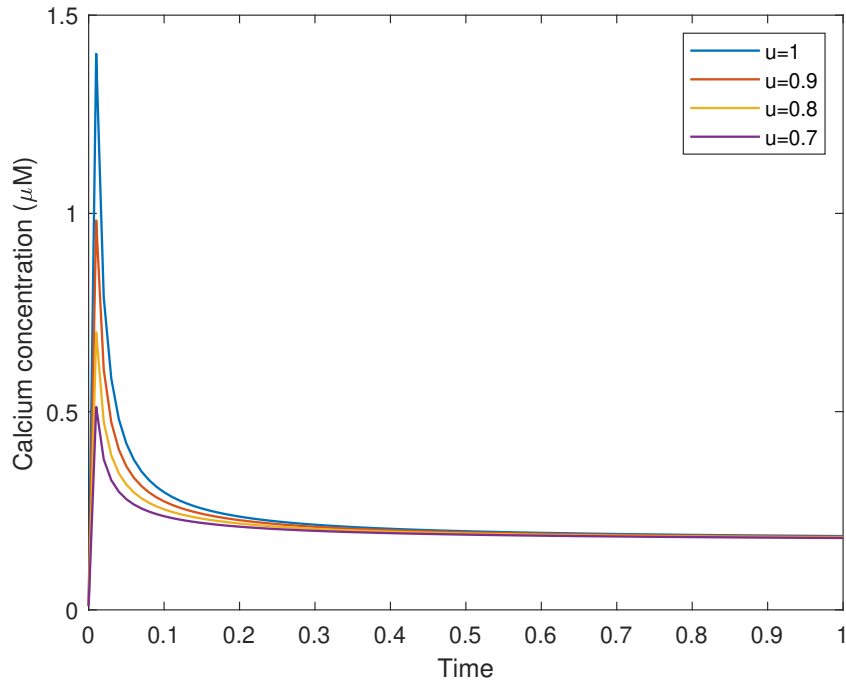


Figure 6. Temporal pattern in Alzheimer’s impact of reduced protein $[B] = 50\mu M$ on calcium ions for a different order

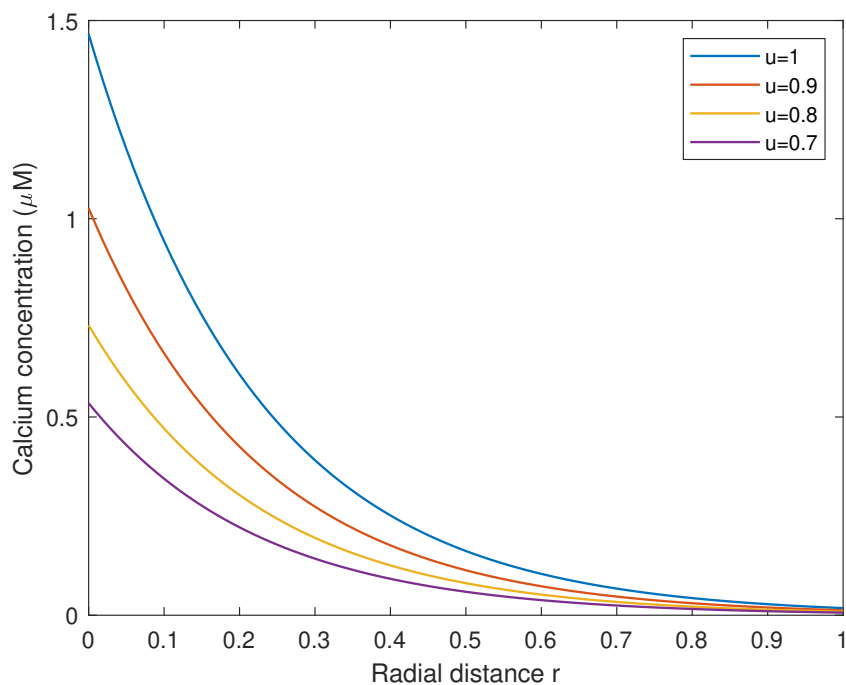


Figure 7. Radial distribution in Alzheimer’s impact of reduced protein $[B] = 50\mu M$ on calcium ions for a different order

Figure 4 displays calcium concentration variations with a diffusion coefficient of $D = 150$ for this fractional temporal reaction-diffusion process. $D = 250$ shows that calcium concentration

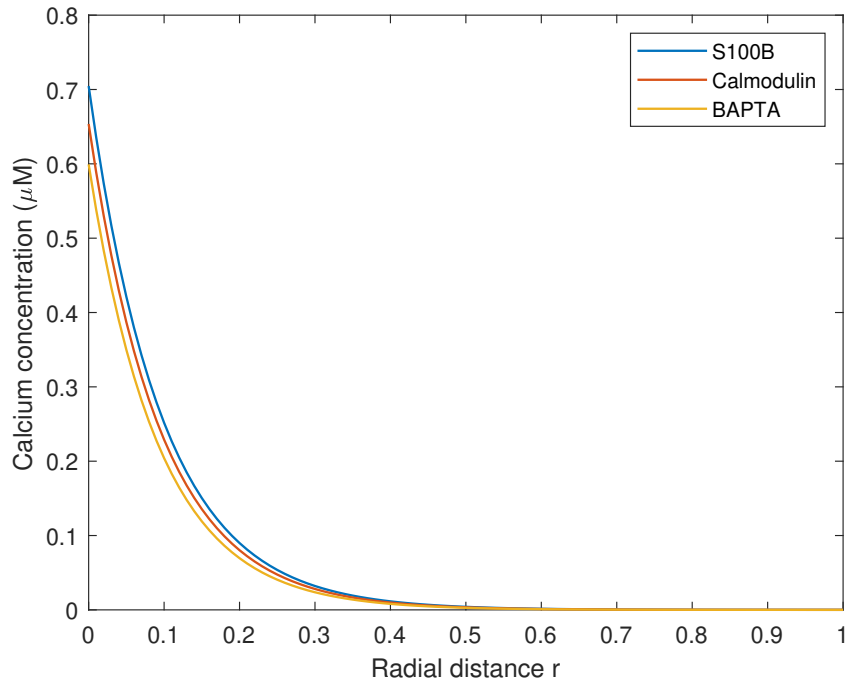


Figure 8. Radial distribution of free calcium ions for various protein impact

increases with a reduced diffusion coefficient, signifying intersection indicates the background calcium level decreased.

In [Figure 5](#), we show calcium concentration with increasing buffer concentration $[B] = 200\mu M$ along the radius. The figure shows that the calcium spectrum is controlled, with enhanced calcium binding activity, showing that increasing buffer concentrations effectively regulate calcium levels.

In [Figure 6](#), we illustrate the effect of the reduced buffer presence observed in Alzheimer's impacted neurons. This can increase the amount of calcium ions, degenerating neuronal homeostasis and leading to neuronal death. The temporal pattern is higher than the normal neuronal cell.

In [Figure 7](#), it illustrates the effect of the reduced buffer presence observed in the radial distance with different temporal order. It can be observed that calcium spread and peak levels are higher and prolonged than normal neuronal conditions. Long-term calcium behavior is harmful to neurons, which leads to cell death.

In [Figure 8](#), it illustrates the nature of the endogenous buffer calmodulin, S100B can control the calcium spectrum in a well-controlled manner. The presence of the BAPTA buffer in the cytosol could disperse calcium in a narrow spectrum. This effect can be useful for well-controlled calcium dispersion in the Alzheimer's impacted neuron.

Table 1. Values of physiological constants [4, 9, 43]

Symbols	Description	Value	Unit
D_{Ca}	Diffusion constant value	150-250	$\mu M^2/s$
C_1	Cell ratio	0.185	-
k_+	Association constant rate (EGTA, S100B, BAPTA)	1.5,1.1,600	$\mu M^{-1}s^{-1}$
$[Ca^{2+}]_{\infty}$	Background concentration level	0.1	μM
V_{SERCA}	Pump conductance	120	$s^{-1}(\mu M)^{-2}$
D_{leak}	Leak flux constant	0.11	s^{-1}
D_{Chan}	Channel flux constant	6	s^{-1}

[P]	Protein level	50-100	μM
ϕ	Opening rate	0.9	-
I_O	Current of Orai	2.1	fA
A_O	Area of Orai	0.25	nm^2
z	Valency of calcium ions	2	-
C_0	extracellular calcium concentration	2	μM
V_{neuron}	Volume of cellular cytosol	523.6	μm^3
V_m	membrane potential	-0.07	V
R	Ideal gas constant	8.31	J/(mol.K)
T	Absolute temperature	300	K
P_V	Permeability of ion	0.5	s^{-1}
K_{SERCA}	Dissociation SERCA rate	0.18	μM
K_{PMCA}	PMCA pump rate	0.425	μM
C_{ER}	ER calcium level	500	μM
V_{PMCA}	PMCA conductance	28	$s^{-1}(\mu M)^{-2}$
K_{IP_3R}	IPR rate	0.52	s^{-1}

7 Conclusion

In this work, we have simulated the interaction of calcium ions and buffers with temporal fractional order, taking into account a variety of characteristics including neuronal membrane flux and ER flux. Different endogenous and exogenous proteins have been investigated in the context of Alzheimer's disease. The Hankel transform has been used for the polar derivative and the Laplace transform for initial conditions, resulting in Mittag-Leffler functions. Green's functions have been used to obtain closed-form solutions, which have also included Mainardi's and Wright's functions. A modified calcium diffusion model, formulated within the Caputo framework, has been successfully solved through a hybrid transform method. The existence and uniqueness of the solution have been demonstrated for fundamental model analysis.

- We have obtained graphical results of the interaction of calcium and other factors with different temporal order, reduced temporal memory reduced the calcium level in neurons.
- The study shows that the time fractional order has a converging effect on calcium levels for radial distance, driven by many characteristics.
- The diffusion coefficient parameter has an inverse influence on calcium distribution, causing calcium concentrations to accumulate near the membrane.
- The impact of Alzheimer's disease is demonstrated by a reduced buffer quantity, resulting in prolonged elevated calcium levels in neurons, which are hazardous. Prolonged conditions could lead to cell death with lower buffer impact.
- Neuroprotection relies heavily on BAPTA binding concentration. Mobile and immobile buffers have distinct effects on calcium levels, with EGTA, Calmodulin, and S100B considerably lowering calcium concentrations.

Thus, our findings provide light on the fractional dynamics of calcium signaling and buffering in neurons, offering insights into protein simulation possibilities for neurodegenerative illnesses such as Alzheimer's. The dual transform approach and fractional-order modeling provide a solid foundation for comprehending the intricate interconnections seen in the neural calcium reaction-diffusion process.

Limitation and future scope

In this work, the experimental setup could play a pivotal role in the understanding of neuronal degenerative diseases.

Declarations

Use of AI tools

The authors declare that they have not used Artificial Intelligence (AI) tools in the creation of this article.

Data availability statement

All data generated or analyzed during this study are included in this article.

Ethical approval

The authors state that this research complies with ethical standards. This research does not involve either human participants or animals.

Consent for publication

Not applicable

Conflicts of interest

The authors declare that they have no conflict of interest.

Funding

There is no funding for this article.

Author's contributions

B.K.J.: Conceptualization, Formal Analysis, Writing-Original Draft. V.H.V.: Methodology, Visualization, Validation, Writing - Review & Editing. T.P.S.: Validation, Writing-Original Draft. The authors have read and agreed to the published version of the manuscript.

Acknowledgements

Not applicable

References

- [1] Workgroup, A.A.C.H and Khachaturian, Z.S. Calcium hypothesis of Alzheimer's disease and brain aging: a framework for integrating new evidence into a comprehensive theory of pathogenesis. *Alzheimer's & Dementia*, 13(2), 178-182, (2017). [[CrossRef](#)]
- [2] Ribe, E.M., Serrano-Saiz, E., Akpan, N. and Troy, C.M. Mechanisms of neuronal death in disease: defining the models and the players. *Biochemical Journal*, 415(2), 165-182, (2008). [[CrossRef](#)]
- [3] Bezprozvanny, I. Calcium signaling and neurodegenerative diseases. *Trends in Molecular Medicine*, 15(3), 89-100, (2009). [[CrossRef](#)]
- [4] Smith, G.D. Analytical steady-state solution to the rapid buffering approximation near an open Ca^{2+} channel. *Biophysical Journal*, 71(6), 3064-3072, (1996). [[CrossRef](#)]

-
- [5] Dupont, G., Berridge, M.J. and Goldbeter, A. Signal-induced Ca^{2+} oscillations: properties of a model based on Ca^{2+} -induced Ca^{2+} release. *Cell Calcium*, 12(2-3), 73-85, (1991). [[CrossRef](#)]
- [6] Dupont, G., Houart, G. and De Koninck, P. Sensitivity of CaM kinase II to the frequency of Ca^{2+} oscillations: a simple model. *Cell Calcium*, 34(6), 485-497, (2003). [[CrossRef](#)]
- [7] Sherman, A., Smith, G.D., Dai, L. and Miura, R.M. Asymptotic analysis of buffered calcium diffusion near a point source. *SIAM Journal on Applied Mathematics*, 61(5), 1816-1838, (2001). [[CrossRef](#)]
- [8] Schmeitz, C., Hernandez-Vargas, E.A., Fliegert, R., Guse, A.H. and Meyer-Hermann, M. A mathematical model of T lymphocyte calcium dynamics derived from single transmembrane protein properties. *Frontiers in Immunology*, 4, 277, (2013). [[CrossRef](#)]
- [9] Friedhoff, V.N., Ramlow, L., Lindner, B. and Falcke, M. Models of stochastic Ca^{2+} spiking. *The European Physical Journal Special Topics*, 230, 2911-2928, (2021). [[CrossRef](#)]
- [10] Marhl, M., Haberichter, T., Brumen, M. and Heinrich, R. Complex calcium oscillations and the role of mitochondria and cytosolic proteins. *BioSystems*, 57(2), 75-86, (2000). [[CrossRef](#)]
- [11] Dave, D.D. and Jha, B.K. Analytically depicting the calcium diffusion for Alzheimer's affected cell. *International Journal of Biomathematics*, 11(7), 1850088, (2018). [[CrossRef](#)]
- [12] Manhas, N., Sneyd, J. and Pardasani, K.R. Modelling the transition from simple to complex Ca^{2+} oscillations in pancreatic acinar cells. *Journal of Biosciences*, 39(3), 463-484, (2014). [[CrossRef](#)]
- [13] Naik, P.A. and Pardasani, K.R. Finite element model to study calcium distribution in oocytes involving voltage gated Ca^{2+} channel, ryanodine receptor and buffers. *Alexandria Journal of Medicine*, 52(1), 43-49, (2016). [[CrossRef](#)]
- [14] Jha, B.K., Joshi, H. and Dave, D.D. Portraying the effect of calcium-binding proteins on cytosolic calcium concentration distribution fractionally in nerve cells. *Interdisciplinary Sciences: Computational Life Sciences*, 10, 674-685, (2018). [[CrossRef](#)]
- [15] Joshi, H. and Yavuz, M. Numerical analysis of compound biochemical calcium oscillations process in hepatocyte cells. *Advanced Biology*, 8(4), 2300647, (2024). [[CrossRef](#)]
- [16] Vatsal, V.H., Jha, B.K. and Singh, T.P. To study the effect of ER flux with buffer on the neuronal calcium. *The European Physical Journal Plus*, 138, 494, (2023). [[CrossRef](#)]
- [17] Vatsal, V.H., Jha, B.K. and Singh, T.P. Deciphering two-dimensional calcium fractional diffusion of membrane flux in neuron. *Journal of Applied Mathematics and Computing*, 70, 4133-4156, (2024). [[CrossRef](#)]
- [18] Joshi, H. and Jha, B.K. Chaos of calcium diffusion in Parkinson's infectious disease model and treatment mechanism via Hilfer fractional derivative. *Mathematical Modelling and Numerical Simulation with Applications*, 1(2), 84-94, (2021). [[CrossRef](#)]
- [19] Vaishali and Adlakha, N. Model of calcium dynamics regulating IP_3 , ATP and insulin production in a pancreatic β -cell. *Acta Biotheoretica*, 72, 2, (2024). [[CrossRef](#)]
- [20] Luchko, Y., Mainardi, F. and Povstenko, Y. Propagation speed of the maximum of the fundamental solution to the fractional diffusion-wave equation. *Computers & Mathematics with Applications*, 66(5), 774-784, (2013). [[CrossRef](#)]
- [21] Pawar, A. and Pardasani, K.R. Computational model of interacting system dynamics of calcium, IP_3 and β -amyloid in ischemic neuron cells. *Physica Scripta*, 99(1), 015025, (2024). [[CrossRef](#)]

- [22] Lai, Y.M., Coombes, S. and Thul, R. Calcium buffers and L-type calcium channels as modulators of cardiac subcellular alternans. *Communications in Nonlinear Science and Numerical Simulation*, 85, 105181, (2020). [[CrossRef](#)]
- [23] Luchko, Y. and Yamamoto, M. General time-fractional diffusion equation: some uniqueness and existence results for the initial-boundary-value problems. *Fractional Calculus and Applied Analysis*, 19(3), 676–695, (2016). [[CrossRef](#)]
- [24] Agarwal, R., Kritika and Purohit, S.D. Mathematical model pertaining to the effect of buffer over cytosolic calcium concentration distribution. *Chaos, Solitons & Fractals*, 143, 110610, (2021). [[CrossRef](#)]
- [25] Tewari, S.G., Camara, A.K.S., Stowe, D.F. and Dash, R.K. Computational analysis of Ca^{2+} dynamics in isolated cardiac mitochondria predicts two distinct modes of Ca^{2+} uptake. *The Journal of Physiology*, 592(9), 1917–1930, (2014). [[CrossRef](#)]
- [26] Jagtap, Y. and Adlakha, N. Numerical model of hepatic glycogen phosphorylase regulation by nonlinear interdependent dynamics of calcium and IP_3 . *The European Physical Journal Plus*, 138, 399, (2023). [[CrossRef](#)]
- [27] Singh, T. and Adlakha, N. Numerical investigations and simulation of calcium distribution in the alpha-cell. *Bulletin of Biomathematics*, 1(1), 40–57, (2023). [[CrossRef](#)]
- [28] Vatsal, V.H., Jha, B.K. and Singh, T.P. Generalised neuronal calcium dynamics of membrane and ER in the polar dimension. *Cell Biochemistry and Biophysics*, (2024). [[CrossRef](#)]
- [29] Jha, B.K., Vatsal, V.H. and Singh, T.P. Navigating the fractional calcium dynamics of Orai mechanism in polar dimensions. *Cell Biochemistry and Biophysics*, (2024). [[CrossRef](#)]
- [30] Joshi, H. Mechanistic insights of COVID-19 dynamics by considering the influence of neurodegeneration and memory trace. *Physica Scripta*, 99(3), 035254, (2024). [[CrossRef](#)]
- [31] Purohit, S.D., Baleanu, D. and Jangid, K. On the solutions for generalised multiorder fractional partial differential equations arising in physics. *Mathematical Methods in the Applied Sciences*, 46(7), 8139–8147, (2023). [[CrossRef](#)]
- [32] Vaishali and Adlakha, N. Disturbances in system dynamics of Ca^{2+} and IP_3 perturbing insulin secretion in a pancreatic β -cell due to type-2 diabetes. *Journal of Bioenergetics and Biomembranes*, 55, 151–167, (2023). [[CrossRef](#)]
- [33] Naik, P.A., Eskandari, Z. and Shahraki, H.E. Flip and generalized flip bifurcations of a two-dimensional discrete-time chemical model. *Mathematical Modelling and Numerical Simulation with Applications*, 1(2), 95–101, (2021). [[CrossRef](#)]
- [34] Manhas, N. Mathematical model for IP_3 dependent calcium oscillations and mitochondrial associate membranes in non-excitable cells. *Mathematical Modelling and Numerical Simulation with Applications*, 4(3), 280–295, (2024). [[CrossRef](#)]
- [35] Kumar, P. and Erturk, V.S. Dynamics of cholera disease by using two recent fractional numerical methods. *Mathematical Modelling and Numerical Simulation with Applications*, 1(2), 102–111, (2021). [[CrossRef](#)]
- [36] Nakul, N., Mishra, V. and Adlakha, N. Finite volume simulation of calcium distribution in a cholangiocyte cell. *Mathematical Modelling and Numerical Simulation with Applications*, 3(1), 17–32, (2023). [[CrossRef](#)]
- [37] Podlubny, I. *Fractional Differential Equations* (Vol. 198). Academic Press: New York, USA, (1999).

- [38] Miller, K.S. and Ross, B. *An Introduction to The Fractional Calculus and Fractional Differential Equations*. John Willey & Sons: New York, (1993).
- [39] Kilbas, A.A., Srivastava, H.M. and Trujillo, J.J. *Theory and Applications of Fractional Differential Equations* (Vol. 204). Elsevier: Amsterdam, (2006).
- [40] Diethelm, K. *The Analysis of Fractional Differential Equations: An Application-Oriented Exposition using Differential Operators of Caputo Type*. Springer: Heidelberg, (2010).
- [41] Mainardi, F. and Pagnini, G. The Wright functions as solutions of the time-fractional diffusion equation. *Applied Mathematics and Computation*, 141(1), 51-62, (2003). [[CrossRef](#)]
- [42] Keener, J. and Sneyd, J. *Mathematical Physiology* (Vol. 8/1). Springer: New York, (2009).
- [43] Prista von Bonhorst, F., Gall, D. and Dupont, G. Impact of β -amyloids induced disruption of Ca^{2+} homeostasis in a simple model of neuronal activity. *Cells*, 11(4), 615, (2022). [[CrossRef](#)]
- [44] Zhang, H., Sun, S., Wu, L., Pchitskaya, E., Zakharova, O., Tacer, K.F. and Bezprozvanny, I. Store-operated calcium channel complex in postsynaptic spines: a new therapeutic target for Alzheimer's disease treatment. *Journal of Neuroscience*, 36(47), 11837-11850, (2016). [[CrossRef](#)]
- [45] Gil, D., Guse, A.H. and Dupont, G. Three-dimensional model of sub-plasmalemmal Ca^{2+} microdomains evoked by the interplay between ORAI1 and $InsP_3$ receptors. *Frontiers in Immunology*, 12, 659790, (2021). [[CrossRef](#)]
- [46] Sneyd, J., Tsaneva-Atanasova, K., Bruce, J.I.E., Straub, S.V., Giovannucci, D.R. and Yule, D.I. A model of calcium waves in pancreatic and parotid acinar cells. *Biophysical Journal*, 85(3), 1392-1405, (2003). [[CrossRef](#)]
- [47] Marambaud, P., Dreses-Werringloer, U. and Vingtdoux, V. Calcium signaling in neurodegeneration. *Molecular Neurodegeneration*, 4, 20, (2009). [[CrossRef](#)]
- [48] Yagami, T., Kohma, H. and Yamamoto, Y. L-type voltage-dependent calcium channels as therapeutic targets for neurodegenerative diseases. *Current Medicinal Chemistry*, 19(28), 4816-4827, (2012). [[CrossRef](#)]
- [49] Bezprozvanny, I.B. Calcium signaling and neurodegeneration. *Acta Naturae*, 2(1), 72-80, (2010).
- [50] Jha, B.K., Adlakha, N. and Mehta, M.N. Finite volume model to study the effect of ER flux on cytosolic calcium distribution in astrocytes. *Journal of Computing*, 3(11), 74-80, (2011).

Bulletin of Biomathematics (BBM)
(<https://bulletinbiomath.org>)



Copyright: © 2024 by the authors. This work is licensed under a Creative Commons Attribution 4.0 (CC BY) International License. The authors retain ownership of the copyright for their article, but they allow anyone to download, reuse, reprint, modify, distribute, and/or copy articles in *BBM*, so long as the original authors and source are credited. To see the complete license contents, please visit (<http://creativecommons.org/licenses/by/4.0/>).

How to cite this article: Jha, B.K., Vatsal, V.H. & Singh, T.P. (2024). The effect of amyloid beta, membrane, and ER pathways on the fractional behavior of neuronal calcium. *Bulletin of Biomathematics*, 2(2), 198-217. <https://doi.org/10.59292/bulletinbiomath.2024009>



RESEARCH PAPER

A mathematical model for the study of HIV/AIDS transmission with PrEP coverage increase and parameter estimation using MCMC with a Bayesian approach

Erick Manuel Delgado Moya ^{1,*}, Ranses Alfonso Rodriguez ^{2,†} and Alain Pietrus ^{3,‡}

¹Institute of Collective Health (ISC), Federal University of Bahia (UFBA), Rua Basilio da Gama, Salvador, 40.110-040 Bahia, Brazil, ²Department of Applied Mathematics, Florida Polytechnic University, Lakeland, FL 33805, USA, ³Department of Mathematics and Computer Sciences, University of Antilles, LAMIA (EA 4540), BP 250, 97159, Pointe-a-Pitre, Guadeloupe, France

* Corresponding Author

† erickdelgadomoya@gmail.com (Erick Manuel Delgado Moya); ranses.alfonso@gmail.com (Ranses Alfonso Rodriguez); alain.pietrus@univ-antilles.fr (Alain Pietrus)

Abstract

In this article, we present a mathematical model for the study of HIV/AIDS considering the implementation of Pre-Exposure Prophylaxis (PrEP). As a novel element in the construction of the model, we consider the diagnosis of cases for attempting to enter the PrEP program, which allows us to study different forms of PrEP. The diagnosis of new infections helps to reduce transmission in the population because these patients are incorporated into the therapy and can achieve an undetectable viral load in blood which prevents them from infecting others. The model contains a compartment of infected persons with undetectable viral load in blood that is reached by adherence to treatment which is separated from those simply infected with the virus as they do not transmit it. Considering the structure of the model, we propose a method to study the effect of increased PrEP use and HIV incidence in a population. In the case of incidence, we took into account the stochasticity of the behavior. Besides, we find the basic reproduction number and present results that allow us to obtain the impact of the parameters associated with transmission, treatment and diagnosis on the basic reproduction number. We perform computational simulations, using demographic and HIV/AIDS data from Brazil, and utilize the Markov Chain Monte Carlo (MCMC) method with a Bayesian approach to estimate model parameters. We study two coverage increases at 25% and 35% that were selected according to the size of the Brazilian population and the daily use of PrEP. We compare the increases in coverage focused on HIV incidence, which is the number of new HIV cases infected and the number of HIV cases avoided, we conclude that by increasing PrEP coverage the incidence of HIV is reduced and the number of cases avoided increases.

Keywords: HIV; incidence; MCMC; parameter estimation; PrEP

AMS 2020 Classification: 37N25; 34A12; 60J22; 97M60

1 Introduction

HIV (human immunodeficiency virus) is a virus that attacks an individual's immune system. HIV is the cause of AIDS (Acquired Immune Deficiency Syndrome) which is an advanced stage of the disease, in which the immune system is compromised [1] and fails to cope with certain diseases. HIV-positive persons are diagnosed with AIDS if they have a CD4 count below 200 cells/mm³ or if they contract certain opportunistic infections [1].

The HIV/AIDS virus is a problem that the world's health systems are facing, and adherence to treatment and preventive programs is an important element in controlling the pandemic. In 2021, 38.4 million [33.9 million - 43.8 million] people worldwide were living with HIV; 1.5 million [1.1 million - 2 million] people had become infected with HIV; 650,000 [510,000 - 860,000] people had died of AIDS-related illnesses; and 28.7 million people were accessing antiretroviral therapy [2–4]. HIV treatment (antiretroviral therapy, ART) is currently available in one-or two-pill daily regimens that can be initiated early in HIV infection and control HIV replication. The life expectancy of persons who have achieved immune reconstitution and remain virologically suppressed should be near normal. A suppressed or undetectable viral load in HIV-infected persons means that the person does not infect his or her sexual partner [5–7].

Oral PrEP uses antiretroviral drugs in pill form to prevent the spread of HIV/AIDS. Currently, there are two approved forms of oral PrEP in use: a combination of tenofovir and emtricitabine or TDF/FTC (brand name Truvada) and a combination of tenofovir, alafenamide, and emtricitabine or F/TAF (brand name Descovy) [8]. PrEP reduces the risk of acquiring HIV sexually by approximately 99% and the risk of acquiring HIV through injection drug use by at least 74% [9].

People using oral PrEP may have adherence problems due to daily use and forgetting to take the pill, searching for the pill over time in places where it is distributed or sold, availability of the product, etc. To counteract these complications generated by daily use, a new model of injectable PrEP has appeared, which avoids interruptions in its use because the injection would only be necessary once every two months [10, 11].

Studies of the impact of PrEP in a population with the use of mathematical models have been increasing [7, 9, 12–21]. Moya et al. [7] presented a mathematical model for studying the influence of PrEP and PEP (Post-Exposure Prophylaxis) in the presence of nondiagnostics and undetectables and Moya and Rodrigues [9] introduced a fractional order mathematical model to study the impact of the oral to the injectable Pre-Exposed Prophylaxis modality. Kim et al. [12] construct a mathematical model of HIV infection among MSM (men who have sex with men) in South Korea and simulate the effects of early antiretroviral therapy (ART), early diagnosis, PrEP, and combined interventions on the incidence and prevalence of HIV/AIDS infection. Omondi et al. [13] presented a mathematical model stratified by sex and sexual preference and included PrEP in the dynamics. Li et al. [14] presented a mathematical model to assess the impact of PrEP, biomedical interventions, and their combinations, and simulated it for a 20-year period. Silva and Torres [15] proposed a mathematical model for HIV/AIDS transmission that includes the PrEP preventive program and demonstrated that PrEP significantly reduces HIV transmission. Nabil and Hamaizia [16] presented three-dimensional discrete-time model to describe the behavior of cancer cells in the presence of healthy cells and HIV-infected cells and performed a theoretical study of the model. Bolaji et al. [17] proposed a model for HIV and tuberculosis co-infection and conclude that concentrating treatment on individuals infected with tuberculosis at the diagnosed latent infection stage could effectively reduce the incidence of HIV in the study population. Naik

et al [18] presented a fractional order model of HIV-1 using Caputo derivatives that involves interactions between cancer cells, healthy CD4+ T cells, and virus-infected CD4+ T cells. Mustapha et al. [19] developed a mathematical model that incorporates public awareness and treatment into the dynamics of HIV/AIDS in an infected population with a detectable and undetectable viral load. Yavuz et al. [20] presented a new mathematical model for the study of the transmission of the hepatitis B virus (HBV). Moya et al. [21] presented a model for Tuberculosis with the incorporation of 3HP treatment for latent tuberculosis and use the Markov Chains Monte Carlo (MCMC) method with a Bayesian approach for the estimation of model parameters and the study in Brazil, a methodology analogous to the presented in this paper.

The aim of our work is to present a model for HIV/AIDS dynamics with the incorporation of PrEP as a compartment. The model allows studying different forms of PrEP based on adherence and variations in PrEP coverage in the population. Furthermore, with the information provided by the model, we can study the incidence of HIV for different increases in PrEP coverage and the basic number reproduction and the impact on it of parameters associated with adherence to treatment and diagnosis of cases. Based on the model structure, we perform parameter estimation using the Markov Chains Monte Carlo (MCMC) method with a Bayesian approach.

Considering the structure of the model, we propose, we can study different forms of PrEP, for example oral PrEP and injectable PrEP, and changes in PrEP coverage. Reproducing the methodology used will allow us to compare these different forms of PrEP and possible increases in coverage and make decisions based on the results of HIV incidence, HIV rate ratio, and the number of cases avoided. In addition, in the dynamics we also have important elements such as the diagnosis of cases due to the use of PrEP through HIV tests applied upon entry into the program and adherence to PrEP (which allows us to study different variants), adherence to antiretroviral treatment based on the undetectability of the viral load in the blood that we quantify in a compartment since these individuals have the virus but do not infect. Using computer simulations of the model, we will study the impact of an increase in PrEP coverage in the population based on the incidence of HIV, the HIV rate ratio and the number of cases avoided. This paper is organized as follows: in [Section 2](#), we present the model, study its mathematical properties, the incidence definition, and the incorporation of the PrEP program. [Section 3](#) evaluates the basic reproduction number and investigates its sensitivity analysis. [Section 4](#) is devoted to parameter estimation, [Section 5](#) presents the computational simulations, and in [Section 6](#) the conclusions of the paper are discussed.

2 Model construction

For the construction of the model, we considered the following compartments: Susceptibles (S), exposed to HIV/AIDS (E), people using PrEP (P), HIV cases (H), AIDS cases (A), and HIV/AIDS positive cases with undetectable viral load in blood (V).

We consider several parameters: Λ is the recruitment rate, so parameter Λ will represent the birth rate, while parameter α_s refers to cases of people who become infected with HIV through non-sexual routes, such as transmission from mother to child during childbirth, drug injection, blood transfusions, among others.

The parameter μ represents the death rate from natural causes (death that is not associated with the disease or its consequences). The virus transmission rate is defined as:

$$\lambda = \beta \frac{(H + \epsilon A)}{N}, \quad (1)$$

where β is the effective contact rate, ϵ is the modification parameter that adapts the AIDS condition

to contagion. and N is the total population ($N = S + E + P + H + A + V$).

We define d_H as disease-associated death in people living with HIV and AIDS. We assume that people who have undetectable viral load due to a low concentration of virus in the body die in a way associated with the disease under the rate d_H . The rate ϕ represents the movement of an HIV/AIDS-positive individual who is diagnosed in HIV status so $(1 - \phi)$ is diagnosed with AIDS, ϵ_{s1} is the HIV/AIDS rate diagnosis in a risk contact.

Compartment V contains virus-infected individuals who, due to the adherence of antiretroviral treatment, reach an undetectable viral load in blood and do not transmit the virus. Parameters σ_{HI} and ν will represent HIV and AIDS cases that by adherence to therapy reach an undetectable viral load in blood and σ_H and ω will represent the loss of undetectability in viral load in blood for different reasons, such as treatment withdrawal, non-adherence to treatment, re-infection, etc, and entry into the HIV and AIDS compartments, respectively. We define the rate of progression from HIV to AIDS as τ .

The parameters ϵ_p and ϵ_f represent the rate of PrEP use (coverage of PrEP use in a population) and the rate of withdrawal and/or non-adherence to therapy. We assume that when the person does not adhere to the treatment, they become susceptible to the virus, but as long as treatment is followed properly, the person does not acquire the virus by any means. We assume that individuals entering the PrEP program are tested for HIV/AIDS so this gives a chance of diagnosing new cases. The parameter ϵ_D is related to the diagnosis of patients who were diagnosed for expressing interest in entering the PrEP program and were tested for HIV/AIDS. In the model, the diagnosis of cases for attempting to enter the PrEP program is studied. The other types of diagnosis are found in the incorporated dynamics of the exit of cases exposed to the HIV (H) and AIDS (A) compartments. Regarding the relationship between the use of PrEP and the diagnosis of new cases due to attempts to enter the PrEP program, we have to take into account factors such as the availability of both PrEP and HIV tests, which both have a cost on the market and in particular the use of PrEP is daily, dissemination of the effectiveness of PrEP and expanding its use in different social groups. These factors can be limiting to a positive impact of PrEP both in prevention and diagnosis.

The model allows the study of different forms of PrEP and also takes into account different forms of infection and the application of antiretroviral therapies.

Figure 1 shows the flow diagram of the model. The model that studies the behavior of HIV/AIDS with the presence of PrEP in a population is described as:

$$\frac{dS}{dt} = \Lambda + \epsilon_f P - (\mu + \lambda + \alpha_s + \epsilon_p) S, \quad (2)$$

$$\frac{dE}{dt} = \lambda S - (\epsilon_{s1} + \mu) E, \quad (3)$$

$$\frac{dP}{dt} = \epsilon_p S - (\mu + \epsilon_f + \epsilon_D) P, \quad (4)$$

$$\frac{dH}{dt} = \phi(\epsilon_{s1} E + \epsilon_D P) + \sigma_H V + \alpha_s S - (\mu + d_H + \tau + \sigma_{HI}) H, \quad (5)$$

$$\frac{dA}{dt} = (1 - \phi)(\epsilon_{s1} E + \epsilon_D P) + \omega V + \tau H - (\mu + d_H + \nu) A, \quad (6)$$

$$\frac{dV}{dt} = \sigma_{HI} H + \nu A - (\mu + d_H + \sigma_H + \omega) V, \quad (7)$$

with initial conditions:

$$S(t_0) > 0, E(t_0) > 0, P(t_0) \geq 0, H(t_0) > 0, A(t_0) > 0 \text{ and } V(t_0) > 0.$$

The initial conditions for the PrEP compartment can start with the value zero because we can make a prospective study of the epidemic after the implementation of PrEP in the population.

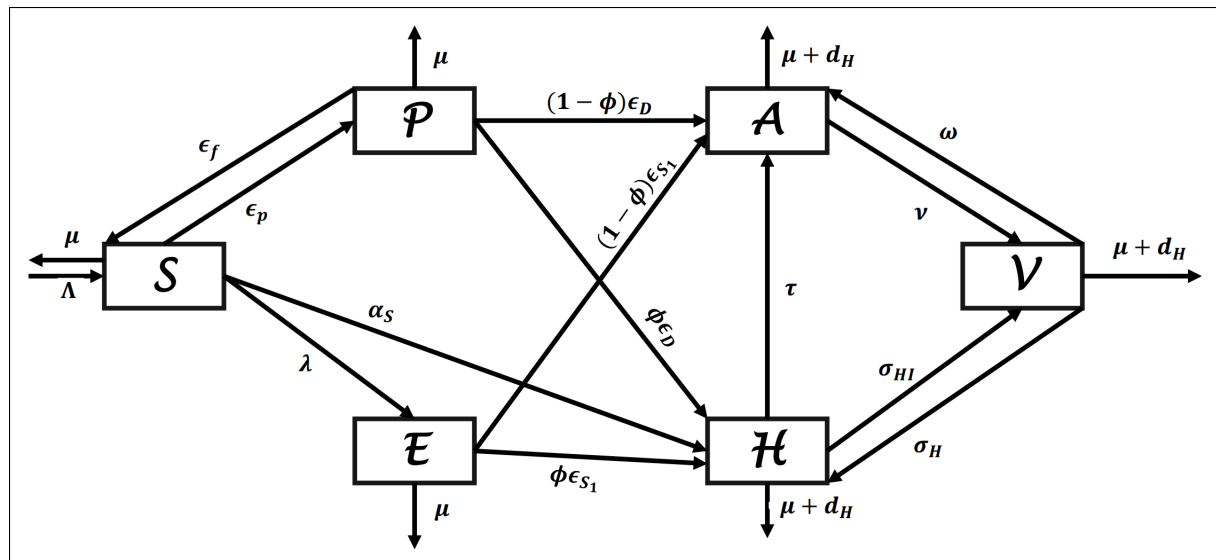


Figure 1. Flow chart of model (2)-(7). The recruitment rate is Λ and the death rate from natural causes is μ and is the same in all compartments. The use of PrEP is only admitted to those susceptible and parameters ϵ_p and ϵ_f represent the rate of PrEP use and failure to use PrEP. Before entering the PrEP program it is necessary to do HIV tests and with this, we help in the detection of new cases of HIV and AIDS, and is defined in parameter ϵ_D . Those who are susceptible are exposed to the virus with the transmission rate of virus λ . The α_s rate defines the individuals who become infected through non-sexual routes. The exposed (E compartment) who acquire the virus are diagnosed with HIV or AIDS with the diagnosis rate, ϵ_{s1} . The τ is the rate of evolution of the disease from HIV to AIDS. Parameters σ_{HI} and ν are associated with those infected with HIV (H compartment) and AIDS (A compartment) who, using retroviral treatment, achieve an undetectable viral load and enter V compartment, and parameters ω and σ_H are when undetectability is lost and depending on the disease stages enters H or A . The parameter d_H represents death associated with HIV/AIDS

The parameters and their definitions are given in [Table 1](#).

Table 1. Definition of model parameters (2)-(7)

Parameter	Definition
Λ	Recruitment rate
ϵ	Modification parameter associated with virus transmission from AIDS patient
ϵ_p	PrEP use selection rate
ϵ_f	PrEP therapy failure rate
ϵ_D	Diagnosis rate of patients who attempted to enter the PrEP program
α_s	HIV infection rate by non-sexual routes
μ	Death rate due to natural causes
β	Effective contact rate
ν	Rate of progression from AIDS to undetectable
ϕ	Virus progression rate
ϵ_{s1}	Rate of detection and diagnosis of persons at risk contact
τ	Rate of progression from HIV to AIDS
σ_{HI}	Rate of progression from HIV to undetectable
ω	Rate of progression from undetectable to AIDS
σ_H	Rate of progression from undetectable to HIV
d_H	Death rate associated with HIV/AIDS

Basic properties of model

Now, let us prove the existence and non-negativity of the solution of model (2)-(7), and let's find the biologically feasible region.

Non-negativity and boundless of solutions

Theorem 1 *Let initial data be $S(t_0) > 0, E(t_0) > 0, P(t_0) > 0, H(t_0) > 0, A(t_0) > 0$ and $V(t_0) > 0$. Then, the solutions $(S(t), E(t), P(t), H(t), A(t), V(t))$ of model (2)-(7) are positive for all $t > 0$. Furthermore,*

$$\limsup_{t \rightarrow \infty} N(t) \leq \frac{\Lambda}{\mu}. \tag{8}$$

Proof By first equation of model (2)-(7), we have that:

$$\frac{dS}{dt} = \Lambda + \epsilon_f P - (\mu + \lambda + \alpha_s + \epsilon_p)S \leq \Lambda - (\mu + \lambda + \alpha_s + \epsilon_p)S, \tag{9}$$

can be rewritten as

$$\frac{d}{dt} \left[S(t) \exp \left\{ (\mu + \lambda + \alpha_s + \epsilon_p)t + \int_{t_0}^t \lambda(s)ds \right\} \right] \geq \Lambda \exp \left\{ (\mu + \lambda + \alpha_s + \epsilon_p)t + \int_{t_0}^t \lambda(s)ds \right\}. \tag{10}$$

Hence, for $0 \leq t_0 \leq t^*$,

$$S(t^*) \exp \left\{ (\mu + \lambda + \alpha_s + \epsilon_p)t^* + \int_{t_0}^{t^*} \lambda(s)ds \right\} - S(t_0) \geq \int_{t_0}^{t^*} \Lambda \exp \left\{ (\mu + \lambda + \alpha_s + \epsilon_p)u + \int_{t_0}^u \lambda(w)dw \right\} du. \tag{11}$$

So that,

$$S(t^*) \geq S(t_0) \exp \left\{ - \left((\mu + \lambda + \alpha_s + \epsilon_p)t^* + \int_{t_0}^{t^*} \lambda(s)ds \right) \right\} + \exp \left\{ - \left((\mu + \lambda + \alpha_s + \epsilon_p)t^* + \int_{t_0}^{t^*} \lambda(s)ds \right) \right\} \times \int_{t_0}^{t^*} \Lambda \exp \left\{ - \left((\mu + \lambda + \alpha_s + \epsilon_p)u + \int_{t_0}^u \lambda(w)dw \right) \right\} du > 0. \tag{12}$$

Similarly, it can be shown that $E(t), P(t), H(t), A(t)$ and $V(t) > 0$ for all $t > 0$.

Moreover, we have

$$\frac{dN}{dt} = \Lambda - \mu N - d_H(H + A + V). \tag{13}$$

Then,

$$\Lambda - (\mu + d_H)N \leq \frac{dN}{dt} \leq \Lambda - \mu N, \tag{14}$$

which gives

$$\frac{\Lambda}{\mu + d_H} \leq \liminf_{t \rightarrow \infty} N(t) \leq \limsup_{t \rightarrow \infty} N(t) \leq \frac{\Lambda}{\mu}. \tag{15}$$

So, we have that

$$\limsup_{t \rightarrow \infty} N(t) \leq \frac{\Lambda}{\mu}.$$

Biologically feasible region

Now, let's define the biologically feasible region for the model (2)-(7).

Lemma 1 *The closed set $\Omega = \left\{ (S, E, P, H, A, V) \in \mathbb{R}_+^6 : N(t) \leq \frac{\Lambda}{\mu} \right\}$ is positively-invariant and attracts all solutions of model (2)-(7).*

Proof The derivative of N (total population) is

$$\frac{dN}{dt} = \Lambda - \mu N - d_H(H + A + V). \quad (16)$$

Since $\frac{dN}{dt} \leq \Lambda - \mu N$, it follows that $\frac{dN}{dt} \leq 0$, if $N(t) \geq \frac{\Lambda}{\mu}$. Hence, the standard comparison theorem from [22] can be used to show that $N(t) \leq N(t_0) \exp\{-\mu t\} + \frac{\Lambda}{\mu} \left(1 - \exp\{-\mu t\} \right)$.

In particular, if $N(t_0) \leq \frac{\Lambda}{\mu}$, then $N(t) \leq \frac{\Lambda}{\mu}$ for all $t > 0$. Hence, the domain Ω is positively invariant.

Furthermore, if $N(t_0) > \frac{\Lambda}{\mu}$, then either the solution enters the domain Ω in finite time or $N(t)$ approaches $\frac{\Lambda}{\mu}$ asymptotically as $t \rightarrow \infty$. Hence, the domain Ω attracts all solutions in \mathbb{R}_+^6 .

Existence of solution

Theorem 2 *The solutions of model (2)-(7) with non-negative initial conditions exist for all time.*

Proof The right-hand side of the model is locally Lipschitz continuous, and this proves the local existence of the solution. The global existence of the solution follows from the bound found in Theorem 1, inequality (8).

Incidence

Incidence is the number of newly diagnosed cases of a disease. The incidence rate is the number of new cases of a disease divided by the number of people at risk of contracting the disease [23, 24]. Prevalence differs from incidence in that prevalence includes all active cases, both new and pre-existing, in the population at the specified time, whereas incidence is limited to new cases only. New entries in the HIV compartment are incorporated into the model with the following differential equation respectively:

$$\frac{dI}{dt} = \phi(\epsilon_{s1}E + \epsilon_D P) + \alpha_s S. \quad (17)$$

The HIV incidence is defined as:

$$I^*(t) = I(t) - I(t-1), \quad (18)$$

where t is the current time and $t - 1$ is the moment of time immediately preceding. Then, the HIV incidence rate is:

$$\text{HIV Incidence Rate } (t) = \frac{I^*(t) * 100000}{N}. \quad (19)$$

Given that this methodology is deterministic by itself, we introduce stochasticity by considering the negative binomial distribution (*Negbin*), one of the most general for modeling count data. Its density function is given by:

$$f_Y(y) = \binom{y + v - 1}{y} \left(\frac{s}{s + v} \right)^y \left(\frac{v}{s + v} \right)^v, \quad y \in \mathbb{N}, \quad (20)$$

where $E(Y) = s > 0$ is the expected value and $v > 0$ is the parameter that controls for overdispersion. Let \mathbf{Y}_1 be a random vector representing the annual new cases. Considering stochasticity, we have that $\mathbf{Y}_1 = (Y_{11}, \dots, Y_{1t})$ with $\mathbf{Y}_{1t} \sim \text{Negbin}(s_{1t}, v)$, where:

$$s_{1t} = I(t) - I(t - 1) = I^*(t). \quad (21)$$

In this way, we are not only able to get a point estimate but also a confidence interval for allowing stochasticity.

Increased PrEP coverage

The new PrEP coverage is based on the percentage increase of the current coverage, so the parameter ϵ_p in the period 2025-2035 will have the following structure:

$$\epsilon_p(t) = \epsilon_p(t - 1) + p_s \epsilon_p(t - 1), \quad (22)$$

where $\epsilon_p(t)$ is the current coverage in that year, $\epsilon_p(t - 1)$ is the coverage in the previous year, and p_s is the percent increase in coverage.

3 Basic reproduction number

In a population composed only of susceptible individuals, the average number of infections caused by an infected individual is defined as basic reproduction number \mathfrak{R}_0 . In our study, we have that the compartment of undetectable infected individuals cannot be infected by the virus but upon losing undetectability they pass to the infectious state of HIV or AIDS depending on the state of the disease in which the individual is. The incorporation of these individuals in the study of the basic reproduction number allows us to study the effect of reaching a state of virus undetectability and the impact it has when it is lost.

If $0 < \mathfrak{R}_0 < 1$, the infection will disappear in the long term, and if $\mathfrak{R}_0 > 1$ the infection can spread in a population [25, 26]. The higher the \mathfrak{R}_0 , the more difficult it will be to control the epidemic. \mathfrak{R}_0 can be affected by several factors, such as the duration of infectivity of the affected patients, the infectivity of the organism, and the degree of contact between susceptible and infected populations.

Our interest is to study the disease-free equilibrium point due to its relationship with the basic

reproduction number. The disease-free equilibrium point (DFE) is:

$$\epsilon_0 = \left(\frac{\Lambda}{(\mu + \alpha_s + \epsilon_p)}, 0, 0, 0, 0, 0 \right). \tag{23}$$

To find the basic reproduction number, we use the next-generation matrix method presented in [25–27], where

$$F = \begin{pmatrix} 0 & 0 & \frac{\beta\Lambda}{N(\mu + \epsilon_p + \alpha_s)} & \frac{\epsilon\beta\Lambda}{N(\mu + \epsilon_p + \alpha_s)} & 0 \\ 0 & 0 & 0 & 0 & 0 \\ 0 & 0 & 0 & 0 & 0 \\ 0 & 0 & 0 & 0 & 0 \\ 0 & 0 & 0 & 0 & 0 \end{pmatrix},$$

$$V = \begin{pmatrix} k_0 & 0 & 0 & 0 & 0 \\ 0 & k_p & 0 & 0 & 0 \\ -\phi\epsilon_{s1} & -\phi\epsilon_D & k_1 & 0 & 0 \\ -(1-\phi)\epsilon_{s1} & -(1-\phi)\epsilon_D & -\tau & k_2 & -\omega \\ 0 & -\sigma_{HI} & 0 & -\nu & k_3 \end{pmatrix},$$

are the matrices of transmission and transition terms, respectively and $k_p = \mu + \epsilon_f + \epsilon_p$, $k_0 = \mu + \epsilon_{s1}$, $k_1 = \mu + d_H + \tau + \sigma_{HI}$, $k_2 = \mu + d_H + \nu$ and $k_3 = \mu + d_H + \sigma_H + \omega$. Then, for model (2)-(7) the basic reproduction number is

$$\mathfrak{R}_0 = \rho(FV^{-1}) = \left| \frac{\Lambda\beta\epsilon_{s1} \left(k_3(k_2\phi + \epsilon(k_1(1-\phi) + \phi\tau)) + (\epsilon\sigma_{HI} - \nu)(\sigma_H(\phi - 1) + \phi\omega) \right)}{N(\mu + \alpha_s + \epsilon_p)k_0 \left(k_2(\sigma_H\sigma_{HI} - k_1k_3) + \nu(\sigma_H\tau + k_1\omega) \right)} \right|, \tag{24}$$

where $\rho(FV^{-1})$ is the spectral radius of matrix FV^{-1} .

To find the basic reproduction number with the next-generation matrix method, we use the infection-free equilibrium point (ϵ_0) and now we will briefly present results that relate the stability of this point with the behavior of the \mathfrak{R}_0 .

Theorem 3 *The infection-free equilibrium point (ϵ_0) of model (2)-(7), is locally asymptotically stable (LAS) if $\mathfrak{R}_0 < 1$ and unstable if $\mathfrak{R}_0 > 1$.*

The threshold quantity \mathfrak{R}_0 is the basic reproduction number of HIV/AIDS model (2)-(7). It measures the average number of new diseases generated by a single infectious agent in a fully susceptible population. Consequently, the disease-free equilibrium of model (2)-(7) is locally asymptotically stable (LAS) whenever $\mathfrak{R}_0 < 1$ and unstable if $\mathfrak{R}_0 > 1$. This means that HIV/AIDS can be removed from the community (when $\mathfrak{R}_0 < 1$) if the population sizes of model (2)-(7) are in the basin of attraction of the disease-free equilibrium ϵ_0 .

Now, we prove the global stability of the infection-free equilibrium point. Following [27], we can

rewrite the model (2)-(7) as

$$\begin{aligned} \frac{dX}{dt} &= f(S, I), \\ \frac{dI}{dt} &= g(S, I), \quad g(S, 0_{\mathbb{R}^5_+}) = 0, \end{aligned} \tag{25}$$

where $S \in \mathbb{R}_+$ is the susceptible compartment, $I \in \mathbb{R}^5_+$ have the compartments exposed, HIV, AIDS and undetectable of model (2)-(7) and $0_{\mathbb{R}^5_+}$ is the null vector of the space \mathbb{R}^5_+ .

The disease-free equilibrium is now denoted by $E_0 = (S_0, 0_{\mathbb{R}^5})$ where $S_0 = \frac{\Lambda}{\mu + \alpha_s + \epsilon_p}$.

The conditions (H_1) and (H_2) below must be satisfied to guarantee the global asymptotic stability of E_0 .

$$\begin{aligned} (H_1) : & \text{ For } \frac{dS}{dt} = f(S, 0_{\mathbb{R}^5}), \quad S_0 \text{ is globally asymptotically stable,} \\ (H_2) : & \quad g(S, I) = AI^T - g^*(S, I), \quad g^*(S, I) \geq 0, \quad \text{for } (S, I) \in \Omega, \end{aligned} \tag{26}$$

where $A = D_I g(S_0, 0_{\mathbb{R}^5})$ ($D_I g(S_0, 0_{\mathbb{R}^5})$ is the Jacobian of g at $(S_0, 0_{\mathbb{R}^5})$) is a M-matrix (the off-diagonal elements of A are non-negative) and Ω is the biologically feasible region.

The following theorem shows the global stability of the infection-free equilibrium point.

Theorem 4 *The fix point E_0 is a globally asymptotically stable equilibrium (G.A.S) of model (2)-(7) provided that $\mathfrak{R}_0 < 1$ and that the conditions (H_1) and (H_2) are satisfied.*

Proof Let

$$f(S, 0_{\mathbb{R}^5}) = \Lambda - (\mu + \alpha_s + \epsilon_p).$$

As $f(S, 0_{\mathbb{R}^5})$ is linear, then S_0 is globally stable. Then, (H_1) is satisfied. Let

$$A = \begin{pmatrix} -k_0 & 0 & \beta & \epsilon\beta & 0 \\ 0 & -k_p & 0 & 0 & 0 \\ \phi\epsilon_{s1} & \phi\epsilon_D & -k_1 & 0 & \sigma_H \\ (1-\phi)\epsilon_{s1} & (1-\phi)\epsilon_D & \tau & -k_2 & \omega \\ 0 & 0 & \sigma_{HI} & \nu & -k_3 \end{pmatrix},$$

$$I = (E, P, H, A, V),$$

$$g^*(S, I) = AI^T - g(X, I),$$

$$g^*(S, I) = \begin{pmatrix} g_1^*(X, I) \\ g_2^*(X, I) \\ g_3^*(X, I) \\ g_4^*(X, I) \\ g_5^*(X, I) \end{pmatrix} = \begin{pmatrix} \beta(H + \epsilon A) \left(1 - \frac{S}{N}\right) \\ 0 \\ 0 \\ 0 \\ 0 \end{pmatrix}.$$

Since $\frac{S}{N} \leq 1$ then $1 - \frac{S}{N} \geq 0$. Thus $g^*(S, I) \geq 0$ for all $(S, I) \in \Omega$. Consequently, E_0 is a globally asymptotically stable point. Analogous proofs can be found in the bibliographical references [28–30]. We will study the joint influence of parameters $\epsilon_{s1}, \sigma_{HI}, \sigma_H, \nu$ and ω on the basic reproduction number. These parameters are associated with treatment adherence and effectiveness (undetected virus in the blood), treatment failure, and diagnosis of cases exposed to the virus. These parameters are defined in the interval $[0, 1]$ and we want to study the joint behavior when they are at the extreme values of the interval. At the extremes of the interval are the critical behaviors because they may represent all individuals or none and it is of interest to study this epidemiological situation together.

Firstly, we will study the undetectability in HIV and its impact on the basic reproduction number. The following limit characterizes the increase in the number of patients with HIV who achieve undetectability of the virus in the blood and the decrease in the number of patients who lose it and pass to the HIV state:

$$\lim_{\substack{\sigma_{HI} \rightarrow 1 \\ \sigma_H \rightarrow 0}} \mathfrak{R}_0 = \frac{\beta \Lambda \epsilon_{s1} \left((\mu + d_H + \omega) (k_2 \phi + \epsilon((\mu + d_H + \tau + 1)(1 - \phi) + \phi \tau)) + (\epsilon - \nu) \phi \omega \right)}{N(\mu + \epsilon_p + \alpha_s) k_0 (\nu(\mu + d_H + \tau + 1) \omega - k_2(\mu + d_H + \tau + 1)(\mu + d_H + \omega))}. \quad (27)$$

The opposite case is defined as:

$$\lim_{\substack{\sigma_{HI} \rightarrow 0 \\ \sigma_H \rightarrow 1}} \mathfrak{R}_0 = \frac{\beta \Lambda \epsilon_{s1} \left((\mu + d_H + \omega + 1) (k_2 \phi + \epsilon((\mu + d_H + \tau)(1 - \phi) + \phi \tau)) - \nu((\phi - 1) + \phi \omega) \right)}{N(\mu + \epsilon_p + \alpha_s) k_0 (\nu(\tau + (\mu + d_H + \tau) \omega) - k_2(\mu + d_H + \tau)(\mu + d_H + \omega + 1))}. \quad (28)$$

With the expressions (27)-(28) of \mathfrak{R}_0 , we can characterize the impact that the increase and decrease in the number of patients with HIV who achieve undetectable virus loads in the blood has together with the increase and decrease in the number of patients who lose undetectability and acquire detectable levels of HIV.

Now, we are going to study the case of patients with AIDS who achieve undetectability of the virus in the blood and patients who lose undetectability and enter the compartment of AIDS. The expressions that characterize this situation are:

$$\lim_{\substack{\nu \rightarrow 1 \\ \omega \rightarrow 0}} \mathfrak{R}_0 = \frac{\beta \Lambda \epsilon_{s1} \left((\mu + d_H + \sigma_H) ((\mu + d_H + 1) \phi + \epsilon(k_1(1 - \phi) + \phi \tau)) + (\epsilon \sigma_{HI} - 1) \sigma_H (\phi - 1) \right)}{N(\mu + \epsilon_p + \alpha_s) k_0 ((\mu + d_H + 1) (\sigma_H \sigma_{HI} - k_1(\mu + d_H + \sigma_H)) + \sigma_H \tau)}, \quad (29)$$

$$\lim_{\substack{\nu \rightarrow 0 \\ \omega \rightarrow 1}} \mathfrak{R}_0 = \frac{\beta \Lambda \epsilon_{s1} \left((\mu + d_H + \sigma_H + 1) ((\mu + d_H) \phi + \epsilon(k_1(1 - \phi) + \phi \tau)) + \epsilon \sigma_{HI} (\sigma_H (\phi - 1) - \phi) \right)}{N(\mu + \epsilon_p + \alpha_s) k_0 ((\mu + d_H) (\sigma_H \sigma_{HI} - k_1(\mu + d_H + \sigma_H + 1)))}. \quad (30)$$

We will find the expressions for the increase and decrease in cases of HIV and AIDS that achieve the virus's undetectability in the blood and when they lose it and become infectious again. The expressions for achieving the undetectability of the virus in the blood for HIV and AIDS together

are:

$$\lim_{\substack{\sigma_{HI} \rightarrow 1 \\ \nu \rightarrow 1}} \mathfrak{R}_0 = \frac{\beta \Lambda \epsilon_{s1} \left(k_3 ((\mu + d_H + 1)\phi + \epsilon((\mu + d_H + \tau + 1)(1 - \phi) + \phi\tau)) + (\epsilon - 1)(\sigma_H(\phi - 1) + \phi\omega) \right)}{N(\mu + \epsilon_p + \alpha_s)k_0((\mu + d_H + 1)(\sigma_H - (\mu + d_H + \tau + 1)k_3) + (\sigma_H\tau + (\mu + d_H + \tau + 1)\omega))}, \quad (31)$$

$$\lim_{\substack{\sigma_{HI} \rightarrow 0 \\ \nu \rightarrow 0}} \mathfrak{R}_0 = \frac{\beta \Lambda \epsilon_{s1} k_3 \left((\mu + d_H)\phi + \epsilon((\mu + d_H + \tau)(1 - \phi) + \phi\tau) \right)}{-N(\mu + \epsilon_p + \alpha_s)k_0(\mu + d_H)(\mu + d_H + \tau)k_3}. \quad (32)$$

For the loss of the undetectability of the virus and return to the infectious state in the HIV and AIDS compartments are:

$$\lim_{\substack{\sigma_{HI} \rightarrow 1 \\ \omega \rightarrow 1}} \mathfrak{R}_0 = \frac{\beta \Lambda \epsilon_{s1} \left((\mu + d_H + 2)(k_2\phi + \epsilon(k_1(1 - \phi) + \phi\tau)) + (\epsilon\sigma_{HI} - \nu)(2\phi - 1) \right)}{N(\mu + \epsilon_p + \alpha_s)k_0(k_2(\sigma_{HI} - k_1(\mu + d_H + 2)) + \nu(\tau + k_1))}, \quad (33)$$

$$\lim_{\substack{\sigma_H \rightarrow 0 \\ \omega \rightarrow 0}} \mathfrak{R}_0 = \frac{\beta \Lambda \epsilon_{s1} (\mu + d_H) \left(k_2\phi + \epsilon(k_1(1 - \phi) + \phi\tau) \right)}{-N(\mu + \epsilon_p + \alpha_s)k_0k_2k_1(\mu + d_H)}. \quad (34)$$

Besides, we are interested in studying the impact of the growth and decrease of the parameters associated with HIV cases that reach AIDS (τ) and the achievement of undetectability of the virus in the blood of cases with AIDS (ν). This factor is interesting because if a case reaches the stage of AIDS and, with adherence to the treatment, we manage to have the undetectable status of the virus in the blood, we would be avoiding new infections. The expressions of the limits of \mathfrak{R}_0 for this situation are:

$$\lim_{\substack{\tau \rightarrow 1 \\ \nu \rightarrow 0}} \mathfrak{R}_0 = \frac{\beta \Lambda \epsilon_{s1} \left(k_3(\phi(\mu + d_H) + \epsilon((\mu + d_H + \sigma_{HI} + 1)(1 - \phi) + \phi)) + \epsilon\sigma_{HI}(\sigma_H(\phi - 1) + \phi\omega) \right)}{N(\mu + \epsilon_p + \alpha_s)k_0((\mu + d_H)(\sigma_H\sigma_{HI} - (\mu + d_H + \sigma_{HI} + 1)k_3))}, \quad (35)$$

$$\lim_{\substack{\tau \rightarrow 0 \\ \nu \rightarrow 1}} \mathfrak{R}_0 = \frac{\beta \Lambda \epsilon_{s1} \left(k_3(\phi(\mu + d_H + 1) + \epsilon(\mu + d_H + \sigma_{HI})(1 - \phi)) + (\epsilon\sigma_{HI} - 1)(\sigma_H(\phi - 1) + \phi\omega) \right)}{N(\mu + \epsilon_p + \alpha_s)k_0((\mu + d_H + 1)(\sigma_H\sigma_{HI} - (\mu + d_H + \sigma_{HI})k_3) + (\mu + d_H + \sigma_{HI})\omega)}. \quad (36)$$

Now, we are going to study the increase in the diagnosis of cases rate (ϵ_{s1}) in conjunction with the undetectability of the virus in the blood, which leads to the diagnosis and effectiveness in treatment in cases with HIV and AIDS. The following expressions characterize these situations:

$$\lim_{\substack{\epsilon_{s1} \rightarrow 1 \\ \sigma_{HI} \rightarrow 0}} \mathfrak{R}_0 = \frac{\beta \Lambda \left(k_3(k_2\phi + \epsilon((\mu + d_H + \tau + 1)(1 - \phi) + \phi\tau)) - \nu(\sigma_H(\phi - 1) + \phi\omega) \right)}{N(\mu + \epsilon_p + \alpha_s)(\mu + 1)(\nu(\sigma_H\tau + (\mu + d_H + \tau + 1)\omega) - k_2k_3(\mu + d_H + \tau + 1))}. \quad (37)$$

$$\lim_{\substack{\epsilon_{s1} \rightarrow 1 \\ \sigma_{HI} \rightarrow 1}} \mathfrak{R}_0 = \frac{\beta\Lambda \left(k_3(k_2\phi + \epsilon((\mu + d_H + \tau)(1 - \phi) + \phi\tau)) + (\epsilon - \nu)(\sigma_H(\phi - 1) - \phi\omega) \right)}{N(\mu + \epsilon_p + \alpha_s)(\mu + 1)(k_2(\sigma_H - k_3(\mu + d_H + \tau)) + \nu(\sigma_H\tau + (\mu + d_H + \tau + 1)\omega))}. \tag{38}$$

Finally, we will find the expressions of the limits for the cases of the increase in the diagnosis of cases (ϵ_{s1}), the increase in the undetectability of the virus and the decrease in the loss of the undetectability of the virus in the blood (we will call the positive scenario) and the increase in the diagnosis of cases with the increase in the loss of undetectability of the virus and the decrease in cases that achieve undetectability of the virus (we will call it semi-positive because case detection is still a positive factor but here we see the infectiousness of the treatment, regarding the undetectability of the virus or adverse situations). Then we have

$$\lim_{\substack{\epsilon_{s1} \rightarrow 1 \\ \sigma_{HI} \rightarrow 1 \\ \nu \rightarrow 1 \\ \sigma_H \rightarrow 0 \\ \omega \rightarrow 0}} \mathfrak{R}_0 = \frac{\beta\Lambda(\mu + d_H) \left((\mu + d_H + 1)\phi + \epsilon((\mu + d_H + \tau + 1)(1 - \phi) + \phi\tau) \right)}{-N(\mu + \epsilon_p + \alpha_s)(\mu + 1)(\mu + d_H + 1)(\mu + d_H)(\mu + d_H + \tau + 1)}, \tag{39}$$

$$\lim_{\substack{\epsilon_{s1} \rightarrow 1 \\ \sigma_{HI} \rightarrow 0 \\ \nu \rightarrow 0 \\ \sigma_H \rightarrow 1 \\ \omega \rightarrow 1}} \mathfrak{R}_0 = \frac{\beta\Lambda(\mu + d_H + 2) \left((\mu + d_H)\phi + \epsilon((\mu + d_H + \tau)(1 - \phi) + \phi\tau) \right)}{-N(\mu + \epsilon_p + \alpha_s)(\mu + 1)(\mu + d_H)(\mu + d_H + 2)(\mu + d_H + \tau)}. \tag{40}$$

By definition, the basic reproduction number is in the closed interval $[0, 1]$, then in cases where the result of the limits is negative, we use the modulus. In the next subsection, we are going to study and obtain expressions for the impact of the parameters associated with the transmission, the rate of PrEP use, the desistence of PrEP use, and contagion by means other than sexual, on the basic reproduction number.

Sensitivity index

The sensitivity analysis of the basic reproduction number determines the relative importance of the parameters present in the basic reproduction number, such as the parameters of transmission, resistance, and recovery, among others. The sensitivity index can be defined using the partial derivatives, provided that the variable is differentiable with respect to the parameter under study. Sensitivity analysis also helps to identify the vitality of the parameter values in the predictions using the model [31–33].

Definition 1 ([33]) *The normalized forward sensitivity index of a variable, v , that depends on the differentiability of a parameter p is defined as:*

$$Y_p^v := \frac{\partial v}{\partial p} \times \frac{p}{v}. \tag{41}$$

The sensitivity index of \mathfrak{R}_0 helps to determine the parameters that have an impact on it. We can characterize the sensitivity index as follows:

- A positive value of the sensitivity index implies that an increase in the parameter value causes an increase in the basic reproduction number.

- A negative value of the sensitivity index implies that an increase in the parameter value causes a decrease in the basic reproduction number.

The expressions of the sensitivity indices of the selected parameters are:

$$Y_{\alpha_s}^{\mathfrak{R}_0} = -\frac{\alpha_s}{\alpha_s + \epsilon_p + \mu} < 0, \quad (42)$$

$$Y_{\epsilon_p}^{\mathfrak{R}_0} = -\frac{\epsilon_p}{\alpha_s + \epsilon_p + \mu} < 0. \quad (43)$$

Parameters α_s and ϵ_p have a negative sensitivity index with respect to \mathfrak{R}_0 , which implies that an increase in these parameters will mean a decrease in \mathfrak{R}_0 . Epidemiologically, we have that an increase in the parameters associated with cases that do not acquire the virus in a risk contact, individuals who enter the PrEP contagion preventive method cause a reduction in the basic reproduction number. In the case of α_s , it also happens that an increase in this parameter causes a decrease in the basic reproduction number because this is a different form of contagion by contact between a susceptible and an infected human. In the case of the parameters associated with deaths and entries into the susceptible community, they are logical values and associated with demographics, since if more people infected with HIV/AIDS die, it leads to fewer infected and if more elements enter the population, the number of susceptible increases, therefore, we have more elements in the dynamics with the possibility of becoming infected with the virus.

4 Parameters estimation

Parameters selection

For the estimation of the model parameters, we used the MCMC (Markov Chains Monte Carlo) with a Bayesian approach. The theory and examples of the MCMC technique with a Bayesian approach that we use can be found in [34–36].

We select to estimate six parameters, the effective contact rate β , since it influences the HIV/AIDS transmission rate; parameters σ_H and ω , which are related to the loss of undetectable viral load and entry into the HIV and AIDS compartments, respectively; τ , which is associated with disease progression to AIDS; ν , which is related to AIDS cases reaching undetectability; and d_H , which is death from the disease. These parameters are associated with treatment efficacy, progression to AIDS, disease-associated death and transmission, and were selected because we are focusing our study on HIV incidence.

Rate ratio

The a posteriori distribution of $\theta|\mathbf{Y}_1 = (Y_{11}, \dots, Y_{1t})^T$, is given by:

$$\pi(\theta|\mathbf{Y}_1) \propto L(\theta|\mathbf{Y}_1)\pi(\theta), \quad (44)$$

with $L(\theta|\mathbf{Y}_1)$ being the likelihood corresponding to the negative binomial distribution in (20) and $\pi(\theta)$ the independent prior structure generated by:

$$\pi(\theta) \propto \pi(\nu) \times \pi(\sigma_H) \times \pi(\tau) \times \pi(\omega) \times \pi(d_T) \times \pi(\beta), \quad (45)$$

where θ denote the vector of parameters to estimate, for the active tuberculosis model, this vector will be $\theta = (\nu, \sigma_H, \tau, \omega, d_T, \beta)$ keeping the remaining parameters fixed. To forecast a new response,

we use the a posteriori predictive distribution. It is given by,

$$p\left(\mathbf{Y}_{i,pred}|\mathbf{Y}_{i,obs}\right) = \int p\left(\mathbf{Y}_{i,pred}|\boldsymbol{\theta}\right) p\left(\boldsymbol{\theta}|\mathbf{Y}_{i,obs}\right) d\boldsymbol{\theta}. \quad (46)$$

By sampling from (46), we can compute quantities of interest for prediction, the same way we did it with the parameters. For example, one could compute the median and the 2.5% and 97.5% quantiles of this distribution to get a point and a symmetric credibility interval for the new response.

An important element to be analyzed in this study is the rate ratio between a reference scenario which in our case is the scenario where we maintain the implementation of PrEP at this moment and the different types of PrEP studied and the increases in PrEP use. For this analysis, we use the following procedure:

- Generate M vectors $\mathbf{Y}_{i,pred}$ from $p_{\theta_1}\left(\mathbf{Y}_{i,pred}|\mathbf{Y}_{i,obs}\right)$ and $p_{\theta_2}\left(\mathbf{Y}_{i,pred}|\mathbf{Y}_{i,obs}\right)$, where θ_1 and θ_2 are defined for two different scenarios, and then we have M vectors for each scenario.
- Define each vector as $\mathbf{Y}_{sc1,j}$ and $\mathbf{Y}_{sc2,j}$ for $j = 1, \dots, M$ for each scenario.
- For $i = 1, \dots, M$, we compute,

$$Ratio_j = \frac{\mathbf{Y}_{sc1,j}}{\mathbf{Y}_{sc2,j}} = \left(\frac{Y_{sc1,1,j}}{Y_{sc2,1,j}}, \dots, \frac{Y_{sc1,npred,j}}{Y_{sc2,npred,j}} \right)^T,$$

where $npred$ is the number of predicted observations.

- With the above steps, we obtain the rate ratio ($Ratio_j$) with have dimension m .

So, as done for estimation and prediction, quantities of interest such as the median and quantiles for constructing credibility intervals, can be obtained from the distribution of the rate ratio.

Estimation and prediction intervals

The algorithm was implemented in R through the Rstan package [34, 37, 38]. To solve the deterministic system, we used a predictor-corrector method based on the Runge-Kutta predictor of order 4 and corrector of order 5 [39].

Also, an extension of the Hamiltonian Monte Carlo (HMC) algorithm [35, 39–41], was used to perform the statistical analysis. Once the sample is obtained quantities of interest such as the median and the 2.5% and 97.5% quantiles can be computed to get a point and a symmetric credibility interval.

To construct the prediction intervals of HIV Incidence, we ran 20000 simulations, and for each of those solved the system of differential equations. The vector of 20000 solutions was then considered as the vector of medians and using as many values of the overdispersion parameter we were able to sample the 2.5% and 97.5% quantiles from the negative binomial distribution, such that the interval formed by these two quantiles is what we consider as the credibility region [34, 36, 37, 42].

5 Computational simulations

Parameters values and demographic data

The initial conditions for the initialization of the simulations were extracted from demographic data and for those concerning HIV, AIDS, undetectable (viral load), and incidence, we used the data reported by the Brazilian Ministry of Public Health between 2003-2019 [43–47].

For the compartment of individuals who are in the PrEP program and the parameters that are related to the use of PrEP in the population (ϵ_p, ϵ_f), we assume a value of zero until 2018, and the values for the incorporation of PrEP in 2018 of the compartment and the parameters come from [48, 49].

The initial conditions are $H(0) = 260000$, $A(0) = 150000$, $V(0) = 0.4 \times I(0)$, $P(0) = 0$, $E(0) = 100000$ and $S(0) = 1.91 \times 10^8 - V(0) - H(0) - A(0)$. We conducted simulations from 2003 until 2035 and compared with the actual data reported from 2003-2019.

For our study, we used that the probability of retention of the oral PrEP is 3 months after initiation is 72.5% and the probability of full adherence to oral PrEP is 92.3% using more than 4 pills per week [10, 49–51]. We assume that the probability of full adherence to oral PrEP is 96.3%. This information is used to give value to the parameter ϵ_f .

The data about HIV incidence was obtained from [52].

The a priori distributions for the parameters to be estimated were selected by the parameter definition space, taking a normal distribution for the parameters that can take values outside the unit interval and beta for those that are defined in $(0, 1)$ because the support of it is in that interval. Then, we picked a normal distribution ($N(\cdot, \cdot)$) for β , and ω , whose space of definition is greater than $(0, 1)$; and for other parameters a beta distribution ($Beta(a, b)$) with a and b entries defined as follows [53–55]:

$$a = \text{Mean} \left(\frac{\text{Mean}(1 - \text{Mean})}{\text{Var}} - 1 \right), \quad (47)$$

$$b = (1 - \text{Mean}) \left(\frac{\text{Mean}(1 - \text{Mean})}{\text{Var}} - 1 \right), \quad (48)$$

if $\text{Var} < \text{Mean}(1 - \text{Mean})$ where Mean is mean and Var is variance.

Table 2 shows the values of the parameters that are fixed, the intervals, and distributions a priori for the parameters to be estimated with the MCMC with a Bayesian approach.

Table 2. Parameter values and a priori distributions

Parameter	Point	Interval	A Priori Distribution	Reference
Λ	4,590,490,56	-	Fixed	[43]
α_s	0.00000001	-	Fixed	Assumed
μ	1/75.50	-	Fixed	[43]
β	-	(0, 10)	$N(2.5, 0.1)$	Assumed
ϵ	1.02	-	Fixed	Assumed
ϵ_D	0.00002	-	Fixed	Assumed
ϵ_{s1}	0.007	-	Fixed	[2]
ν	-	(0, 0.4)	$Beta(0.021, 3.812)$	[56–59]
ϕ	0.65	-	Fixed	Assumed
τ	-	(1/15, 1/10)	$Beta(0.389, 4.680)$	[44, 60, 61]
σ_H	-	(0, 0.4)	$Beta(0.091, 2.549)$	[56–59]
σ_{HI}	2	-	Fixed	[61]
d_H	-	(0, 0.1)	$Beta(0.069, 3.091)$	[62]
ω	-	(0.2, 2.5)	$N(0.52, 0.1)$	[61, 63]

Results

In [Figure 2](#), we can observe the posterior density functions of the parameters estimated with the MCMC with a Bayesian approach.

For our study, we used two chains and [Figure 3](#) show the traceplots for the chains representing each parameter. In addition, the convergence of the Hamiltonian Monte Carlo (HMC) was verified by the criterion shown in [[35](#), [39–41](#)]. Using the expressions of the limits ([27](#))-([40](#)) and the mean

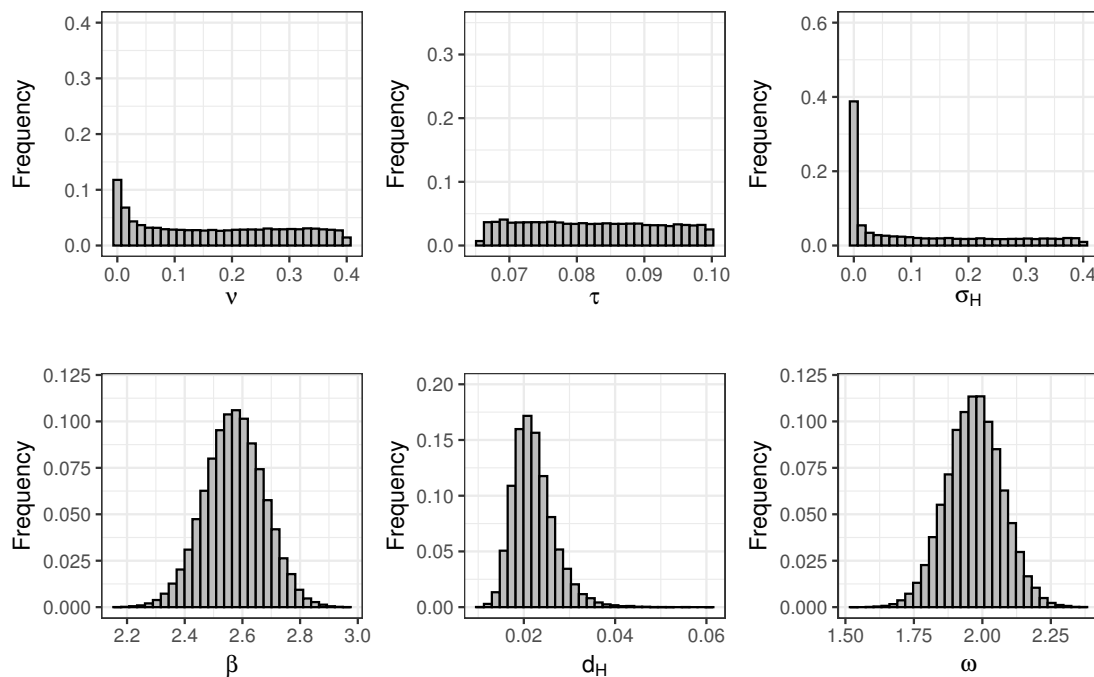


Figure 2. The posterior density functions obtained using MCMC with a Bayesian approach

of the values of the estimated parameters we have that the value obtained for the expression ([27](#)) is 0.25, and for ([28](#)) is 1.15 which means that when the parameter associated with adherence to treatment grows with HIV patients achieving the undetectability of the virus in blood the basic reproduction number is less than the unit so that the epidemic under these conditions can disappear in the population. The case when the adherence to HIV treatment tends to 0 and the number of cases that lose the undetectability and are HIV positive is higher than the unit, leads to an adverse epidemiological situation.

For expressions ([29](#)) and ([30](#)), the values obtained were 1.02 and 1.15, both greater than unity, which means that the number of AIDS cases that achieve undetectability while maintaining HIV status and other factors without intervention does not improve the epidemiological situation.

When the parameters associated with adherence to treatment and achieving undetectability of the virus in blood grow together and when the parameters associated with the loss of this undetectability for HIV and AIDS grow together, the basic reproduction number is less than unity, so we would be in a favorable situation, see expressions ([31](#)) and ([34](#)) and [Table 3](#). In the opposite cases, by means of expressions ([32](#)) and ([33](#)), the basic reproduction number is greater than unity. In the case when the diagnosis rate increases and the parameters associated with adherence to HIV treatment increase and decrease, the basic reproduction number is less than unity but is more favorable when the latter decreases.

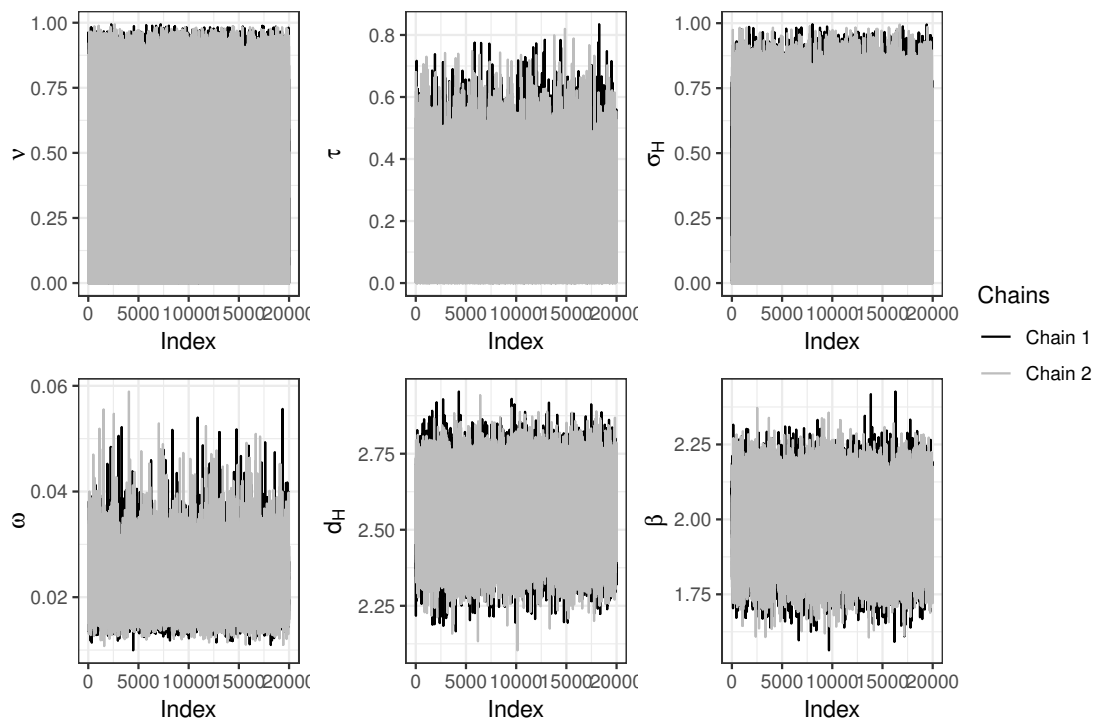


Figure 3. In this plot, each line represents an MCMC chain (2 chains), and each point represents the sampled value of a specific parameter in each MCMC iteration

When we increase the number of patients who progress from HIV to AIDS and decrease the number of AIDS cases who achieve undetectability according to formula (35), the basic reproduction number is greater than unity, which means that this epidemiological situation has a negative effect on the control of virus transmission. In the opposite situation by formula (36), the basic number reproduction is lower than unity, which we can say from the information provided by the model and the values of the parameters that if the number of cases with progression to AIDS increases, we need to increase adherence to treatment to counteract it.

In the case of increased case detection and adherence to HIV treatment according to formula (38), we have a positive impact on the basic reproduction number because it is less than unity. But if the number of diagnoses increases but adherence to treatment decreases according to formula (37), the basic reproduction number is greater than unity, so in order to have a positive effect on the decrease of HIV/AIDS cases we must have greater adherence to treatment in HIV.

Generally, when the parameters associated with the diagnosis and adherence to treatment in HIV and AIDS tend to the limit of the definition interval and the parameters of loss of the virus's undetectability in the blood tend to zero and return to the HIV and AIDS state, we are in a favorable situation for the control and future eradication of the epidemic and the opposite case we would be in an unfavorable situation because the basic reproduction number is greater than unity, see expressions (39) and (40) in Table 3.

Table 4 shows the evolution of the parameters associated with PrEP use when we implement the 25% coverage increase and 35% in 2025. Also, we assume that the health system has enough medication to cover the number of new individuals starting to use PrEP per year, which is logical taking into account the size of the Brazilian population. In the case a patient stops the PrEP use by decision or due to adverse effects, he/she can re-enter after a period of time to use the preventive method again, always remembering that our study, given the characteristics of the HIV/AIDS

Table 3. Values of the expressions (27)-(40) related to the joint variation over the \mathfrak{R}_0 of the parameters associated with treatment and diagnosis. The first column represents where the parameters will tend together, the second column links the respective expression of the basic reproduction number and the last column shows the value of the basic reproduction number when the parameters tend together to those values

Parameters	Expressions	Value of \mathfrak{R}_0
$\sigma_{HI} \rightarrow 1$ and $\sigma_H \rightarrow 0$	(27)	0.25
$\sigma_{HI} \rightarrow 0$ and $\sigma_H \rightarrow 1$	(28)	1.15
$\nu \rightarrow 1$ and $\omega \rightarrow 0$	(29)	1.02
$\nu \rightarrow 1$ and $\omega \rightarrow 0$	(30)	1.15
$\sigma_{HI} \rightarrow 1$ and $\nu \rightarrow 1$	(31)	0.16
$\sigma_{HI} \rightarrow 0$ and $\nu \rightarrow 0$	(32)	1.21
$\sigma_H \rightarrow 1$ and $\omega \rightarrow 1$	(33)	1.07
$\sigma_H \rightarrow 0$ and $\omega \rightarrow 0$	(34)	0.91
$\tau \rightarrow 1$ and $\nu \rightarrow 0$	(35)	1.01
$\tau \rightarrow 0$ and $\nu \rightarrow 1$	(36)	0.83
$\epsilon_{s1} \rightarrow 1$ and $\sigma_{HI} \rightarrow 0$	(37)	1.02
$\epsilon_{s1} \rightarrow 1$ and $\sigma_{HI} \rightarrow 1$	(38)	0.64
$\epsilon_{s1} \rightarrow 1, \sigma_{HI} \rightarrow 1, \nu \rightarrow 1,$ $\sigma_H \rightarrow 0,$ and $\omega \rightarrow 0$	(39)	0.11
$\epsilon_{s1} \rightarrow 1, \sigma_{HI} \rightarrow 0, \nu \rightarrow 0,$ $\sigma_H \rightarrow 1,$ and $\omega \rightarrow 1$	(40)	1.24

epidemic and the data, is annual. We compare two possible increases in coverage, Coverage I,

Table 4. Value of PrEP use rate with increases in coverage and number of new PrEP users per year from 2025-2035

Year	ϵ_p with Coverage I	Number of individuals who started using PrEP	ϵ_p with Coverage II	Number of individuals who started using PrEP
2025	0.000375	82136	0.000405	88707
2026	0.00046875	103273	0.00054675	120458
2027	0.0005859375	129812	0.0007381125	163525
2028	0.0007324219	163120	0.0009940063	221378
2029	0.0009155274	204914	0.0013419085	300347
2030	0.0011444093	257342	0.0018115765	407366
2031	0.0014305116	323087	0.0024462831	552355
2032	0.0017881395	394781	0.0033015982	728920
2033	0.0022235174	510597	0.0044571576	1018180
2034	0.0027939681	638246	0.0060176282	1374650
2035	0.0034921721	802668	0.0081231698	1867099

which is an increase of 25% per year, and Coverage II, an increase of 35% per year, both following formula (22), where the percentage increases are the p_s value, with respect to keeping the current rate of PrEP use fixed. We quantified the impact with the HIV incidence rate, HIV rate ratio and number of avoided cases and began implementation in 2025 to study its effect until 2035.

With Coverage I basic number that, the HIV incidence reported by the model was 17.06 ([15.96, 18.92]), which represented a decrease of 18.98% ([18.04%, 18.62%]) with respect to the scenario where we maintain the current coverage which was 20.85 ([19.61, 22.23]).

With Coverage II of HIV incidence rate was 15.15 ([14.15, 16.22]), which is a decrease of 27.66% ([27.03%, 27.84%]) with respect to the scenario where we maintain the current coverage until 2035.

Using HIV incidence as a quantification of the impact of increased coverage, we can conclude that from the values reported by the model and the estimation technique, an increase in PrEP coverage in Brazil favors the reduction of new cases of HIV, but we must take into account that given the

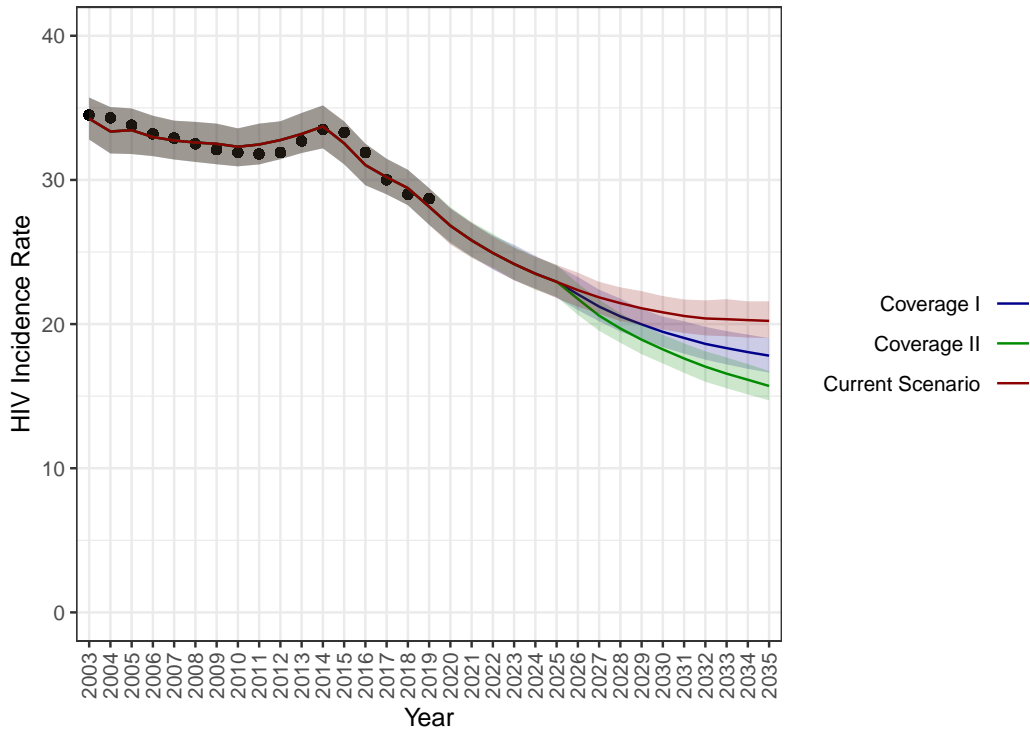


Figure 4. Behavior of the HIV incidence rate for the different increases in coverage starting in 2025 using the formula (22), and when we maintain PrEP use at current coverage (Current Scenario) until 2035. The credibility intervals between 2.5% and 97.5% are shown and the black points are the real data reported [43–46, 52]

demographics of Brazil, we need to further reduce the incidence of HIV for future eradication of the virus, see Figure 4.

The number of averted cases of HIV infection with the increased coverage is significant. The 35% annual increase in coverage (Coverage II) reported the highest number of averted cases with respect to the 25% increase in coverage, with a difference of 26790 fewer cases for 2.5%, 26390 for 50% and 26420 cases averted for 97.5%, see Table 5.

The reported values of the rate ratio show that Coverage I has at the end of the study in 2035 a value of 0.82 ([0.75, 0.89]) and Coverage II of 0.73 ([0.66, 0.80]), see Table 6, showing again that an increase in PrEP coverage in the population has a positive impact.

Based on the data reported by model (2)-(7), and the parameter estimation method, we obtained that through the HIV incidence, the number of HIV cases avoided, and the rate ratio that an increase in PrEP coverage can reduce the impact of HIV/AIDS in Brazil. In this case, two annual increases in PrEP coverage in Brazil of 25% and 35% were studied and the difference in the values obtained was significant and we recommend increasing the use of PrEP and extending its use not only to the vulnerable part of the population. to reduce the impact of the virus on the population.

Table 5. Number of cases avoided in 2035 with the different coverage increases started in 2025 and the difference in the number of cases avoided between Coverage I and Coverage II

	2.5%	50%	97.5%
Coverage I	15985	50879	85448
Coverage II	42774	77269	111868
Difference	26790	26390	26420

Table 6. Rate ratio for the different coverage increases initiated in 2025 and studying the impact until 2035

Year	Coverage I			Coverage II		
	Estimated	Lower Limit	Upper Limit	Estimated	Lower Limit	Upper Limit
2025	1.00	0.93	1.07	1.00	0.93	1.07
2026	0.98	0.91	1.05	0.97	0.90	1.04
2027	0.96	0.89	1.03	0.93	0.86	1.00
2028	0.94	0.87	1.01	0.90	0.84	0.97
2029	0.92	0.85	0.99	0.87	0.81	0.94
2030	0.90	0.83	0.97	0.85	0.78	0.92
2031	0.88	0.81	0.96	0.82	0.76	0.89
2032	0.87	0.80	0.94	0.80	0.73	0.87
2033	0.85	0.78	0.92	0.77	0.71	0.84
2034	0.83	0.76	0.91	0.75	0.68	0.82
2035	0.82	0.75	0.89	0.73	0.66	0.80

6 Conclusions

In this article, we presented a mathematical model for HIV/AIDS transmission that incorporates current PrEP programs. We presented a methodology that incorporates increasing PrEP coverage in the population into the model. The model allows for the study of different PrEP variants, different coverages and takes into account the importance of antiretroviral treatment in the transmission of the virus, in particular, adherence to treatment which leads to having an undetectable viral load in the blood and not infecting, and the diagnosis of cases due to the attempt to enter the PrEP program. We demonstrated the basic properties of the model: that it has a solution, such solution is positive, and in which region it makes epidemiological sense. We focus on the incidence of HIV cases because antiretroviral therapies allow the patient not to reach that state of the disease, in addition to being the most advanced cases of the disease. In the model, we have a compartment for people with undetectable viral load in the blood with the use of treatment because they will not represent a problem in the transmission of the virus and we can monitor the patient's health status and try to control the evolution of the disease. Using the next-generation matrix, we found the basic reproduction number and studied the joint and independent impact of parameters associated with the effectiveness of the treatment, the number of cases with HIV that reach the stage of AIDS, the use of PrEP, and contagion by other non-sexual ways.

To estimate parameters, we used the Markov Chains Monte Carlo (MCMC) with a Bayesian approach and as a value to quantify the impact we have on the HIV incidence rate ratio. The parameters selected to estimate are related to the effectiveness of antiretroviral treatment, death associated with the disease, and transmission. Using demographic data from Brazil and data from the bibliography for parameters and initial conditions, we performed computer simulations. We presented a test to observe the behavior of the estimation of the selected parameters of the model. We studied two possible increases in PrEP program coverage of 25% and 35%. With the results reported by the model, the accumulated cases of the individuals and the new individuals who enter the program are studied, since it is important that the results are logical with respect to the study population. The results obtained are acceptable, as can be seen in [Table 4](#).

We compare the behavior after increasing coverage by 25% and 35% in 2025 compared to maintaining the current coverage with oral PrEP using as a basis the incidence of HIV, HIV rate ratio and the number of cases avoided.

The results of the study showed the potential of PrEP use to reduce the incidence of HIV in Brazil. The model, after adapting the initial conditions and parameters, can be utilized to predict HIV incidence in other regions, countries, or localities.

In future work, we intend to study the model in other scenarios and study the cost-benefit problem of implementing injectable PrEP and increasing coverage.

Declarations

Use of AI tools

The authors declare that they have not used Artificial Intelligence (AI) tools in the creation of this article.

Data availability statement

All data generated or analyzed during this study are included in this article.

Ethical approval

The authors state that this research complies with ethical standards. This research does not involve either human participants or animals.

Consent for publication

All authors authorize the publication of the work.

Conflicts of interest

The authors declare that they have no conflict of interest.

Funding

There is no funding for this research.

Author's contributions

E.M.D.M.: Conceptualization, Formal Analysis, Methodology, Software, Validation, Visualization, Data Curation, Writing-Original Draft. R.A.R and A.P.: Visualization, Validation, Writing - Review & Editing. All authors discussed the results and contributed to the final manuscript. The authors have read and agreed to the published version of the manuscript.

Acknowledgements

The authors express their profound gratitude to the journal and reviewers for their excellent work and contributions to improving the manuscript.

References

- [1] Boniphace, I., Omari, M., Susan Fred, R., Ferdinand, M. and Marcel, T. HIV/AIDS clinical manifestations and their implication for patient clinical staging in resource-limited settings in Tanzania. *The Open AIDS Journal*, 5(1), 9-16, (2011). [[CrossRef](#)]
- [2] UNAIDS, Global HIV & AIDS statistics - Fact Sheet, (2023). <https://www.unaids.org/en/resources/fact-sheet>
- [3] U.S. Food & Drug Administration, FDA Approves First Injectable Treatment for HIV Pre-Exposure Prevention, (2021). <https://www.fda.gov/news-events/press-announcements/fda-approves-first-injectable-treatment-hiv-pre-exposure-prevention>

- [4] World Health Organization (WHO), WHO Recommends Long-Acting Cabotegravir for HIV Prevention, (2022). <https://www.who.int/news/item/28-07-2022-who-recommends-long-acting-cabotegravir-for-hiv-prevention>
- [5] Tseng, A., Seet, J. and Phillips, E.J. The evolution of three decades of antiretroviral therapy: challenges, triumphs and the promise of the future. *British Journal of Clinical Pharmacology*, 79(2), 182-194, (2015). [[CrossRef](#)]
- [6] Günthard, H.F., Saag, M.S., Benson, C.A., Del Rio, C., Eron, J.J., Gallant, J.E. et al. Antiretroviral drugs for treatment and prevention of HIV infection in adults: 2016 recommendations of the International Antiviral Society–USA panel. *JAMA*, 316(2), 191-210, (2016). [[CrossRef](#)]
- [7] Moya, E.M.D., Rodrigues, D.S., Pietrus, A. and Severo, A.M. A mathematical model for HIV/AIDS under pre-exposure and post-exposure prophylaxis. *Biomath*, 11(2), 208319, (2022). [[CrossRef](#)]
- [8] D’Angelo, A.B., Westmoreland, D.A., Carneiro, P.B., Johnson, J. and Grov, C. Why are patients switching from tenofovir disoproxil fumarate/emtricitabine (Truvada) to tenofovir alafenamide/emtricitabine (Descovy) for pre-exposure prophylaxis?. *AIDS Patient Care and STDs*, 35(8), 327-334, (2021). [[CrossRef](#)]
- [9] Moya, E.M.D. and Rodrigues, D.S. Fractional order modeling for injectable and oral HIV pre-exposure prophylaxis. *Mathematical Modelling and Control*, 3(2), 139-151, (2023). [[CrossRef](#)]
- [10] Biello, K.B., Mimiaga, M.J., Santostefano, C.M., Novak, D.S. and Mayer, K.H. MSM at highest risk for HIV acquisition express greatest interest and preference for injectable antiretroviral PrEP compared to daily, oral medication. *AIDS and Behavior*, 22(4), 1158-1164, (2018). [[CrossRef](#)]
- [11] Hosek, S.G., Rudy, B., Landovitz, R., Kapogiannis, B., Siberry, G., Rutledge, B. et al. An HIV preexposure prophylaxis demonstration project and safety study for young MSM. *Journal of Acquired Immune Deficiency Syndromes*, 74(1), 21-29, (2017). [[CrossRef](#)]
- [12] Kim, S.B., Yoon, M., Ku, N.S., Kim, M.H., Song, J.E., Ahn, J.Y. et al. Mathematical modeling of HIV prevention measures including pre-exposure prophylaxis on HIV incidence in South Korea. *PloS One*, 9(3), e90080, (2014). [[CrossRef](#)]
- [13] Omondi, E.O., Mbogo, R.W. and Luboobi, L.S. Mathematical analysis of sex-structured population model of HIV infection in Kenya. *Letters in Biomathematics*, 5(1), 174-194, (2018). [[CrossRef](#)]
- [14] Li, J., Peng, L., Gilmour, S., Gu, J., Ruan, Y., Zou, H. et al. A mathematical model of biomedical interventions for HIV prevention among men who have sex with men in China. *BMC Infectious Diseases*, 18, 600, (2018). [[CrossRef](#)]
- [15] Silva, C.J. and Torres, D.F.M. Modeling and optimal control of HIV/AIDS prevention through PrEP. *Discrete and Continuous Dynamical Systems–Series S*, 11(1), 119-141, (2018). [[CrossRef](#)]
- [16] Nabil, H. and Hamaizia, T. A three-dimensional discrete fractional-order HIV-1 model related to cancer cells, dynamical analysis and chaos control. *Mathematical Modelling and Numerical Simulation with Applications*, 4(3), 256-279, (2024). [[CrossRef](#)]
- [17] Bolaji, B., Onoja, T., Agbata, C., Omede, B.I. and Odionyenma, U.B. Dynamical analysis of HIV-TB co-infection transmission model in the presence of treatment for TB. *Bulletin of Biomathematics*, 2(1), 21-56, (2024). [[CrossRef](#)]
- [18] Naik, P.A., Owolabi, K.M., Yavuz, M. and Zu, J. Chaotic dynamics of a fractional order HIV-1 model involving AIDS-related cancer cells. *Chaos, Solitons & Fractals*, 140, 110272, (2020).

[CrossRef]

- [19] Mustapha, U.T., Ado, A., Yusuf, A., Qureshi, S. and Musa, S.S. Mathematical dynamics for HIV infections with public awareness and viral load detectability. *Mathematical Modelling and Numerical Simulation with Applications*, 3(3), 256-280, (2023). [CrossRef]
- [20] Yavuz, M., Akyüz, K., Bayraktar, N.B. and Özdemir, F.N. Hepatitis-B disease modelling of fractional order and parameter calibration using real data from the USA. *AIMS Biophy*, 11(3), 378-402, (2024). [CrossRef]
- [21] Delgado Moya, E.M., Ordoñez, J.A., Alves Rubio, F., Niskier Sanchez, M., De Oliveira, R.B., Volmir Anderle, R. and Rasella, D. A mathematical model for the impact of 3HP and social programme implementation on the incidence and mortality of Tuberculosis: Study in Brazil. *Bulletin of Mathematical Biology*, 86, 61, (2024). [CrossRef]
- [22] Lakshmikantham, V., Leela, S. and Martynuk, A.A. *Stability Analysis of Nonlinear Systems*. Springer: New York, (1989).
- [23] Gerstman, B.B. *Epidemiology Kept Simple: An Introduction to Traditional and Modern Epidemiology*. John Wiley & Sons: Hoboken, NJ, (2003).
- [24] Rothman, K.J. *Epidemiology: An Introduction* (Vol.2). Oxford University Press: USA, (2012).
- [25] Diekmann, O., Heesterbeek, J.A.P. and Roberts, M.G. The construction of next-generation matrices for compartmental epidemic models. *Journal of the Royal Society Interface*, 7(47), 873-885, (2010). [CrossRef]
- [26] Van den Driessche, P. and Watmough, J. Reproduction numbers and sub-threshold endemic equilibria for compartmental models of disease transmission. *Mathematical Biosciences*, 180(1-2), 29-48, (2002). [CrossRef]
- [27] Castillo-Chavez, C., Feng, Z. and Huang, W. On the computation of \mathfrak{R}_0 and its role on global stability. In *Mathematical Approaches for Emerging and Reemerging Infectious Diseases: An Introduction* (pp. 229-250). New York, USA: Springer, (2002).
- [28] Moya, E.M.D., Pietrus, A. and Oliva, S.M. Mathematical model with fractional order derivatives for Tuberculosis taking into account its relationship with HIV/AIDS and Diabetes. *Jambura Journal of Biomathematics*, 2(2), 80-95, (2021). [CrossRef]
- [29] Pinto, C.M.A. and Carvalho, A.R.M. Diabetes mellitus and TB co-existence: Clinical implications from a fractional order modelling. *Applied Mathematical Modelling*, 68, 219-243, (2019). [CrossRef]
- [30] Pinto, C.M.A. and Carvalho, A.R.M. The HIV/TB coinfection severity in the presence of TB multi-drug resistant strains. *Ecological Complexity*, 32, 1-20, (2017). [CrossRef]
- [31] Ngoteya, F.N. and Nkansah-Gyekye, Y. Sensitivity analysis of parameters in a competition model. *Applied and Computational Mathematics*, 4(5), 363-368, (2015). [CrossRef]
- [32] Chitnis, N., Hyman, J.M. and Cushing, J.M. Determining important parameters in the spread of malaria through the sensitivity analysis of a mathematical model. *Bulletin of Mathematical Biology*, 70, 1272-1296, (2008). [CrossRef]
- [33] Zamir, M., Zaman, G. and Alshomrani, A.S. Sensitivity analysis and optimal control of anthroponotic cutaneous leishmania. *PLoS One*, 11(8), e0160513, (2016). [CrossRef]
- [34] Roberts, G.O. and Rosenthal, J.S. General state space Markov Chains and MCMC algorithms. *Probability Surveys*, 1, 20-71, (2004). [CrossRef]
- [35] Neal, R.M. MCMC using Hamiltonian dynamics. In *Handbook of Markov Chain Monte Carlo*

- (pp. 113-162). London, England: Chapman and Hall/CRC, (2011).
- [36] Grinsztajn, L., Semenova, E., Margossian, C.C. and Riou, J. Bayesian workflow for disease transmission modeling in Stan. *Statistics in Medicine*, 40(27), 6209-6234, (2021). [[CrossRef](#)]
- [37] Chatzilena, A., Van Leeuwen, E., Ratmann, O., Baguelin, M. and Demiris, N. Contemporary statistical inference for infectious disease models using Stan. *Epidemics*, 29, 100367, (2019). [[CrossRef](#)]
- [38] Carpenter, B., Gelman, A., Hoffman, M.D., Lee, D., Goodrich, B., Betancourt, M. et al. Stan: A probabilistic programming language. *Journal of Statistical Software*, 76(1), 1-32, (2017). [[CrossRef](#)]
- [39] Gelman, A. and Rubin, D.B. Inference from iterative simulation using multiple sequences. *Statistical Science*, 7(4), 457-472, (1992). [[CrossRef](#)]
- [40] Duane, S., Kennedy, A.D., Pendleton, B.J. and Roweth, D. Hybrid Monte Carlo. *Physics Letters B*, 195(2), 216-222, (1987). [[CrossRef](#)]
- [41] Metropolis, N., Rosenbluth, A.W., Rosenbluth, M.N., Teller, A.H. and Teller, E. Equation of state calculations by fast computing machines. *The Journal of Chemical Physics*, 21, 1087-1092, (1953). [[CrossRef](#)]
- [42] Margossian, C. and Gillespie, B. Differential equations based models in Stan. In Proceedings, *StanCon 2017*, New York, USA, (2017, January). [[CrossRef](#)]
- [43] Instituto Brasileiro de Geografia e Estatística (IBGE), Projeção da População, (2024). <https://www.ibge.gov.br/apps/populacao/projecao/index.html>
- [44] Boletim Epidemiológico, HIV AIDS 2018, (2019). <https://central.to.gov.br/download/101448>
- [45] Boletim Epidemiológico Especial - HIV/AIDS 2019, (2019). <https://www.gov.br/saude/pt-br/centrais-de-conteudo/publicacoes/boletins/epidemiologicos/especiais/2019/boletim-epidemiologico-especial-hiv-aids-2019/view>
- [46] Boletins Epidemiológicos Especiais, Boletim Epidemiológico Especial - HIV/Aids 2021, (2021). <https://www.gov.br/saude/pt-br/centrais-de-conteudo/publicacoes/boletins/epidemiologicos/especiais/2021/boletim-epidemiologico-especial-hiv-aids-2021.pdf/view>
- [47] Rubio, F.A., Amad, A.A.S., Aransiola, T.J., De Oliveira, R.B., Naidoo, M., Moya, E.M.D. et al. Evaluating social protection mitigation effects on HIV/AIDS and Tuberculosis through a mathematical modelling study. *Scientific Reports*, 14, 11739, (2024). [[CrossRef](#)]
- [48] Agência de Notícias da AIDS: Ativistas Consideram um Retrocesso a Decisão do Ministério da Saúde de Proibir Farmacêuticos de Prescreverem PrEP e Dizem Que Exclusão Vai na Contramão do SUS, (2022). <https://agenciaaids.com.br/noticia/ativistas-consideram-um-retrocesso-a-decisao-do-ministerio-da-saude-de-proibir-farmacuticos-de-prescreverem-prep-e-dizem-que-exclusao-vai-na-contramao-do-sus/>
- [49] Fonner, V.A., Dalglish, S.L., Kennedy, C.E., Baggaley, R., O'reilly, K.R., Koechlin, F.M. et al. Effectiveness and safety of oral HIV preexposure prophylaxis for all populations. *Aids*, 30(12), 1973-1983, (2016). [[CrossRef](#)]
- [50] Jamieson, L., Johnson, L.F., Nichols, B.E., Delany-Moretlwe, S., Hosseinipour, M.C., Russell, C. and Meyer-Rath, G. Relative cost-effectiveness of long-acting injectable cabotegravir versus oral pre-exposure prophylaxis in South Africa based on the HPTN 083 and HPTN 084 trials: a modelled economic evaluation and threshold analysis. *The Lancet HIV*, 9(12), e857-e867,

(2022). [CrossRef]

- [51] Marshall, B.D.L., Goedel, W.C., King, M.R.F., Singleton, A., Durham, D.P., Chan, P.A. et al. Potential effectiveness of long-acting injectable pre-exposure prophylaxis for HIV prevention in men who have sex with men: a modelling study. *The Lancet HIV*, 5(9), e498-e505, (2018). [CrossRef]
- [52] Szwarcwald, C.L., Souza Júnior, P.R.B., Pascom, A.R.P., Coelho, R.A., Ribeiro, R.A., Damacena, G.N. et al. HIV incidence estimates by sex and age group in the population aged 15 years or over, Brazil, 1986-2018. *Revista da Sociedade Brasileira de Medicina Tropical*, 55, e0231-2021, (2002). [CrossRef]
- [53] Wadsworth, G.P. and Bryan, J.G. *Introduction to Probability and Random Variables*. McGraw-Hill: New York, (1960).
- [54] Gnanadesikan, R., Pinkham, R.S. and Hughes, L.P. Maximum likelihood estimation of the parameters of the beta distribution from smallest order statistics. *Technometrics*, 9(4), 607-620, (1967). [CrossRef]
- [55] Pearson, K. Method of moments and method of maximum likelihood. *Biometrika*, 28(1/2), 34-59, (1936). [CrossRef]
- [56] Leng, X., Liang, S., Ma, Y., Dong, Y., Kan, W., Goan, D. et al. HIV virological failure and drug resistance among injecting drug users receiving first-line ART in China. *BMJ Open*, 4(10), e005886, (2014). [CrossRef]
- [57] Jobanputra, K., Parker, L.A., Azih, C., Okello, V., Maphalala, G., Kershberger, B. et al. Factors associated with virological failure and suppression after enhanced adherence counselling, in children, adolescents and adults on antiretroviral therapy for HIV in Swaziland. *PLoS One*, 10(2), e0116144, (2015). [CrossRef]
- [58] Hassan, A.S., Nabwera, H.M., Mwaringa, S.M., Obonyo, C.A., Sanders, E.J., Rinke de Wit, T.F. et al. HIV-1 virologic failure and acquired drug resistance among first-line antiretroviral experienced adults at a rural HIV clinic in coastal Kenya: a cross-sectional study. *AIDS Research and Therapy*, 11(1), 9, (2014). [CrossRef]
- [59] Rupérez, M., Pou, C., Maculuve, S., Cedenó, S., Luis, L., Rodríguez, J. et al. Determinants of virological failure and antiretroviral drug resistance in Mozambique. *Journal of Antimicrobial Chemotherapy*, 70(9), 2639-2647, (2015). [CrossRef]
- [60] World Health Organization (WHO), HIV and AIDS, (2024). <https://www.who.int/news-room/questions-and-answers/item/hiv-aids>
- [61] Ali, J.H. and Yirtaw, T.G. Time to viral load suppression and its associated factors in cohort of patients taking antiretroviral treatment in East Shewa zone, Oromiya, Ethiopia, 2018. *BMC Infectious Diseases*, 19, 1084, (2019). [CrossRef]
- [62] Todd, J., Glynn, J.R., Marston, M., Lutalo, T., Biraro, S., Mwita, W. et al. Time from HIV seroconversion to death: a collaborative analysis of eight studies in six low and middle-income countries before highly active antiretroviral therapy. *AIDS*, 21, S55-S63, (2007). [CrossRef]
- [63] CDC, Evidence of HIV Treatment and Viral Suppression in Preventing the Sexual Transmission of HIV, (2022). <https://www.cdc.gov/hiv/risk/art/evidence-of-hiv-treatment.html>

Bulletin of Biomathematics (BBM)
(<https://bulletinbiomath.org>)



Copyright: © 2024 by the authors. This work is licensed under a Creative Commons Attribution 4.0 (CC BY) International License. The authors retain ownership of the copyright for their article, but they allow anyone to download, reuse, reprint, modify, distribute, and/or copy articles in *BBM*, so long as the original authors and source are credited. To see the complete license contents, please visit (<http://creativecommons.org/licenses/by/4.0/>).

How to cite this article: Delgado Moya, E.M., Rodriguez, R.A. & Pietrus, A. (2024). A mathematical model for the study of HIV/AIDS transmission with PrEP coverage increase and parameter estimation using MCMC with a Bayesian approach. *Bulletin of Biomathematics*, 2(2), 218-244. <https://doi.org/10.59292/bulletinbiomath.2024010>